AD_____
(Leave blank)

Award Number: W81XWH-08-1-0352

TITLE: Optimizing and Evaluating an Integrated SPECT-CmT System Dedicated to Improved 3-D Breast Cancer Imaging

PRINCIPAL INVESTIGATOR: Dominic J. Crotty

CONTRACTING ORGANIZATION: Duke University
Durham, NC, 27710

REPORT DATE: May 2009

TYPE OF REPORT: Annual Summary

PREPARED FOR: U.S. Army Medical Research and Materiel Command
Fort Detrick, Maryland 21702-5012

DISTRIBUTION STATEMENT: (Check one)

[X] Approved for public release; distribution unlimited

[ ] Distribution limited to U.S. Government agencies only; report contains proprietary information

REPORT DOCUMENTATION PAGE

Form Approved OMB No. 0704-0188

1. REPORT DATE	2. REPORT TYPE	3. DATES COVERED *(From - To)*
31-05-2009	Annual Summary	*01 MAY 2008-30 APR 2009*

4. TITLE AND SUBTITLE
Optimizing and Evaluating an Integrated SPECT-CmT System Dedicated to Improved 3-D Breast Cancer Imaging

5a. CONTRACT NUMBER

5b. GRANT NUMBER
W81XWH-08-1-0352

5c. PROGRAM ELEMENT NUMBER

6. AUTHOR(S)
Dominic Crotty

Email: dominic.crotty@duke.edu

5d. PROJECT NUMBER

5e. TASK NUMBER

5f. WORK UNIT NUMBER

7. PERFORMING ORGANIZATION NAME(S) AND ADDRESS(ES)
Duke University
Office of Sponsored Programs
Box 104135
Durham, NC 27708
Dominic.crotty@duke.edu

8. PERFORMING ORGANIZATION REPORT NUMBER

9. SPONSORING / MONITORING AGENCY NAME(S) AND ADDRESS(ES)
U.S. Army Medical Research and Materiel Command Fort Detrick, Maryland 21702-5012

10. SPONSOR/MONITOR'S ACRONYM(S)

11. SPONSOR/MONITOR'S REPORT NUMBER(S)

12. DISTRIBUTION / AVAILABILITY STATEMENT
Approved for Public Release

13. SUPPLEMENTARY NOTES

14. ABSTRACT The overall objective of this research is to optimize the development of a combined dual-modality single photon emission computed tomography (SPECT) and x-ray computed mammotomography (CmT) system for the earlier detection and staging of breast cancer, improving surgical biopsy guidance, and the monitoring of patient therapy response. Co-registered acquisition of emission (nuclear) and transmission (x-ray) data using both 3D imaging modalities in a common field of view may aid to accurately localize the radioactive tumor uptake in the emission image by using anatomical structure from the transmission image. In the first year of this grant the complete hybrid imaging system, including a custom designed patient bed, were successfully integrated and used to complete single and dual-modality patient imaging studies. The tradeoffs inherent in the design of the custom-made bed for prone-patient imaging were investigated by evaluating the effects of limited angle tomography on reconstructed CmT image quality of the pendant breast volume. Novel 3D system trajectories to help overcome the design tradeoffs were also investigated with an observer study used to quantify the results. Initial steps in the process of designing a fully integrated imaging system with both modalities capable of full 3D motion were also taken. In addition to research, experience in other areas of breast cancer screening and detection were explored through shadowing clinical procedures.

15. SUBJECT TERMS X-ray imaging, Nuclear Medicine Imaging, SPECT, CT, Molecular Breast Imaging, Mammotomography

16. SECURITY CLASSIFICATION OF:			19a. NAME OF RESPONSIBLE PERSON	19b. TELEPHONE NUMBER
			Dominic Crotty	(919) 684 7948
a. REPORT	**b. ABSTRACT**	**c. THIS PAGE**	**17. LIMITATION OF ABSTRACT**	**18. NUMBER OF PAGES - 64**
Unclassified	Unclassified	Unclassified	Unlimited	

Standard Form 298 (Rev. 8-98)
Prescribed by ANSI Std. Z39.18

TABLE OF CONTENTS

A. Introduction

The objective of this pre-doctoral trainee project is to enhance the development of a combined dual-modality single photon emission computed tomography (SPECT) and x-ray computed mammotomography (CmT) system for the earlier detection and staging of breast cancer, improving surgical biopsy guidance, and the monitoring of patient therapy response. Co-registered acquisition of emission (nuclear) and transmission (x-ray) data using both 3D imaging modalities in a common field of view may help to accurately localize the radioactive tumor uptake in the emission image by using the anatomical structure visible in the transmission image.

In the first year of this grant the complete hybrid imaging system, including a custom designed patient bed, were successfully integrated and used to complete some dual-modality patient imaging studies. The novel design of the patient bed for prone patient imaging introduces tradeoffs between maximizing the imaged breast volume and the ability to complete a full 360° scan of the patient's pendant breast. In Year 1 the feasibility of solutions to overcome these limitations using novel source-detector trajectories were also comprehensively investigated.

In addition, the x-ray source and detector, decoupled in the initial prototype CmT system, were once again coupled in a newly modified prototype system design using a C-arm extension. The newly re-coupled source-detector CmT system, a precursor to the future integration of fully 3D SPECT and CmT systems, has reduced the uncertainties in relative orientation of the x-ray source and detector and helped increase system stability and robustness.

Patient imaging trials using the integrated system and the patient bed took place that gave valuable information to guide the design of future iterations of the imaging system and its various constituent components.

Several supplementary aspects of the training program have been initiated including presentations of research at international conferences, shadowing of healthcare professionals in their dedicated work of breast cancer screening and detection, publishing manuscripts in conference proceedings, and the co-authoring of a peer reviewed manuscript accepted for publication in an international journal.

B. Body

The Statement of Work along with the original projected timeline is attached in Appendix A of this Progress Report. In Year 1, Task 2 was completed in addition to several aspects of Task 3. It is expected that Task 1 will be completed in the early part of Year 2 in addition to making both sub-systems capable of fully 3D motion. The system as it stands currently is shown in Figure 1.

Task 2: Investigate the effect on image quality of the limited 3D motion of the prototype dual-modality imaging system (Months 4-10).

Task 2(a) Integrate the existing prototype dual-modality breast imaging device along with a new customized clinical patient bed.

As shown in Figure 1, a patient bed was designed and integrated with the dual-modality imaging system. The overarching objective of the bed design was to allow for comfortable imaging of a prone patient while also enabling the hybrid system to maximize the imaged volume of breast and chest wall.

Figure 1 Image of the custom deisgned patient bed positioned over the initial prototype integrated SPECT-CmT imaging system.

To design the bed, the x-ray tube, cone beam limits and detector of the CmT sub-system were modeled at different x-ray source to image distances (SIDs) (55-80cm) and at varying polar tilt and patient bed angles (0- 20°) using computer aided design (CAD) software (*Autodesk Inventor Professional R10*, *Autodesk Inc.*, CA). For each iteration, a pendant breast was modeled in the field of view (FOV) of the detector at varying source to object distances, thus changing image magnification. The total imaged breast volume was calculated by the intersection of the cone beam and the breast. Using the design criterion of fixing to 5mm the gap between the top of the source and detector and the bottom of the bed, a skeleton outline of possible bed designs was superimposed on the CmT system for each source-detector setup (see Figure 2 for one such example).

To achieve comfortable patient imaging with the downstream effect of reducing motion induced artifacts, the approach was to design a shallow trough at the head to minimize neck strain and also design an angled waist section over which the patient extends her torso, making her breast protrude through a centered hole.

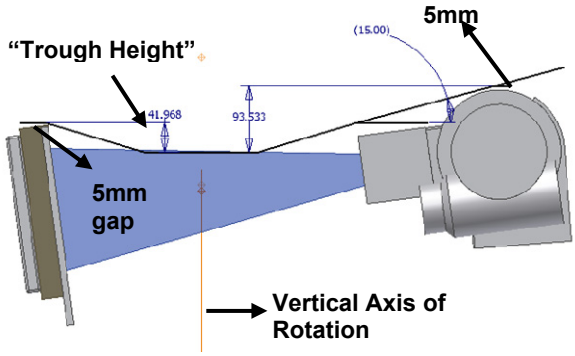

Figure 2 An example skeleton outline of a bed design superimposed on the modeled CmT source (right) and detector (left) sub-system with a 60cm SID and 15° bed angle. The bed is designed to allow the cone beam (blue) x-ray system image while rotating about the vertical axis of rotation.

The final $\frac{1}{8}$" thick stainless steel bed was designed, manufactured and integrated with the hybrid imaging system (see Figures 1, 3). The tiered bed design, angled sides and octagonally shaped trough allow for system rotation underneath the patient while providing comfort for the prone patient. To allow for flexibility in future CmT system designs the steel bed was designed with an octagonal center that could be removed or replaced by a radiolucent or more flexible radio-opaque materials (see Figure 3). In fact, the bed is now used with the center section entirely removed and replaced with layered neoprene and layers of thin leaded sheets (see Task 2(b)).

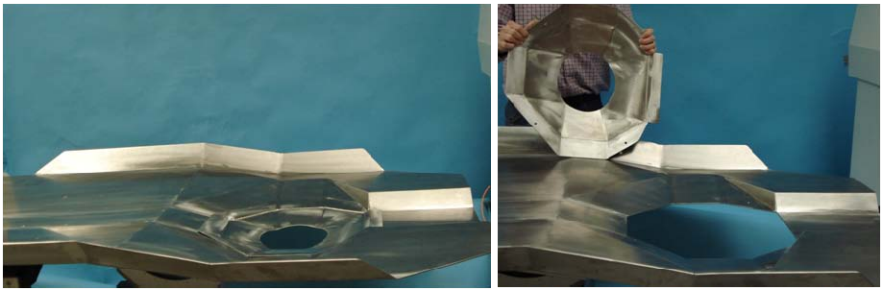

Figure 3 Photographs of the patient bed illustrating the tiered nature of the bed and the removable torso section to allow imaging deeper into the patient's breast and chest wall.

We made a number of modifications following initial delivery of the manufactured bed to increase patient comfort and improve reconstructed image quality. Due to an observed degradation in transmission image quality due to emission contamination photons emanating from radioactivity inside the patient's torso [1], the bed was lined with a $^{1}/_{16}$" lead sheet that acts as a barrier to primary and scattered ^{99m}Tc 140keV gamma rays. Further protection to both the patient from backscattered x-rays and to the transmission image from emission source (^{99m}Tc) contamination was additionally provided by modifying a standard protective lead apron having 0.5mm thick sheeting. It is planned in Year 2 to replace these temporary lead aprons with permanent lead sheets of standard thickness. Additionally, as stated above, the center stainless steel section was removed and has been replaced with flexible neoprene lining that's radiolucent to incident radiation but importantly gives the subject support as she bends into the FOV. A lining of comfortable foam has also been added to increase patient comfort as she lies prone during the 10-20 minute dual modality scan. Subsequent to its integration with the hybrid imaging system, the bed has been successfully used in a few patient studies under Dr. Tornai's NIH R01 grant (see Unlisted Tasks).

There are recognized limitations to the bed design that span both ergonomic and technical details. Feedback from subjects involved in early studies includes their feeling some physical discomfort in certain areas of the body (i.e. their necks) that may ultimately contribute to motion-induced artifacts. This feedback will be used in the design of an improved bed that increases the subject's comfort level. In contrast to the limited range of motion of the current CmT sub-system, restricted to circular trajectories, we will implement full 3D tilting for the CmT sub-system in future designs. This will necessitate designing a new bed with angled sides that enable system tilting. Other novel CmT sub-system trajectories were also investigated as solutions to overcome the inability of the CmT sub-system to view more of the chest wall (see Task 2(b) and Task 3(a)).

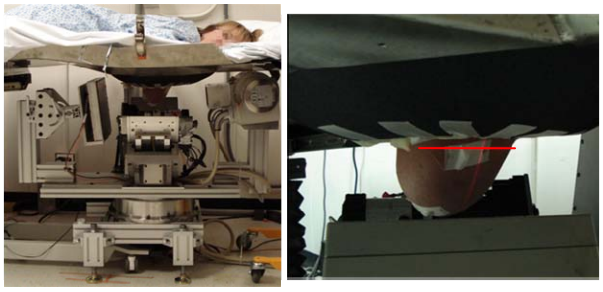

Figure 4 (Left) Images of a subject being scanned using the dual modality imaging system. This volunteer was scanned using a 360° trajectory with the x-ray tube shown passing underneath the subject's head. (Right) the red line on the pendant breast indicates the approximate depth of imaging into the breast using this imaging trajectory.

Task 2(b) Investigate quality of images reconstructed using limited tomographic acquisition for the hybrid system.

Using a sequential image acquisition protocol, with the SPECT and CmT sub-systems acquiring data in succession, the 3D hemispherical positioning flexibility of the integrated SPECT sub-system enables the gamma camera to avoid all physical impediments and contour the pendant breast, ensuring visualization of molecular imaging information inside the patient's chest wall. In contrast, experience with initial patient imaging trials has shown that a combination of challenges in effective patient positioning, the tiered bed design, its truncated trough height at the head, imaging dead zones inherent to the components of the CmT sub-system and bed manufacturing tolerances all combine to separate the top plane of the CmT cone beam from the chest wall (see Figure 4).

A study was therefore designed to investigate circumventing the positioning limitations of the prototype CmT system by using limited angle tomography to acquire vital CmT projections views through the patient's chest wall. The premise of the experiment was that, to accommodate a 360° acquisition, the bed has to be raised up to allow the CmT system to rotate around the lowest part of the bed (the head section). Because of this, vital volumetric information about the breast volume closest to the chest wall is lost. To regain this lost volumetric information, it is proposed to lower the bed more into the FOV of the CmT system and acquire data using <360° of projections. Depending on the height the bed was lowered to, the maximum possible angular rotation was restricted to as little as 250°.

While limited angle tomography was also investigated using the SPECT sub-system, the SPECT sub-system is still capable of full 3D motion in this initial prototype. Therefore, the emphasis of the dual-modality study was on investigating novel trajectories to allow the less flexible CmT system to better image the breast and chest wall area.

The flexibility of the bed positioning system used in the lab (model 830-058, *Biodex Medical Systems*, Shirley, NY), having five degrees of controlled movement, allows implementation of a number of 3D x-ray source and detector trajectories applicable to overcoming the issue of limited angle tomography while avoiding contact with the patient and/or bed.

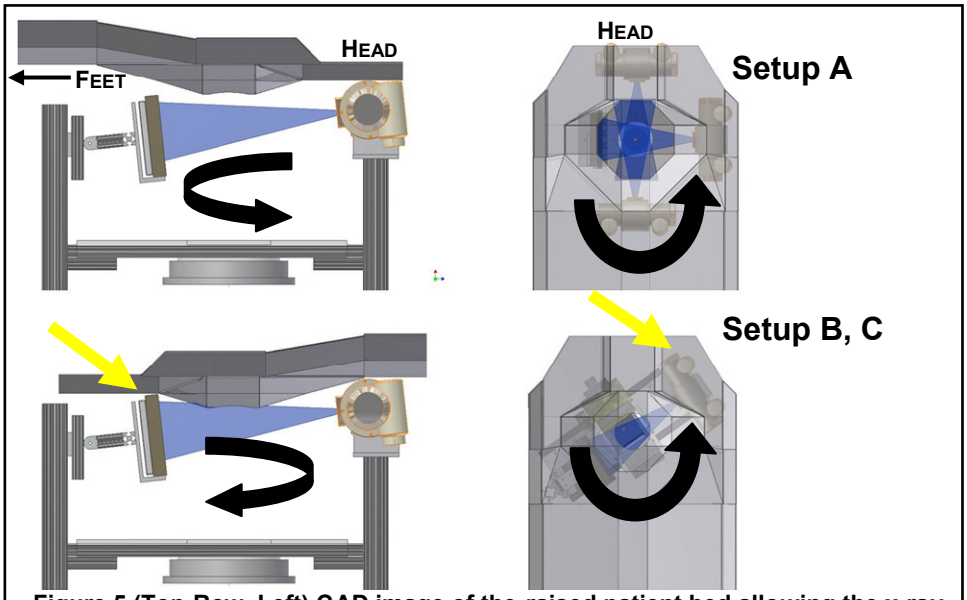

Figure 5 (Top Row, Left) CAD image of the raised patient bed allowing the x-ray tube to rotate underneath the head section. Note the separation of the top plane of the modeled x-ray cone beam (blue) from the under surface of the bed. (Top Row, Right) Top down view of the modeled x-ray tube completing a full 360° trajectory with the raised bed. (Bottom row, Left) The patient bed is lowered, with the top plane of the cone beam penetrating the assumed position of the chest wall of the patient. Note the top of the x-ray tube is above the level of the head section (black broken line). (Bottom Row, Right) Tube impacts the side of the head section of the bed. Conversely, the detector remains capable of traversing under the head section (yellow arrows).

Before the dual-modality SPECT-CmT experiments were performed, simulations were initially made using software to quantify the expected changes in imaged breast volume using various limited angle trajectories described in more detail in the accompanying manuscript in Appendix D. The trajectories modeled a combination of raising or lowering the patient bed and rotating the modeled x-ray tube around the vertical axis of rotation until the tube housing (a model of our Sapphire housing, *Varian Medical Systems*, Salt Lake City, UT) made contact with the patient bed.

Three potential trajectory setups were tested. The first (A) simulates raising the bed just enough to allow for full 360° rotation of the imaging system, including underneath the head section, trading increased tomographic sampling for a reduction in imaged breast volume (since the bed is raised to allow for full rotation, it therefore increases the separation of the chest wall from the top plane of the cone beam). The second and third setups (B and C) simulate lowering the bed until the system rotates up to the inner and outer circular edges of the x-ray tube housing, respectively (see Figure 1, Figure 4 for photographs of these limited angle and full 360° trajectory setups, respectively).

Representative illustrations of the setup for the simulated cases are shown in Figure 5 with the breast and anterior chest wall (not shown) modeled as hanging pendant from the center of the octagonal opening in the bed. Table 1 quantifies tradeoffs involved in vertically shifting the system in order to allow more of the breast and chest wall to be included in the cone beam FOV. A negative number in the far right column indicates that the top plane of the cone beam lies anterior to the simulated chest wall, i.e. the chest wall is not sampled. A positive number indicates that the top plane of the cone beam images into and through the chest wall.

There is a 120° azimuthal difference between a full 360° rotation at a higher system height where the x-ray tube is allowed to pass below the head section of the bed (Setup A) and a 240° trajectory with the system lowered to view more of the breast, but where the outer edge of the tube housing impacts the head section (Setup C).If this 120° reduction in azimuthal sampling is acceptable, simulation results indicate that there is an approximate 19mm increase in visualization towards the chest wall i.e. the range from -10mm to +9.3mm. This result demonstrates the potential advantages for using limited angle trajectories to increase the imaged volume of breast tissue.

Table 1 Effect of limited angle trajectories to increase the volume of breast imaged near the chest wall

	Imaging Setup	Total azimuthal projection range	Distance from anterior chest wall to cone beam (mm) *
A	Tube passes below head section of the bed	360°	-10
B	Tube housing inner edge impacts bed	300°	-2.9
C	Tube housing outer edge impacts bed	240°	+9.3

* Negative values indicate the top plane of the cone beam is anterior to the chest wall, positive values mean the beam penetrates the chest wall.

The phantom used in the dual modality SPECT-CmT experiments can be viewed in the manuscripts in Appendix D. Each phantom consists of 4 thin walled balloon lesions (*Harvard Apparatus Inc.*, Holliston, MA), 2600, 500, 140 and 70μL arranged on the same radius circle at 90° intervas. Attached to an acrylic ring, two such disks were stacked, vertically separated by ~1.5", placed in a water-filled cylinder (to mimic dense breast tissue) and suspended in the common FOV of the imaging system. For dual mode scanning, the lesions were filled with a mixture of CmT contrast (1:60 Iodine:water concentration) and activity-filled water (40μL/mCi ^{99m}Tc). Three lesion:background concentrations were employed for SPECT imaging: inifinity:1, 10:1 and 3:1. Two trajectories were used for contoured SPECT imaging: a three-lobed sinewave projected onto the hemispherical surface (projsine), and a simple vertical axis of rotation (VAOR) [2-4]. For CmT imaging a 360° data set was acquired with both disks in the FOV. The SPECT and CmT projection data sets were post-processed to mimic limited angle data sets by removing projections in contiguous sectors from desired positions around the phantom.

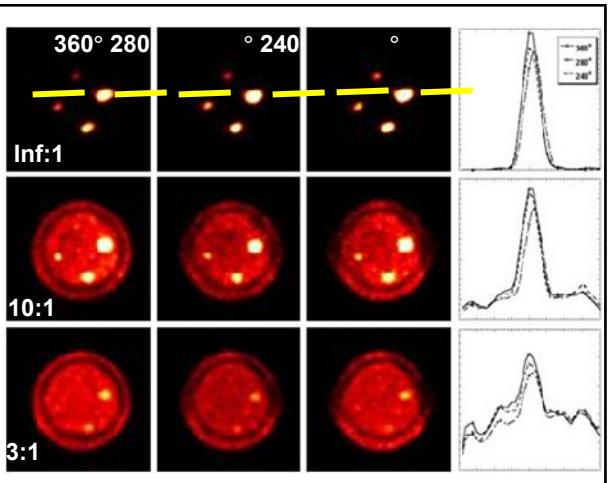

Figure 6 Coronal images of the lower disk of lesions for different activity ratios. Images are divided into 360° data set (left col.), 280° (middle col.) and 240° (right col.). Profiles (yellow lines) through the 2.6mL lesion show little change from the 360° to the 280° trajectory.

Reconstructed images from the SPECT study using a projsine trajectory are shown in Figure 6, for a full 360° and limited angle data sets using 280° and 240° of projections. Images are shown for lesion:background activity ratios of infinity, 10:1 and 3:1. Image quality degrades with a reduction in the activity ratio and the angular range of projections with increased distortion visible in the profiles (yellow

lines) of the largest lesion closer to the edge of the cylinder especially for the 3:1 data set. However, the same profiles indicate that lesions remain clearly discernable.

Figure 7 shows maximum intensity projection (MIP) CmT images of lesions reconstructed using limited angle methods. The fu lly sampled data set is also shown for comparison. Incr easing disto rtion is evident in the images as the number of omitted proj ections is in creased. In addition, smaller lesion s become harder to visualize as more projectio ns are remove d from the f ull 360°. Pr ofiles through each 'lesion' in th e upper disk taken from lim ited angle reconstructions, also shown in Figure 7, emphasize the increase d distortion and reduction in peak reconstructe d attenuation coefficient value. A trend of reduced balloon lesion SNR and contrast with a reduction in the projections is also seen (Table 2).

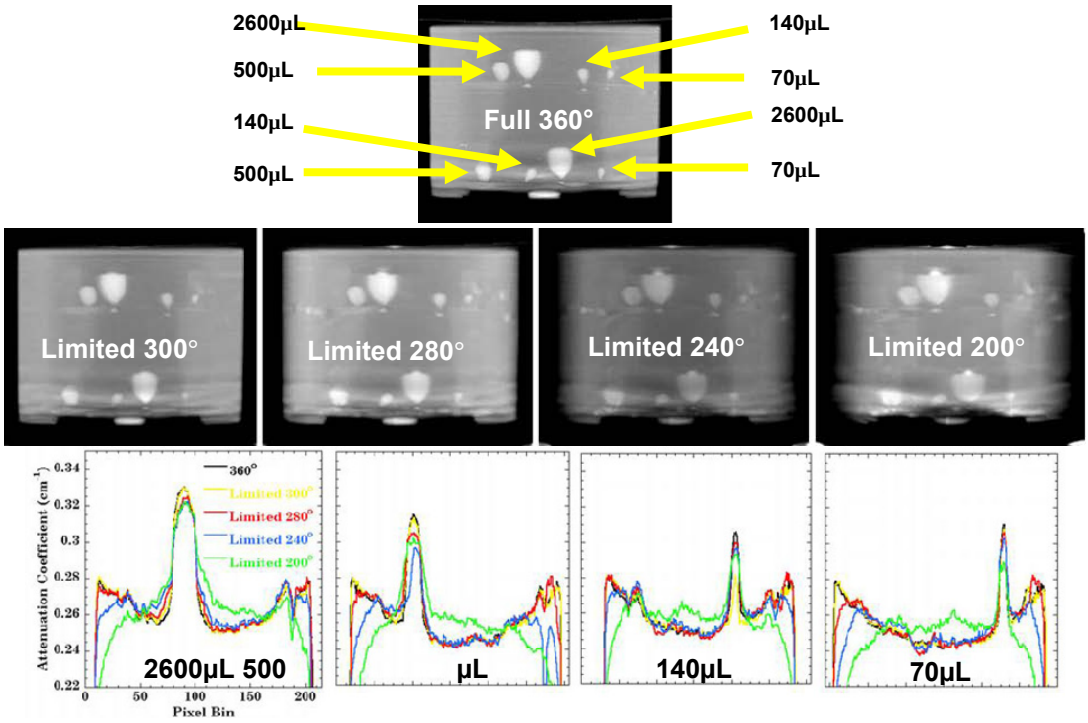

Figure 7 T ransverse MIP imag es of the cylindrical phantom showing the (top row) upper and lower disks of balloons with the full 360°in the FOV acquisition contrasted with (middle row) images from limited d ata sets. L imited 280° in dicates th at 2 80° of p rojections were u sed w ith 80° rem oved. (Bottom ro w) Pro files fro m th e imag es sh ow increased d istortion in lesio n sh ape an d esp ecially towards the edges of the cylinder as projections are increasingly removed.

Table 2 SNR an d contrast metrics calculated for the upper disk of balloon lesions from the CmT ima ges using a full 360° data acquisition and limited angle trajectories.

	SNR		Contrast	
Lesion Size	**2.6mL**	**140uL**	**2.6mL**	**140uL**
Full 360°	38.53 19.46		0.29	0.17
Limited - 280º	27.34 15.65		0.26	0.18
Limited - 240º	21.84 14.22		0.23	0.17

Task 3: Implement s ynchronized 3-D positi oning and data acquisition for the prototype dual-modality imaging system (Months 10-22)

Task 3(a): Novel 3D data acquisit ion trajectories involving CmT sub-system vertical shifting – an initial feasibility study

A study wa s conducted to evaluate the feasibility of implementing vertical sh ifting of the CmT sub-system. This was the first step to restoring the fully 3D positioning capability of the CmT sub-system as part of the integrated hybrid imaging system.

Using the results of the simulation study completed for the limited angle tomography study (Table 1), it can be seen that a trajectory involving vertical shifting of the system as the system rotates could be used to concurrently satisfy a full 360° azimuthal sampling of a lower portion of the breast while accepting partial sampling of the full breast volume. Such a trajectory could be implemented by imaging at one height for a portion of the trajectory (e.g. setup B or C in Table 1 see also Figure 5) and at a different height for the remainder of the trajectory (i.e. setup A, Table 1, Figure 5) to complete the 360° rotation by passing the x-ray tube beneath the head section of the bed. Trajectories B or C view more of the breast volume with reduced azimuthal range while trajectory A results in the least amount of imaged breast volume while maximizing azimuthal range.

The same disk phantom (see Appendix D) used in the limited angle tomography study was also used in this study. For vertical shift imaging, 2 separate complete tomographic data sets were acquired. The first scan acquired data with one (the lower) disk in the system FOV for 360 projections at 1° intervals, acquired at 60kVp, 100mA, 2.5mAs per projection. This trajectory mimicked trajectory A. The disk phantom was then lowered and a follow up 360° data set acquired with both disks in the FOV (mimicking B or C). Vertically shifted CmT projection data sets were created by concatenating projections in specific angle sectors from the first data acquisition with portions of the complete projection set from the second data acquisition that had both disks visible in projection images.

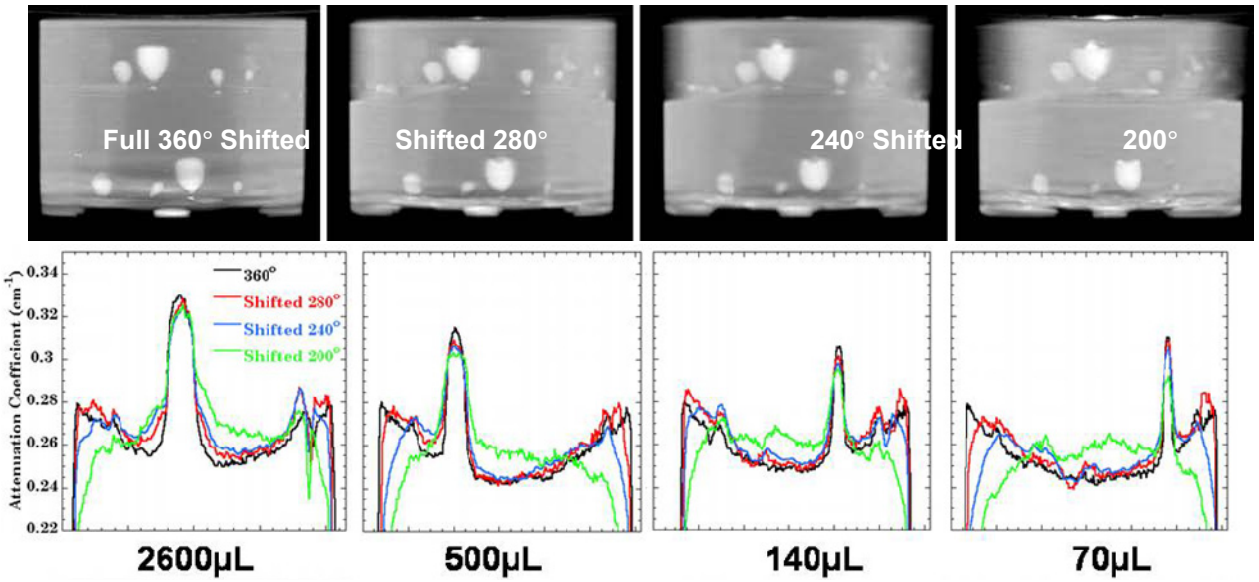

Figure 8 (Upper row) Reconstructed MIP images of balloons in both the upper and lower disks with the full 360° acquisition (upper row, left) contrasted with images reconstructed from shifted data sets. Shifted 280° indicates that 280° of projections have both disks in the FOV with the remaining 80° containing 1 disk. Note the increased distortion in lesion shape in the upper disk as shifting increases. (Lower Row) Single slice profiles of the upper disk of balloon lesions similarly indicate increased distortion.

Figure 8 shows maximum intensity projection (MIP) images of lesions reconstructed using vertical system shifting with the angular range of projections shifted (2 planes in the FOV) noted on each image. Distortion in the upper row of lesions increases with an increase in the number of projections with 1 disk in the FOV while reconstructions of the lower disk have image quality apparently similar to that of the full 360° data set. Reconstructed profiles of each plastic lesion in the upper disk taken from shifted data sets emphasize this trend in increased distortion and a reduction in peak reconstructed attenuation coefficient value. Despite the apparent increase in image distortion, the high contrast lesions are still clearly visible even down to missing 120° of projections of the upper disk indicating the feasibility of implementing this type of 3D motion in the second iteration of the hybrid imaging system. Quantative SNR and contrast results shown in Table 3 again support a trend in reduced image quality as projections are increasingly removed.

Table 3 SNR and contrast metrics calculated for the upper disk of balloon lesions from the CmT images using a full 360° data acquisition and 3D trajectories where the CmT sub-system is vertically shifted.

	SNR		Contrast	
Lesion Size	2.6mL	140uL	**2.6mL**	**140uL**
Full 360°	38.53	19.46	0.29	0.17
Shifted 280^0	27.36	14.12	0.26	0.15
Shifted 240^0	21.79	11.3	0.24	0.15

An observer study was also carried out to investigate the effects of using limited angle tomography and the 3D vertically shifted trajectories on the detectability of low-contrast 5mm acrylic lesions in water. The extensive details of the methodology and results are included in manuscripts in the Appendix. The various limited angle and shifted data sets were reconstructed and shown to 5 observers who were asked to indicate the quality of the reconstructed images and to also note the number of spheres detectible under the various conditions.

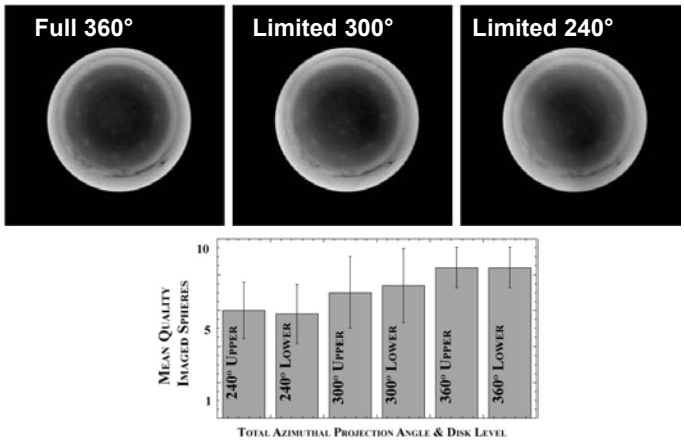

Figure 9 (Upper row) Coronal images of the observer study disk phantom using limited angle tomography with 360° and limited 300° and 240° rotations. (Lower row) Results when observers rated the quality of the spheres imaged on the lower and upper disks under these limited angle conditions.

Sample images of reconstructed slices under various conditions of limited angle tomography are illustrated in Figure 9 with one set of observer study results indicated. In general, despite the low contrast environment, using iterative reconstruction techniques it was possible to view essentially the same number of 5mm acrylic spheres in water while missing between 60° and 120° of data.

Additional unlisted tasks completed in Year 1:

Initial Patient Studies using the Common Field of View SPECT-CmT imaging system

Although trial patient imaging studies using the integrated SPECT-CmT system do not form part of the Statement of Work for this pre-doctoral award, the studies, with funding provided by Dr. Tornai's NIH R01 grant, formed part of the cumulative work of the research lab in Year 1. Patient studies are described here to illustrate the system's clinical potential and to demonstrate the valuable practical training that routinely occurs in this research lab.

The results of the patient studies additionally provided a rich vein of quantifiable, observational and anecdotal evidence into many aspects of the imaging system's required clinical performance. This evidence ranged from the ability of the CmT system to image close to the chest wall (see Task 2 and Task 3) to the effectiveness of the current patient bed design (Task 2) in maximizing patient comfort so as to minimize patient motion artifacts. Other vital aspects of the imaging procedure that were tested included enhancing patient positioning, streamlining system preparation and calibration procedures, and optimizing data acquisition methods, all with the ultimate objective of improving both the patient experience and imaging outcomes. Experience with these described patient studies will be used to inform the design of the fully 3D integrated SPECT-CmT system and new patient bed (Task 3).

During Year 1 of this award, two human subjects with biopsy confirmed breast cancer volunteered to be scanned using the dual-modality SPECT-CmT system. All subjects were imaged using a protocol

approved by the institutional review board (IRB) of Duke University Medical Center with informed written consent obtained from the volunteers prior to imaging. A data acquisition sequence protocol, previously generated with input from all members of the research laboratory, was employed. Sections of this work was presented by me and another member of the research lab at the *2008 Duke Cancer Comprehensive Cancer Center annual meeting* and the *2008 AAPM (American Association of Physicists in Medicine) Annual Conference* in addition to other conference venues. The abstracts are attached in the Appendix.

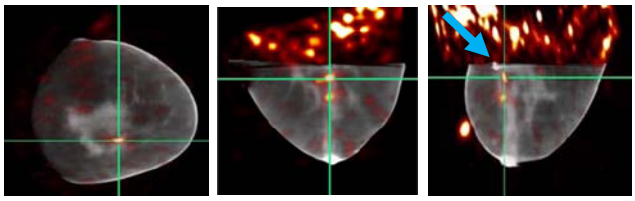

Figure 10 Fused SPECT-CmT reconstructed slices of a breast cancer patient (54 yrs, 96 kg). Green crosshairs indicate radiotracer uptake by a suspect lesion. Above this area is a biopsy clip (blue arrow). Bright area s above breast are radiotracer uptake by heart and liver.

One patient, with biopsy confirmed DCIS anterior to her chest wall, was scanned using both imaging modalities. The subject was injected with 660MBq of ^{99m}Tc-sestamibi prior to scanning and four fiducial markers (in this case nylon balls soaked in ^{99m}Tc acting as dual modality markers) were taped to the surface of the breast at the 3, 6, 9, and 12 o'clock position in a helical fashion to be visible in the CmT image at varying heights and orientations. The initial CmT scan was carried out using an x-ray tube potential of 60 kVp, an exposure per projection of 2.5mAs for 240 equally spaced projections around 360°. These specific x-ray exposure parameters had previously been shown to generate a dose in the patient's breast (modeled as a 15cm thick breast with 50-50% adipose-glandular composition) equivalent to 2/3rd of dual mammography.

A circular trajectory at a fixed height above the horizontal was used along with a fixed source-detector tilt of -6.2° to the vertical. Using a sequential imaging protocol, SPECT imaging was subsequently performed using a 15-45° PROJSINE (three-lobed sinusoid) trajectory, specifically tailored to closely contour the individual patient's breast surface. Such a SPECT system trajectory has been used before in this lab [2-4]. Reconstructed images from the CmT acquisition illuminated the location of the biopsy clip and with reconstructed SPECT images showing signs of ^{99m}Tc-sestamibi uptake beneath the biopsy clip, a lesion in this patient was suspected (Figure 10). This suspicion was confirmed in subsequently viewed MRI images. This dual modality study illustrated the significance and benefits of correlating anatomical information from the CmT images with the functional information from SPECT to localize the position of potential cancerous lesions.

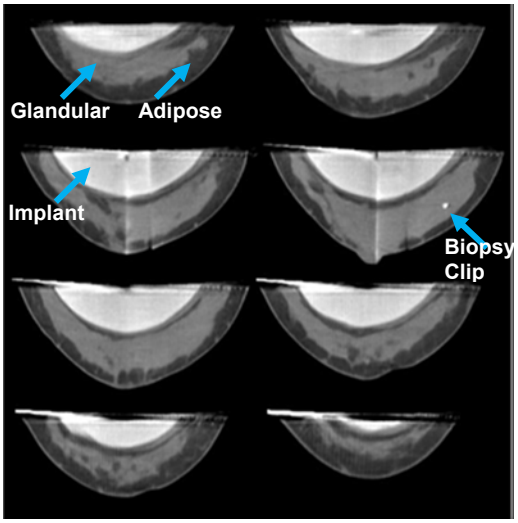

Figure 11 CmT reconstructed sagittal slices of a breast cancer patient (42yrs, 68kg) with implant and biopsy clip and various identified tissues.

A second volunteer subject in Year 1 underwent a single modality imaging procedure using the CmT sub-system of the combined imaging system. Imaging parameters used were a tube potential of 60 kVp with a 2.5mAs exposure per projection for a total of 240 equally-spaced projections in a full 360° rotation. Several reconstructed slices of the acquired breast data are shown in Figure 11. This patient possessed an implant in her breast which can be a difficult imaging task in mammography due to the risk of implant rupture from routine breast compression as well as the possible occlusion of a cancerous lesion in images due to tissue/implant superposition. However, the fully tomographic images demonstrate the ability of

volumetric imaging to effectively differentiate between normal glandular, adipose tissue and the artificial implants.

It is expected that further patient scans will occur in Year 2 of this award.

Development of a C-arm based modification to the initial prototype hybrid imaging system to improve CmT Sub-system Stability

To maximize overall system stability and robustness, the x-ray source and detector in the independent CmT sub-system were coupled to each other through a common base plate. However, to increase design flexibility, the x-ray source and detector were physically decoupled in the initial prototype integrated SPECT-CmT imaging system (see Figure 1). This decoupling increased the likelihood of geometric misalignment between the separated source and detector components and reduced the physical robustness of the system. It was decided to try to restore overall CmT system robustness by re-coupling the x-ray source and detector to a common stage – this was accomplished by the design and development of a c-arm-based plate that connected the source and detector together.

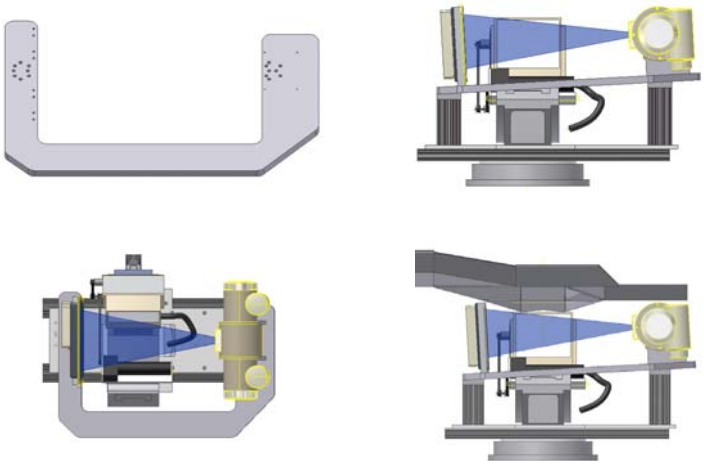

Figure 12 CAD images of the new C-arm (top row, left) from an oblique angle showing the design complete with attachment holes for the various components for the CmT sub-system. The C-arm integrated with the SPECT sub-system from (top row, right) side-on tilted at 3.11° to the horizontal (bottom row, left) top down and (bottom row, right) integrated with the patient bed.

Accurate computer based models of the separate hybrid system components were first designed using Autodesk Inventor (see Task 2(a)). Based on experience gleaned from initial patient studies, modified CmT sub-system design criteria were generated including a reduced source-detector tilt to the horizontal axis (now -3.11° versus -6.20° previously) in order to increase the imaged breast and chest wall volume. The c-arm component was then designed in software and subsequently manufactured to these specifications. The final design (see Figure 12) is made from a 7/8th" thick aluminum plate, strong enough to support the heavy components without deflecting under their weight. The c-arm plate, directly attached to the common base plate of the combined imaging system under both the x-ray source and detector, also helps to dampen vibrations transmitted by the motion of the azimuthal motor as it accelerates in the step-and-shoot mechanism employed by our imaging system. The x-ray detector is firmly attached to a newly designed u-shaped holder that ensures detector stability once screwed into place. A photograph of the modified system as it appears in the laboratory is shown in Figure 13.

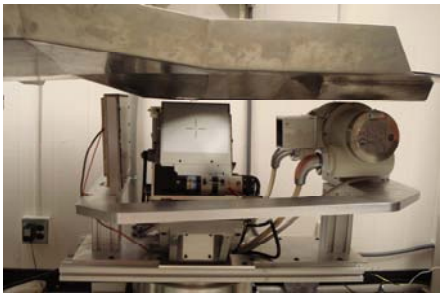

Figure 13 Photograph of the current modified prototype integrated dual modality imaging system showing the integration of the new c-arm plate that couples the x-ray source and detector systems.

The modified hybrid prototype system has not yet been included in patient imaging studies. It is expected that patient trials will recommence during Year 2 and that the closer vertical proximity of both the CmT source and detector to the patient's chest wall will ultimately result in improved volumetric imaging of the breast.

Task 5: Complete other aspects of the breast cancer training program (Months 1-36):

Task 5(a) Shadow a radiologist to observe the clinical and diagnostic side in breast cancer imaging (Nuclear Medicine, Mammography). (Months 1-12)

I arranged to spend a number of hours shadowing staff in the Mammography Clinic of Duke University Medical Center. It was interesting to see the aspects of the clinical breast imaging process: how the patient is cared for from welcoming at the registration desk (for example, an 80-year old woman undergoing dual-view screening mammography of her remaining intact breast seven years after a mastectomy) to completing a medical history to acquiring the mammogram of the ladies breast in both the CC and MLO directions. I additionally observed the back end operation of the clinic: processing of the digital image data onto screen film for backlit displays and also displaying the digital image on monitors for viewing by the radiologists; the resident radiologists reading the patient's various mammograms from this and previous visits to the clinic; how the residents discuss and validate their findings with the attending physician; what the physicians look for in different cases; the radiologists viewing preference (nearly exclusively screen film with a physical magnifying glass); how the radiology team separates roles within the reading room to optimize workflow. I also had the added experience of viewing the digital tomosynthesis research clinic room and viewing data from a recent volunteer subject whose 4-5mm mass was considered indistinct on mammography but was readily apparent in the tomosynthesis image.

In the time between applying for this award and the end of Year 1, I have also observed a new breast cancer screening approach particularly applicable to high risk populations of women using random periareolar fine needle aspiration (rpFNA). In rpFNA, a cellular sample is collected in a random fashion from the entire breast [5]. The protocol involves the volunteer initially lying supine on a table with the breast partially numbed by anesthetic injections before the procedure commences. Both breasts are sequentially interrogated using a needle with several (~9) aspirations taken from approximately the 9 o'clock and 3 o'clock sites of the breast near the nipple surface and areola. While squeezing the breast, the needle is positioned in and moved around the same spot as the anesthetic injection (fulcrum) to collect random samples around the circumference of the breast. Once the sample is collected, the contents of the syringe are transferred to a solution. This procedure is repeated 3 times with separate needles and an additional needle is injected in the outer side to sample fatty cell content. A further four samples are collected from the inner side and transferred to another set of tubes. The procedure takes approximately about 15 minutes per breast. The collected cell count can vary from 5 to more than 5,000 with cells from the different sections of each breast processed separately. Cellular samples are collected in two tubes to test correlation and examine for abnormality. Shadowing this procedure was an extremely interesting experience and it was amazing to witness the volunteer's willingness to undergo this relatively invasive procedure in the hope of uncovering an early stage cancer.

Task 5(b) Prepare and submit research work to peer-reviewed journals

In Year 1, I submitted no manuscripts for peer review – however, a draft manuscript is being reviewed internally within the lab at the time of writing this report and it is expected that this manuscript will be submitted soon to a major international journal in the early part of Year 2. It is expected that several other manuscripts will be submitted to internationally known journals in Year 2.

I was first author on other manuscripts that were published in non-peer reviewed conference proceedings; these manuscripts are included in the Appendix.

I was a co-author on a manuscript submitted by another lab member that has been accepted to the Physics in Medicine and Biology journal.

Task 5(c) Attend and present at local seminars offered at Duke University

After the award had been granted but immediately prior to its commencement, I presented work on the dual modality system at the *2008 Duke Cancer Comprehensive Cancer Center annual meeting* in March 2008. The abstract is attached in the Appendix.

Task 5(d) Attend international conferences such as SPIE Medical Imaging Conference, DOD BCRP Era of Hope Meeting, IEEE Medical Imaging Conference, RSNA Conference, and San Antonio Breast Cancer Symposium. (Months 13-36)

Although not required to do so in Year 1 of the award, I attended and presented my research at the *SPIE Medical Imaging Conference* in Orlando, Florida in February 2008 on the use of novel 3D trajectories to image more of the breast and chest wall. Although unable to attend, my work was also presented my work at the *IEEE Molecular Radiology of Breast Cancer* in November 2008 in Dresden, Germany.

C. Key Research Accomplishments

From the proposed Statement of Work, accomplishments in Year 1 included:

- Task 2 completed.
- Task 3(a) has been initially investigated with new designs currently being developed in software to also complete Task 3(d). It is hoped that these designs will be implemented in Year 2.
- Research was presented at major international and local imaging conferences and manuscripts published in conference proceedings as first author.
- Co-author on a of peer-reviewed paper submitted by another member of this research lab.
- Using a previously designed patient imaging protocol, a number of patient subject volunteers were imaged, providing data for a successful renewal of a major NIH-funded grant.
- A more stable C-arm type connection between the x-ray source and detector was designed and developed for improved imaging system robustness.
- Arrangements to complete Task 1(a) are being made and this should be completed in early part of Year 2.

D. Reportable Outcomes

Peer Reviewed Publications

P Madhav, **DJ Crotty**, RL McKinley and MP Tornai **"**Evaluation of tilted cone-beam CT orbits in the development of a dedicated hybrid mammoTomograph" *Phys. Med. Biol.* **54**:3659-3676. http://stacks.iop.org/PMB/54/3659 and doi:10.1088/0031-9155/54/12/004 .

DJ Crotty, CN Brzymialkiewicz, RL McKinley, MP Tornai. "Quantifying Transmission Source Contamination of the Emission Image in a Comm on Field-of-View Dual Modality SPECT-CT Mammotomography System." In preparation for *Phys. Med. Biol.*

Conference Proceedings

DJ Crotty, SJ Cutler, RL McKinley, P Madhav, KL Perez, MP Tornai. "Improved chest wall imaging through combined complex trajectories in dedicated dual modality SPECT-CT breast molecular

imaging." Presented at *4th International Workshop on the Molecular Radiology of Breast Cancer*, Dresden, Germany, 20-21 October, 2008, and published in *2008 IEEE Nuclear Science Symposium & Medical Imaging Conference Record*, 5650-5665.

DJ Crotty, RL McKinley, P Madhav SJ Cutler, MP Tornai "Initial Investigation of Novel Trajectories to Improve Chest Wall Imaging in a Dedicated Breast Computed Tomography System." Presented at the SPIE Medical Imaging Conference, Orlando Florida, 8-12 February, 2009 and published in the *Proceedings of the SPIE Medical Imaging Conference*.

SJ Cutler, **DJ Crotty**, MP Tornai "Dynamic Laser-Guided Contouring for Dedicated Emission Mammotomography" Presented at the *2008 IEEE Nuclear Science Symposium & Medical Imaging Conference*, Dresden, Germany, 20-21 Oct. 2008 and and published in *2008 IEEE Nuclear Science Symposium & Medical Imaging Conference Record*, 4789-4793..

Abstracts and Presentations

DJ Crotty, P Madhav, SJ Cutler, KL Perez, RL McKinley, MP Tornai, "Performance of a new dual-modality molecular-anatomical imaging system dedicated to breast cancer." Presented at the *2008 Duke Cancer Center Annual Meeting*, Durham, NC, 10 Mar. 2008.

P Madhav, SJ Cutler, **DJ Crotty**, KL Perez, RL McKinley, PK Marcom, TZ Wong, MP Tornai. "Dedicated molecular and anatomical breast imaging - initial patient studies." Presented at the *2008 Duke Cancer Center Annual Meeting*, Durham, NC, 10 Mar. 2008.

P Madhav, SJ Cutler, **DJ Crotty**, KL Perez, RL McKinley, L Wilke, TZ Wong, MP Tornai. "Pilot patient studies using a dedicated dual-modality SPECT-CT system for breast imaging." Presented at the *2008 American Association of Physicists in Medicine Meeting*, Houston, TX, 27-31 Jul. 2008, and published in Med. Phys. 35(6): 2894.

E. Conclusion

Progress has been made in Year 1 towards the stated goals of the award. A new patient bed is now integrated with the imaging system and novel feasible 3D trajectories were investigated that may be solutions for overcoming the physical limitations of the bed design and may allow increased imaging of the patient's breast and chest wall. Year 2 should see many more advancements including a new imaging system that permits fully 3D movement of the CmT system and empirical characterization of the dose delivered to a pendant breast using our device. Manuscripts will be submitted for peer review in international journals and progress will also be made in learning more about breast cancer and leading methods for its detection and treatment.

F. References

[1] D. J. Crotty, C. N. Brzymialkiewicz, R. L. McKinley, and M. P. Tornai, "Investigation of emission contamination in the transmission image of a dual modality computed mammotomography system," *Proc SPIE: Phys Med Imag,* vol. 6142, pp. 664-674, 11-17 Feb. 2006 2006.

[2] S. J. Cutler, K. L. Perez, P. Madhav, and M. P. Tornai, "Comparison of 2D scintimammography and 3D dedicated breast SPECT using a compressible breast phantom and lesions of varying size and tracer uptake," in *Nuclear Science Symposium Conference Record, 2008. NSS '08. IEEE*, 2008, pp. 5640-5646.

[3] P. Madhav, S. J. Cutler, K. L. Perez, D. J. Crotty, R. L. McKinley, T. Z. Wong, and M. P. Tornai, "Initial patient study with dedicated dual-modality SPECT-CT mammotomography," in *2007 IEEE Nucl Sci Symp & Med Imag Conf*, Honolulu, HI, USA, 2007, pp. 3781-7.

[4] K. L. Perez, S. J. Cutler, P. Madhav, and M. P. Tornai, "Novel patient optimized acquisition trajectories for dedicated breast SPECT imaging," in *Nuclear Science Symposium Conference Record, 2008. NSS '08. IEEE*, 2008, pp. 5629-5634.

[5] C. J. Fabian, B. F. Kimler, C. M. Zalles, J. R. Klemp, S. Kamel, S. Zeiger, and M. S. Mayo, "Short-Term Breast Cancer Prediction by Random Periareolar Fine-Needle Aspiration Cytology and the Gail Risk Model," *J. Natl. Cancer Inst.,* vol. 92, pp. 1217-1227, 2000.

Appendix A

Statement of Work

Task 1: Optimize tradeoffs between absorbed dose and image quality for the CmT subsystem (Months 1-6):
a. Embed thermoluminescent dosimeters or available MOSFET detectors in anthropomorphic breast phantoms to evaluate dose for various sizes and compositions of breast equivalent tissue and lesions (Months 1-6).
b. Use quantitative measures of image quality such as SNR, contrast, dose efficiency, and attenuation coefficient accuracy to correlate trends in image quality as a function of measured dose to the breast (Months 1-6).
c. Qualitative metrics to describe observable artifacts will also be used to assess trends in image quality with absorbed dose (Months 1-6).

Task 2: Investigate the effect on image quality of the limited 3-D motion of the current prototype dual modality imaging system (Months 4-10):
a. Integrate the existing prototype dual-modality imaging system with the new custom designed patient bed system (Month 4);
b. Use various geometric and anthropomorphic breast phantoms with embedded lesions to quantify standard image quality metrics from images reconstructed using limited tomographic acquisition for both SPECT and CmT. Objective measures of image quality described in Task 1 will again be used to assess the performance of the system (Months 4-10);

Task 3: Implement synchronized 3-D positioning and data acquisition for the prototype dual-modality imaging system (Months 10-22):
a. Design and manufacture a new physical gantry for the CmT system that supports full 3-D motion (Months 10-16);
b. Modify existing software programs to fully synchronize the 3-D motion and data acquisition of both the SPECT and CmT subsystems. (Months 10-22);
c. Design and manufacture a new comfortable radio-opaque patient bed to allow full 3-D motion of both imaging subsystems positioned below the bed (Months 10-16);
d. Integrate the new CmT positioning system with the existing SPECT subsystem (Month 16);
e. Quantify the effects of this improved 3-D positioning capability on image quality metrics equivalent to those outlined in Task 2 (Months 17-22).

Task 4: Evaluate and Compare performance of the fully 3-D SPECT-CmT system to Mammography and Scintimammography (Months 23-36):
a. Utilize an available breast phantoms containing various dual modality lesions to acquire 2-D planar data under varying compressions for scintimammography and mammography as well as uncompressed breast 3-D dual-modality tomographic imaging (Months 23-29)
b. Conduct an observer study to compare mammography and scintimammography with dual-modality imaging for smallest lesion detectability in reconstructed images of breast phantoms under various operating parameters (Months 30-36).

Task 5: Complete other aspects of the breast cancer training program (Months 1-36):
a. Shadow a radiologist(s) to observe the clinical and diagnostic side in breast cancer imaging (Nuclear Medicine, Mammography). (Months 1-12);
b. Prepare and submit research work to peer-reviewed journals. (Months 1-36);
c. Attend and present at local seminars offered at Duke University through Medical Physics and the Breast and Ovarian Oncology Research Program. (Months 13-36);
d. Attend international conferences such as SPIE Medical Imaging Conference, DOD BCRP Era of Hope Meeting, IEEE Medical Imaging Conference, RSNA Conference, and San Antonio Breast Cancer Symposium. (Months 13-36);
e. Prepare thesis and defend. (Months 30-36).

Appendix B

DUKE COMPREHENSIVE CANCER CENTER ABSTRACT

Performance of a New Dual-Modality Molecular-Anatomical Imaging System Dedicated to Breast Imaging

DJ Crotty, P Madhav, SJ Cutler, KL Perez, RL McKinley, MP Tornai

Dual modality information acquired by combined molecular (SPECT) and anatomical (x-ray CT) 3D systems dedicated to breast cancer imaging offer great promise in the detection and characterization of primary, recurrent and occult cancers, and the monitoring of therapies. X-ray CT images provide structure while function is assessed by observing ^{99m}Tc-sestamibi uptake of the tumors in the SPECT images. Independent SPECT and CT imaging systems, separately developed in our lab, were integrated onto a combined gantry with a common field-of-view. This hybrid system is expected to further enhance the visual and quantitative information over standalone systems, as well as potentially decreasing total patient imaging time. The SPECT sub-system permits fully 3D complex acquisition trajectories around the uncompressed breast to overcome distortions due to inadequate sampling, and allow detection of lesions on the chest wall. The cone-beam CT sub-system implements a unique quasi-monochromatic x-ray beam to reduce breast radiation dose as compared to standard mammography and to improve soft tissue image contrast. Here, we describe the capabilities of the prototype SPECT-CT system, complete with a novel custom-designed patient bed. Data sampling, resolution and image fusion are demonstrated with geometric and anthropomorphic breast phantom measurements using fiducial markers. Initial results indicate clear potential for improved lesion visualization and patient studies have recently commenced.

Appendix C - AAPM ABSTRACT

interchangeably. **Conclusion:** The comparison of the normalized $IAUC_{60}$ showed that both DCE-CT and -MR imaging modalities may be used interchangeably in assessing cervical cancers. The normalized $IAUC_{60}$ may be considered as a reliable quantitative surrogate of the normalized transfer constant for both modalities.

TU-C-332-02

Concomitant Segmentation and Registration of Liver Anatomy Using SPECT-CT Imaging

T Fox*, E Schreibmann, I Crocker, Emory UniversitySchool of Medicine, Atlanta, GA

Purpose: To develop an automatic and accurate technique for concomitant segmentations and registration of liver anatomy using SPECT and CT images for unsealed source radiotherapy. **Method and Materials**: The link between segmentation and registration is given by the using the level set of a liver segmentation into the registration process. In the combined approach, the liver is automatically segmented from the CT image by evolving an initial seed with a level set until it locks to the liver's border as observed in the CT images. The time-crossing map of the level set is then used to match gradients in the SPECT image to the level set by using a data structure containing the signed distance values at a small band of neighboring pixels. **Results:** The technique was applied to three cases of metastatic liver disease treated with unsealed source therapy. Results indicated that the speed map of the level set plays an importance role in obtainng an accurate registration and produce a segmentation that is superior in registration time and accuracy over manual segmentation or the standard registration approach using mutual information. Accuracy measured with the convergence analysis method was of less than 0.5 mm rotation and 1 degree rotation. **Conclusion:** With the proposed combined segmentation-registration technique, the uncertainty of soft-tissue target localization could be greatly reduced ensuring accurate therapy assessment to be precisely delivered as planned. The combined all-in-one approach is automated and provides excellent accuracy over manual segmentation and mutual information approaches.

TU-C-332-03

Automatic Definition of Radiation Targets Using Textural Characteristics of Both Co-Registered PET and CT Images

C Caldwell[1], K Mah[2], H Yu[3]*, (1), Odette Cancer Centre at Sunnybrook Health Science Center, ON, CA, (2) Toronto Sunnybrook Cancer Ctr, Toronto, ON, CA, (3) Univeristy of Toronto, Toronto, ON, CA

Purpose: To automatically segment the radiation target for treatment of head and neck cancer (HNC) from FDG-PET/CT images using a textural classifier and to compare the automated results with contours defined by expert observers. **Method and Materials**: 27 image features, including textural features from Spatial Gray-Level Dependence Matrices and Neighborhood Gray-Tone-Difference Matrices, as well as statistical and structural features were calculated for 476 head and neck regions of interest (ROIs) in PET/CT images of 20 patients with HNC and 20 patients with lung cancer. A voxel based automated segmentation method using a Decision Tree (DT) based K nearest neighbors (KNN) classifier was developed based on the features in these ROIs. PET/CT images of another 10 head and neck patients who had all primary tumors and positive nodes manually segmented by three radiation oncologists were used to evaluate the method. Features were calculated for each voxel from corresponding PET and CT images within a window centered on the voxel. All voxels of head and neck soft tissues from the below the eye to the apex of the lung were automatically segmented. **Results**: The specificity was 95% ± 2% when all "true negative" voxels were considered to be all soft tissue voxels excluding the ROIs considered abnormal by one or more of three radiation oncologists. Sensitivity was 84% ± 19% when "true positive" was considered the intersection of at least two physicians' abnormal ROIs and sensitivity was 90% ± 16% when all "true positive" was the intersection of the abnormal ROIs of all three physicians. **Conclusion:** This work suggests that an automated segmentation method based on texture classification of FDG-PET/CT images has potential to provide accurate delineation of HNC. This could potentially lead to reduction in inter-observer variability in target delineation and improved accuracy of treatment delivery.

TU-C-332-04

Pilot Patient Studies Using a Dedicated Dual-Modality SPECT-CT System for Breast Imaging

P Madhav*, S Cutler, D Crotty, K Perez, R McKinley, P Marcom, T Wong, M Tornai, Duke University Medical Center, Durham, NC

Purpose: Acknowledging the limitations/discomfort of mammography has inspired the development of a dedicated SPECT-CT system to detect breast cancer, monitor therapeutic responses, and improve patient comfort. This system provides semi-quantitative 3D functional/anatomical imaging of a pendant, uncompressed breast. Fused images can potentially provide more valuable clinical information than independent systems alone. **Method and Materials:** The SPECT subsystem permits fully-3D complex acquisition trajectories around the breast, avoiding physical hindrances, overcoming distortions due to inadequate sampling, and allowing lesion detection on the chest wall. The CT subsystem, restricted to circular rotation, uses a quasi-monochromatic, cone-beam x-ray source, which allows for reduced radiation dose and increased contrast between similar soft tissue attenuation coefficients. With no breast compression and an open, common field-of-view geometry system, the patient lies prone on a customized patient bed while the hybrid device non-invasively acquires 3D data underneath. A preliminary investigation on the clinical performance of the hybrid system was done by imaging women with biopsy confirmed breast cancer **Results:** SPECT patient images can clearly visualize the tracer uptake by the tumor and view into the chest wall. Physical system constraints limit chest wall visualization in the CT patient images and thus patient positioning is under modification. Eliminating overlapping tissues through 3D imaging, the CT images improve lesion isolation versus 2D imaging modalities. Complementary functional and anatomical image information helps localize suspicious areas for subsequent analysis. **Conclusion:** Implementation of the world's first dedicated SPECT-CT system promises greatly improved visualization of the 3D breast volume. Complementary information from functional and anatomical imaging can guide lesion localization for subsequent analysis. **Conflict of Interest:** MPT is an inventor of this technology, and is named as an inventor on the patent for this technology applied for by Duke. If this technology becomes commercially successful, he and Duke could benefit financially.

TU-C-332-05

Simulation of Ultrasound Two-Dimensional Array Transducers Using a Frequency Domain Model

M Rao*, T Varghese, J Zagzebski, University of Wisconsin-Madison, Madison, WI

Purpose: Ultrasound imaging with two-dimensional (2D) arrays has garnered broad interest from scanner manufacturers and researchers for real time three-dimensional (3D) imaging. Previously we described a frequency domain B-mode imaging model applicable for linear and phased array transducers. In this study, we extend this model to incorporate 2D array transducers. **Method and Materials:** The pressure field for a 64×64 square array with element dimension of 0.15 mm and center-to-center spacing of 0.2 mm was calculated by applying the paraxial approximation to solve the 2D Rayleigh integral. We assume a rigid baffle, no apodization, a 2.5 MHz center frequency, and a speed of sound of 1540 m/s. A single transmit focus at 30 mm and dynamic receive focus with an F-number of 2 was utilized. The 2D array model is compared with the widely used ultrasound simulation program FIELD II, which utilizes an approximate form of the time domain impulse response function. **Results:** Discrepancies between waveforms computed using our model and FIELD II are less than 4%, regardless of the steering angle for distances greater than 2 cm, yet computation times are on the order of 1/35 of those using FIELD II. Modern beam-forming techniques such as apodization, dynamic aperture, dynamic receive focusing and 3D beam steering can also be simulated. The simulated beam patterns and point spread function images allow evaluation of beam properties for specific transducer parameters. Simulations of B-mode images provide vivid demonstrations of the ability of 2D arrays with specific imaging parameters to detect lesions of a given backscatter contrast and size. **Conclusion:** The frequency domain approach provides an effective and feasible tool to model transmitted and pulse-echo fields as well as B-mode images for 2D array transducers.

Appendix D

2008 IEEE NUCLEAR SCIENCE AND MEDICAL IMAGING CONFERENCE RECORD

Improved Chest Wall Imaging through Combined Complex Trajectories in Dedicated Dual Modality SPECT-CT Breast Molecular Imaging

Dominic J. Crotty, Spencer J. Cutler *Student Member, IEEE,* Randolph L. McKinley, *Member, IEEE,* Priti Madhav *Student Member, IEEE,* Kristy L. Perez, *Student Member, IEEE,* Martin P. Tornai, *Senior Member, IEEE*

***Abstract*–In the hybrid SPECT-CT breast imaging system currently in development in our lab, patient positioning is a practical compromise between comfort and a need to maximize the imaged volume of breast and chest wall. The integrated imaging system rotates under the patient, with the current CT system restricted to purely azimuthal trajectories at a fixed height, while the flexible SPECT system is capable of fully 3D positioning around the pendant breast. The current patient bed, designed with the aforementioned compromises in mind, separates the top of the CT cone beam from the chest wall, thus limiting the system's ability to image this important area. This study examines combined complex trajectories, including limited angle tomography for both modalities and raising the entire imaging system during the scan, to more effectively image lesions in or near the chest wall. While emphasizing new CT system trajectories, SPECT trajectories are also investigated to maximize the imaged volume while avoiding contact with the bed or patient. Various sized lesions filled with low and medium concentrations of ^{99m}Tc activity (10:1 to 3:1) and CT contrast are imaged using different trajectories. Dual modality projections are post-processed to mimic limited angle trajectories or trajectories that raise the CT system for a portion of the scan. Reconstructed images from data sets with trajectories that removed 60° of SPECT and CT azimuthal data and trajectories combining limited angle acquisition with vertical system shift show a significant increase in observed breast volume while maintaining lesion visibility. Two task-based observer studies are used to further evaluate the visibility of small low-contrast lesions reconstructed with decreasing angular acquisitions and system shifting. Observer study results further indicate that limited angle trajectories and system shifting in mid-scan appear to improve chest wall imaging for this dual modality system.**

I. Introduction

Our lab has developed a prototype dedicated dual-modality breast molecular imaging system, integrating independent single photon emission computed tomography (SPECT) and cone beam x-ray CT sub-systems onto a common mechanical gantry. The standard imaging technique calls for the patient to lie prone with her uncompressed breast hanging pendant through a hole in the bed. The hybrid imaging system rotates under the patient acquiring data, with the CT system restricted to purely azimuthal trajectories at a fixed height, while the versatile SPECT system is capable of fully 3D positioning around the pendant breast using simple circular or complex non-circular 3D trajectories [1-5].

For prone patient imaging, the design of the patient bed is a vital component of the overall system and a key determinant of its ultimate utility in the clinic. The design must satisfy often competing demands of ensuring patient comfort while positioning the patient in such a way as to gain access to and maximize the imaged volume of the breast and anterior chest wall. The current patient bed design, constrained by these competing demands, falls short of these requirements. Experience with initial patient imaging trials has shown that a combination of challenges in effective patient positioning, imaging dead zones inherent to the components of the CT sub-system and bed manufacturing tolerances ensure that the top plane of the CT cone beam is practically separated from the chest wall [5-9].

This study details efforts to obtain vital views through the patient's chest wall by using novel x-ray source-detector trajectories to circumvent the current positioning limitations of the prototype system. The 3D hemispherical positioning flexibility of the SPECT sub-system ensures that the gamma camera will practicably avoid all physical impediments and contour the pendant breast, ensuring visualization of molecular imaging information inside the patient's chest wall [10]. The emphasis of this study is then on investigating novel trajectories to allow the less flexible CT system to better image the complete breast and chest wall area.

The feasibility of two potential solutions are examined: Limited angle tomography, i.e. using incomplete (< 360°) trajectories to acquire projections, and vertically raising the imaging system mid-acquisition for a portion of the azimuthal rotation to enable direct viewing of the chest wall.

Limited angle techniques are employed in digital tomosynthesis with promising results for breast imaging [11]. In addition, standard helical CT techniques acquire continuous data while the patient bed, not the imaging system, translates at a constant speed through the gantry, similar to our concept of shifting the system with the patient bed stationary [12]. As far as we are aware, this is the first reported attempt in dedicated breast computed tomography imaging to investigate shifting or raising the entire imaging system mid-acquisition to specifically visualize lesions near the chest wall.

II. Materials and Methods

In the prototype compact dual-modality system (Fig. 1), both the SPECT and CT sub-systems are secured to a common rotation stage capable of 360° azimuthal rotation around the vertical axis of the breast (model RV350CCHL, *Newport*

Corp., Irvine, CA). The SPECT sub-system is positioned orthogonal to the x-ray source-detector axis.

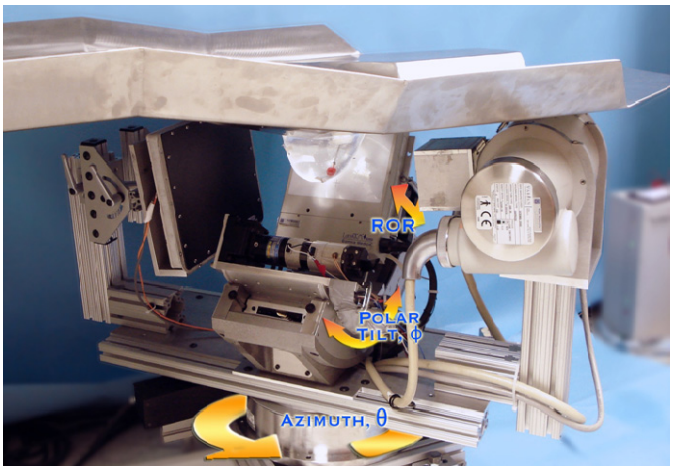

Fig. 1 The initial prototype SPECT-CT system rotating underneath the tiered patient bed. An anthropomorphic breast phantom hangs pendant in the FOV, closely contoured by the flexible SPECT system with noted degrees of freedom of movement. This image illustrates the problem of limited angle tomography with the wide x-ray tube having rotated as far as possible before impacting the lowered head section.

A. SPECT Sub-System

The main component of the SPECT sub-system is a compact 16x20cm^2 field of view Cadmium-Zinc-Telluride (CZT) gamma camera (model *LumaGEM* 3200S, *Gamma Medica, Inc.*, Northridge, CA) with discretized crystals, each 2.3x2.3x5mm^3 on a 2.5mm pitch. The measured mean energy resolution of the gamma camera at 140keV is 6.7% FWHM (full-width-half-maximum) and collimator sensitivity is 37.9 cps/MBq. The camera system includes a parallel-hole collimator with hexagonal holes (a 1.2mm hole size flat-to-flat (inner diameter), 0.2mm septa, and 25.4mm height) and is attached to a laboratory jack (model M-EL120, *Newport Corp.*, Irvine, CA) and goniometric cradle (model BGM200PE, *Newport Corp.*, Irvine, CA) permitting various radii of rotation (RORs – up to 10cm translation range from the initial position) and polar tilt angles (0° to 90°). With this flexible gantry, the camera can be positioned anywhere in a hemisphere to contour and acquire projection data around a pendant, uncompressed breast. Using this flexibility, the small, high performance camera dedicated to breast imaging [13] can easily tailor its trajectories in response to a change in relative positioning of the patient and the imaging system [1, 9, 10, 14-17]. The SPECT reconstruction uses a statistically iterative ordered subset expectation maximization algorithm that accounts for the azimuthal and polar angles of the system trajectory.

B. CT Sub-System

The CT sub-system consists of a rotating tungsten target cone-beam x-ray source (model Rad-94, 0.4mm focal size, 14° anode angle, *Varian Medical Systems*, Salt Lake City, UT) and CsI(T1)-based amorphous silicon digital x-ray detector (model *Paxscan* 2520, *Varian Medical Systems*, Salt Lake City, UT) with a grid size of 1920x1536 and 127μm pixels. The source and detector are secured to a metal plate underneath the SPECT goniometer which is then attached to the azimuthal rotation stage. A Ce 100th attenuating value layer (0.0508cm, calculated at 60kVp) filter (Z=58, ρ=6.77g/cm^3, K-edge=40.4keV, *Santoku America, Inc.*, Tolleson, AZ) was used to yield a mean energy of ~36keV and FWHM of 15%. Such a quasi-monochromatic x-ray source can (1) improve the visualization of tissues with very small differences in attenuation coefficients; (2) lower the x-ray dose for equivalent image quality to mammography; and (3) minimize beam hardening [3, 18, 19]. For these studies, a 60cm source-to-image distance (SID) was used with a magnification of 1.57 for an object located at the system's center of rotation. Unlike the SPECT sub-system, the current CT sub-system is restricted to simple circular motion at a 6.25° fixed tilt. A statistically iterative ordered subset transmission reconstruction algorithm can accommodate system shifting through modification of a user-defined orbit file that is read into the reconstruction algorithm.

C. Patient Bed System

A customized patient bed was designed, in addition to other considerations, to provide patient comfort while enabling the maximum volume of breast to be imaged (Fig. 1). Composed of ⅛" thick stainless steel, the bed is lined with thin layers of lead, neoprene, and polyurethane to protect the patient from errant radiation, enhance comfort during the scan and provide support for the prone patient. The design process is detailed elsewhere [6, 7] and the resultant tiered design (including an octagonal torso section and angled waist and head sections, with the head section at the lowest height of all the sections in the design) both supports and allows the patient to suspend her chest into the common system FOV. With the circular trajectory at a fixed polar tilt, it is the head section that is the main obstacle restricting the angular range of the CT system (see Fig. 2). The octagonal torso section, positioned over the FOV, allows the system to rotate underneath, and a removable insert allows for radiolucent materials to enable imaging up to and, ideally, through the chest wall.

The bed is attached to a positioning system (model 830-058, *Biodex Medical Systems*, Shirley, NY) which has five degrees of movement to aid in extending maximal subject breast volume into the FOV and to negate bowing in the cantilevered bed due to the weight of the subject.

D. Dual-Modality Imaging

Fig. 3 shows the phantom used in the dual modality SPECT-CT experiments. Each phantom consists of 4 thin walled balloon lesions (*Harvard Appartus Inc.*, Holliston, MA), 2600, 500, 140 and 70μL arranged on the same radius circle at 90° intervals. Attached to an acrylic ring, two such disks were stacked, vertically separated by ~1.5" (Fig. 3), placed in a water-filled cylinder (to mimic dense breast tissue) and suspended in the common FOV of the imaging system. For dual mode scanning, the lesions were filled with a mixture

of CT contrast (1:60 Iodine:water concentration) and activity-filled water (40µL/mCi ^{99m}Tc).

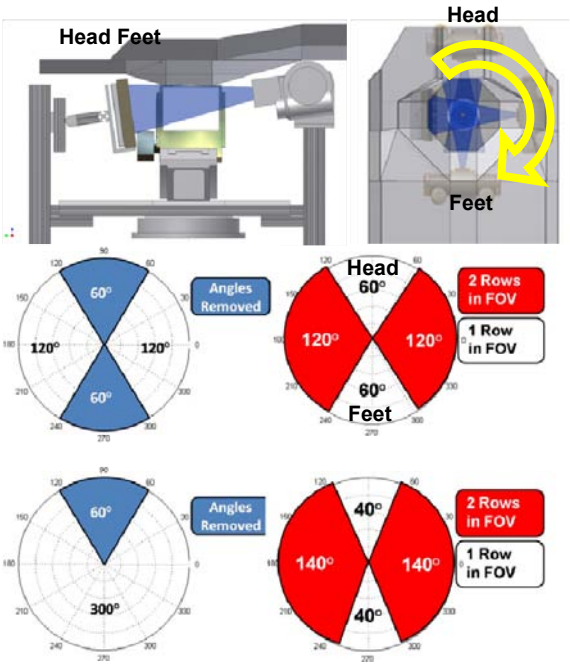

Fig. 2 Illustrations of the patient bed and system from side (top, left) and top-down viewpoints (top, right) showing orientation of the system as the system rotates around the breast. A subset of post-processed limited angle (middle and bottom,left) and system shifted (middle and bottom, right) trajectories are also shown. Polar plots show what projection angles are removed or how system shifted data sets are created.

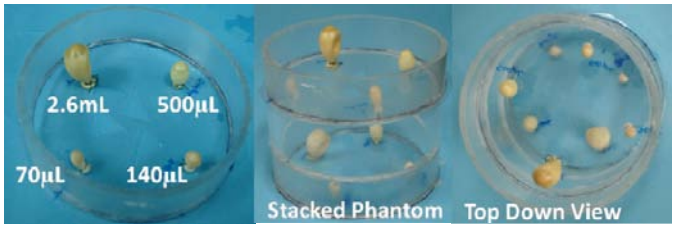

Fig. 3 Images of the dual modality, thin-walled balloon phantom (left) with the noted different-sized lesions.

Three lesion:background concentrations were employed for SPECT imaging: inifinity:1, 10:1 and 3:1 with the ratio modified by adding activity to the water background. Two trajectories were used for contoured SPECT imaging: a three-lobed sinewave projected onto the hemispherical surface (projsine), and a simple vertical axis of rotation (VAOR) [14].

For CT imaging, 2 separate complete tomographic data sets were acquired. The first scan acquired data with only one (the lower) disk in the system FOV for 360 projections at 1° intervals, acquired at 60kVp, 100mA, 2.5mAs per projection (see Fig. 6). The disk phantom was then lowered approximately 2.5cm and a follow up 360° data set acquired with both disks in the FOV. The *Biodex* bed lowered the phantom within the common system FOV.

The CT data sets were post-processed to mimic both limited angle and shifted data sets. Limited angled data sets were created by simply removing projections in contiguous sectors from desired positions around the phantom (Fig. 2). Vertically shifted data sets were created by concatenating projections in specific angle sectors from the first data with projections from the second data set that had both disks visible (Fig.2). In that way, a variety of data sets were created to model the limits of the current equipment in the lab but could also model future x-ray source, detector and patient bed components.

E. Low-Contrast Observer Study

The ability to detect 5mm low-contrast spherical-shaped acrylic lesions in water using system shifting and limited angle tomography techniques was evaluated through an observer study. Two sets of data were used: data collected using a new circular disk phantom and a previously acquired data set using a similar type of resolution sphere phantom [3].

The circular disk phantom (Fig. 4) consisted of concentric circles of 5mm acrylic spheres spaced at 45° intervals around a disk. Two such disks were separated by approximately 3cm and stacked in a water-filled cylinder yielding a low contrast imaging task (~1% intrinsic contrast at 35keV). Similar to the dual modality data, an initial scan of one disk was acquired with a subsequent scan collecting data with both disks in the FOV. Projection sets were post-processed as described above to simulate limited tomography or system-shifted data.

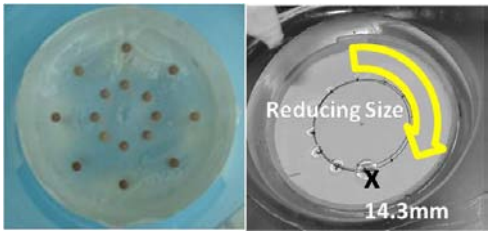

Fig. 4 The circular disk phantom (left) with 5mm acrylic spheres separated at regular 45° intervals, and (right) the phantom consisting of acrylic spheres of continually decreasing size (14.3 – 1mm) arranged on a single circle.

Additionally, a phantom consisting of acrylic spheres of varying size (14.3 to 1mm) equidistant from the center of a circle was used (Fig. 4, right). In this case, a full 360° of data was acquired using 240 equally-spaced projections at 60kVp, 100mA and 25ms per projection. With only one plane of spheres, this data set was only used to probe the feasibility of limited tomographic data acquisitions.

5 observers were asked to assess 58 images. The first task used the previously acquired data set to investigate the effect of limited angle tomography on spheres of different sizes. Initially, contiguous 60° sectors were removed from the projection data set. The data set was then reconstructed missing these sectors of projections and resulting reconstructed images were shown to the observers who were tasked with recording the number of detected spheres. The task was repeated using images reconstructed from data sets that had 120° of angles removed from various sectors.

The second observer task considered the effect of using various system shifts and/or limited angle data acquisition on the detectability of very low contrast spheres in the circular disk phantom. Observers were asked to note the number of

visible spheres from each of the two planes of the reconstructed phantom data, and the objective quality (on a 1 to 10 scale, 10 being best) of the images of the spheres. Three scenarios probed potential solutions to enable increased access to the chest wall: Vertically raising the system only at the head section of the bed for 60° or 120° (Case #1); Raising the system at both head and feet for 60° or 120° each (Case #2); A combination of the first two cases where the bed is raised while traversing 60° or 120° azimuthally either at the head or feet, and a partial angle of 60° and 120° of projection data is removed completely from the other end (Case #3). Observers were also asked to rate the overall image quality on a 1-10 scale given the different reconstruction conditions.

III. Results

A. SPECT Imaging

Reconstructed images from the SPECT study using a projsine trajectory are shown in Fig. 5, using full 360°, 280° and 240° data sets. Images are shown for lesion:background activity ratios of infinity, 10:1 and 3:1. Image quality degrades as the activity ratio and the angular range of projections is reduced, with distortion visible closer to the edge of the cylinder for 280° and 240° of views (yellow arrows, Fig. 5) especially for the 3:1 data set. However profiles (yellow lines) of the 2600μL lesions indicate that lesions remain discernable, confirming conclusions found in preliminary studies concerning limited tomography using the SPECT system [8].

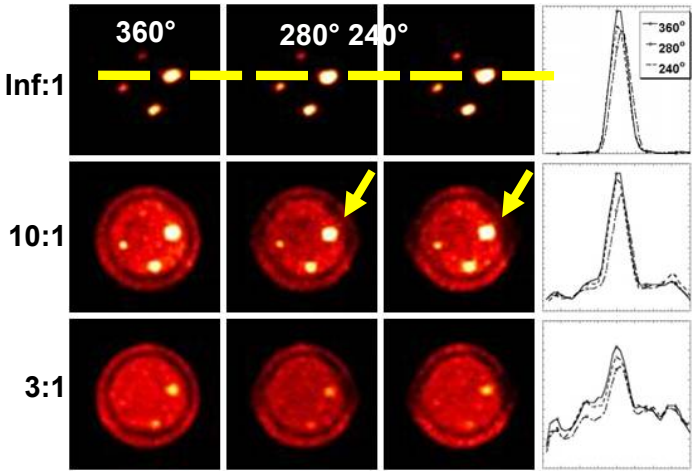

Fig.5 Coronal images of the lower plane of lesions for different activity ratios. Images are divided into 360° data set (left col.), 280° (middle col.) and 240° (right col.). Profiles through the largest lesion are also shown (far right). Note, the distortion towards the edges of the reconstructed cylinder images as the number of angular views is reduced.

B. CT Imaging

Fig. 6 shows sample projections of the imaged phantom with a single (top) and both (bottom) planes in the FOV. CAD drawings accompany the projection views to illustrate the set up for the projections.

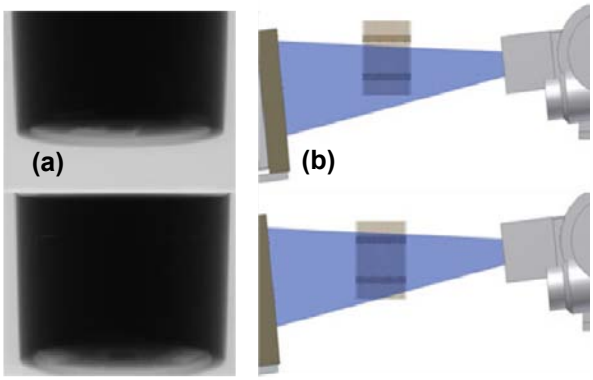

Fig. 6 (a) Sample projection images of the phantom with only the lower disk (top) and both planes (bottom) in the FOV. (b) CAD drawings illustrating the cone beam (blue) emanating from the x-ray tube (right) with one and both layers in the FOV of the detector (left).

Fig. 7 shows maximum intensity projection (MIP) images of lesions reconstructed using both system shifting and partial or limited angle methods with the angular range of projections either shifted (2 planes in the FOV) or removed noted on each image. The fully sampled data set is also shown for comparison. This full 360° reconstruction (16 subsets, 10 iterations) is taken as the standard against which the quality of images reconstructed using partial angle and system shifting methods are compared. Increasing distortion is evident in the images as the number of omitted projections is increased. This is especially evident for the shifted data sets, where the upper plane of lesions is sampled in the FOV for only a subset of the total projection range; the lower plane is always in the FOV and yields reconstructions with apparent image quality similar to that of the full 360° data set. In addition, smaller lesions become harder to visualize as more projections are removed from the full 360°. Separate profiles, taken from both shifted and limited angle reconstructions, of each lesion in the upper plane are shown in Fig. 8 emphasize the trend in increased distortion and a reduction in peak reconstructed attenuation coefficient value. Lower plane phantom lesions in the shifted data sets retain their shape since they are fully sampled around the full 360° but distortion increases in the lower plane of lesions similar to the upper plane since sampling of both planes is reduced as angles are removed. Similar distortion findings are seen in coronal images of the phantom (not shown).

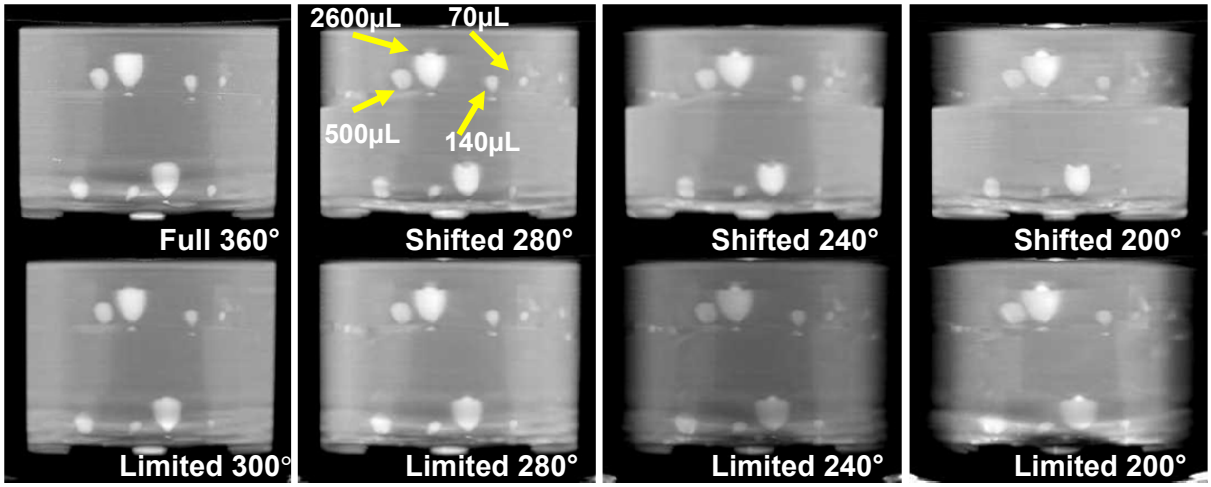

Fig. 7 Transverse MIP images of the cylindrical phantom showing the upper and lower planes of balloons with the full 360°in the FOV acquisition (top row, left) contrasted with images from shifted and limited data sets (lower row of images). Note the increased distortion in lesion shape and towards the edges of the cylinder as projections are increasingly removed.

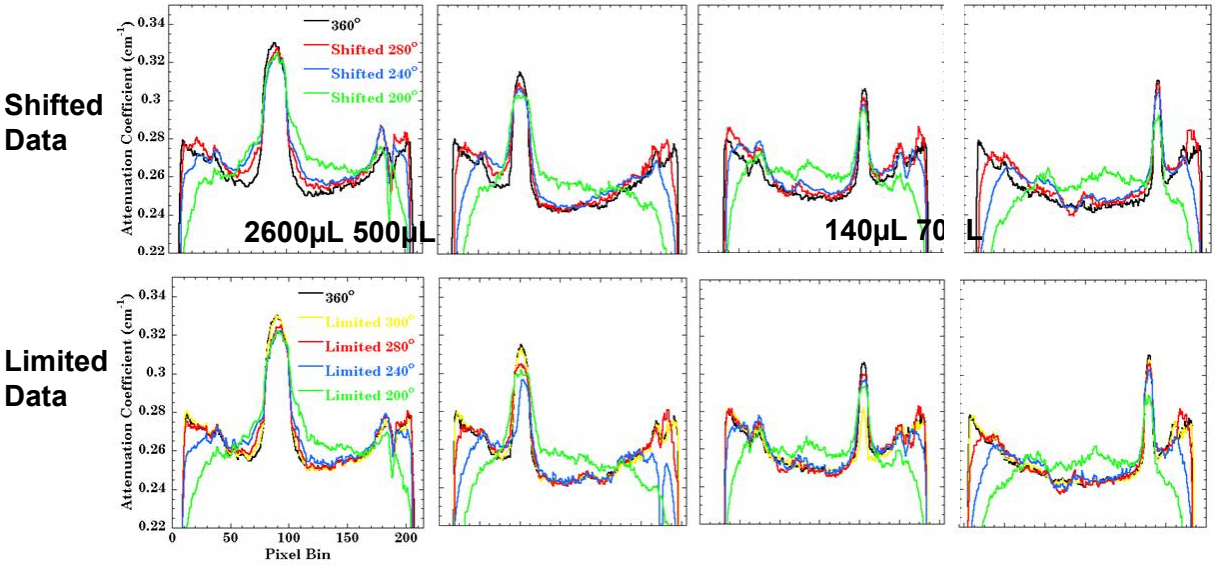

Fig. 8 Separate profiles through the four lesions on the upper plane of the phantom (2600µL to 70µL from left to right) for shifted data sets (top images) and limited angle data sets (bottom images). Note, the increased distortion in the profiles towards the edges as projections are increasingly removed while the peak values for the lesions are maintained..

C. *Fused Data*

Fig. 9 shows reconstructed (left) SPECT and (middle) CT images reconstructed from data acquired using a full 360° of rotation. On the right is an image formed from the fusion of both data sets showing good agreement.

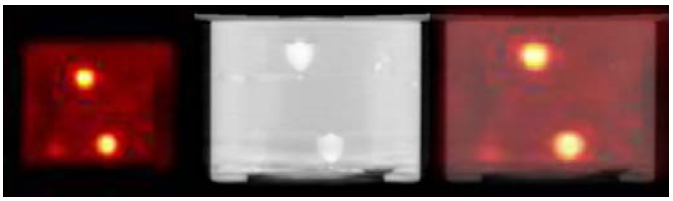

Fig. 9 Transverse sliced images of the SPECT (VAOR trajectory) (left), CT (middle) and fused data (right) showing good agreement.

D. *Observer Data*

Fig. 10a. shows images of the variable sized acrylic spheres in water, reconstructed using various partial angle data sets Although image quality does impact small lesion visibility, the 5mm very low contrast spheres remains visible for the three cases shown here, including the 240° data set. Note that the cupping (dip in the center) seen in all reconstructed CT images is exacerbated by the tight windowing necessary in order to discern the low contrast spheres in the highly attenuating water background.

Fig. 10b. shows the results of the first observer task. They indicate that, for sectors totaling contiguous 60° of missing data (Fig. 10b, left), regardless of the location of that sector around the compass, there is no significant difference in the number nor the size of the smallest sphere observed (3.5mm). However, when repeated with 120° missing (Fig. 10b, right),

there is one sector (0-120°) that shows an non-statistically significant increase in the smallest sphere seen (3.5mm to 3.7mm), shown as a decrease in the mean total spheres . While results for 120° partial angle (not shown) have increased image degradation, small low contrast spheres were still observed in that case. The cumulative finding from these results indicates that a 300° acquisition trajectory, producing minimal image degradation compared to a full 360° may be a solution to viewing more of the chest wall and circumventing the physical restrictions caused by the bed design.

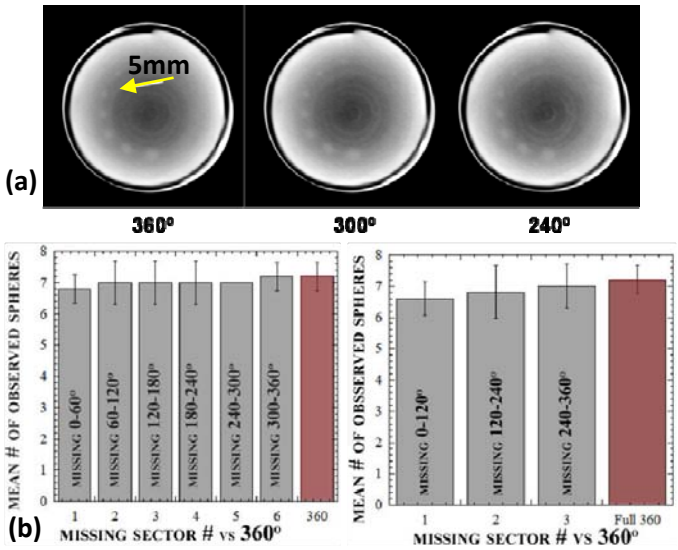

Fig. 10. Selected images used for the first observer task (a, top) and observer results from the task (b, bottom) for different sectors of missing angles compared to a full 360° scan (red bar). Visible 5mm sphere is noted on the images (yellow arrow).

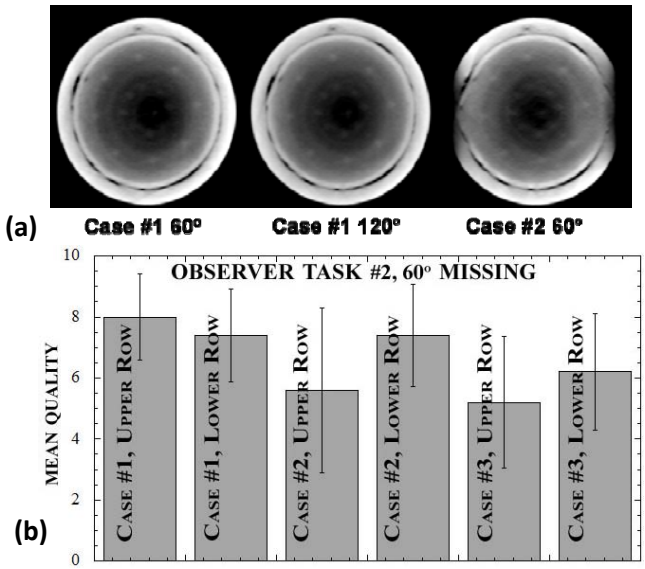

Fig. 11 Sample images of the presented to the observers for task #2 (a) and results of the observer study for task #2 for cases with 60° of projections shifted for each case (b).

For vertical system shifting with the 60° missing span there was no significant difference in the number of spheres observed, although, on average, observers noted a slightly lower number of spheres for case #2, 60° (7 versus 8 spheres). For the lower of the two planes of spheres, there were similarly no significant differences in the number of observed spheres. Note the readily apparent distortion in the outer lateral edges of the cylinder due to missing views for case#2, 60°, where spheres located in the inner portion of the cylinder are still visible. Samples of the images presented to the observers for observer task #2 are shown in Fig. 11a. In terms of quality assessment on a scale of 1 to 10, the results in Fig. 11b indicate that there was no statistically significant difference in the overall quality assessed by observers, despite obvious image artifacts.

For cases #2 and 3 for the 120° span (not shown, although the images are degraded even compared to the image in case #2, 60° shown in Fig. 11a), the reconstructed imaged volume was so visually poor that the embedded objects could not be adequately assessed. Some observers stated that only 2 or 3 spheres were visible. In fact, the reconstructed spheres were so distorted that it is difficult to envision corrections that would do any good to improve the image quality and content. Therefore, cases #2, 3 for 120° were not considered.

IV. Conclusion

In this study, novel trajectories were investigated to improve access to the anterior chest wall in an integrated SPECT-CT imaging system dedicated to breast cancer imaging. Two CT trajectories were specifically explored: intentionally using a limited or partial angle trajectory where <360° of data was acquired at an increased height, and vertically raising the system at various points in mid-acquisition to image more of the chest wall.

The versatile SPECT positioning system improves resolution by modifying the gamma camera's ROR to closely contour the breast. From a practical viewpoint, with the SPECT system ROR capable of extending up to 10cm from its initial position, a 2.5-5cm differential in system height will likely be a tractable problem for the SPECT system. Limited angle tomography is therefore likely to be an issue for the SPECT system only if both modalities acquire data simultaneously, i.e. projections are acquired in an interleaved fashion. This acquisition sequence would necessitate the orthogonally oriented SPECT system to be limited by the CT system's restricted positioning, missing projections from 90°-offset angles as the CT system's trajectory is modified to avoid bed sections. If the modalities acquire data separately, e.g. complete the entire CT scan first and then acquire the entire SPECT data, the issue of limited angle tomography for SPECT does not arise.

For CT imaging, encouraging results point to the viability of the proposed novel system trajectories using iterative reconstruction techniques. While the current system may be able to adequately implement these solutions, a more optimal CT system design will likely include x-ray source and detectors with smaller footprints and imaging dead zones, in addition to an improved bed design. Such system designs having a fully suspended CT system capable of polar tilting are being actively pursued.

ACKNOWLEDGMENTS

This work was supported by DOD grants W81XWH-08-1-0352,W81XWH-06-1-0791,W81XWH-06-1-0765, W81XWH-08-1-0192 and NIH grants R43-CA125924 and R01-CA096821.

REFERENCES

[1] C. N. Brzymialkiewicz, M. P. Tornai, R. L. McKinley, and J. E. Bowsher, "Evaluation of fully 3D emission mammotomography with a compact cadmium zinc telluride detector," *IEEE Trans. Med. Imag.*, vol. 24, pp. 868-877, 2005.

[2] P. Madhav, D. J. Crotty, R. L. McKinley, and M. P. Tornai, "Initial development of a dual-modality SPECT-CT system for dedicated mammotomography," *2006 IEEE Nucl Sci Symp & Med Imag Conf*, 2006.

[3] R. L. McKinley and M. P. Tornai, "Preliminary investigation of dose for a dedicated mammotomography system," *2006 Proc SPIE: Phys Med Imag*, vol. 6142, pp. 60-70, 11-17 Feb. 2006 2006.

[4] M. P. Tornai, Y. C. Tai, and R. L. McKinley, "Initial design considerations of a dedicated hybrid mammotomograph for fully 3D x-ray CT and high resolution PET using object magnification," in *Society of Nuclear Medicine Annual Meeting*, Toronto, ON, 2005.

[5] P. Madhav, S. J. Cutler, K. L. Perez, D. J. Crotty, R. L. McKinley, T. Z. Wong, and M. P. Tornai, "Initial patient study with dedicated dual-modality SPECT-CT mammotomography," in *2007 IEEE Nucl Sci Symp & Med Imag Conf*, Honolulu, HI, USA, 2007, pp. 3781-7.

[6] D. J. Crotty, P. Madhav, R. L. McKinley, and M. P. Tornai, "Patient bed design for an integrated SPECT-CT dedicated mammotomography system," in *2006 Workshop on the Nuclear Radiology of Breast Cancer*, San Diego, CA, 2006.

[7] D. J. Crotty, P. Madhav, R. L. McKinley, and M. P. Tornai, "Investigating novel patient bed designs for use in a hybrid dual modality dedicated 3D breast imaging system," *2007 SPIE Med Imag Conf*, vol. 6150, 2007.

[8] S. J. Cutler, P. Madhav, K. L. Perez, D. J. Crotty, and M. P. Tornai, "Comparison of reduced angle and fully 3D acquisition sequencing and trajectories for dual-modality mammotomography," Honolulu, HI, USA, 2007, pp. 4044-50.

[9] P. Madhav, S. J. Cutler, D. C. Crotty, K. L. Perez, R. L. McKinley, L. Wilke, T. Wong, and M. P. Tornai, "Pilot Patient Studies Using a Dedicated Dual-Modality SPECT-CT System for Breast Imaging " in *2008 AAPM* Houston TX, 2008.

[10] C. N. Brzymialkiewicz, R. L. McKinley, and M. P. Tornai, "Towards patient imaging with dedicated emission mammotomography," *2005 IEEE Nucl Sci Symp & Med Imag Conf*, vol. 3, pp. 1519-1523, 23-29 Oct. 2005 2005.

[11] J. W. Eberhard, D. Albagli, A. Schmitz, B. E. H. Claus, P. Carson, M. Goodsitt, C. Heang-Ping, M. Roubidoux, J. A. Thomas, and J. Osland, "Mammography tomosynthesis system for high performance 3D imaging," Manchester, UK, 2006, pp. 137-43.

[12] C. R. Crawford and K. F. King, "Computed tomography scanning with simultaneous patient translation," *Medical Physics*, vol. 17, pp. 967-982, 1990.

[13] C. N. Brzymialkiewicz, M. P. Tornai, R. L. McKinley, S. J. Cutler, and J. E. Bowsher, "Performance for dedicated emission mammotomography for various breast shapes and sizes," *Phys Med Biol*, vol. 51, pp. 5051-5064, 2006.

[14] C. N. Brzymialkiewicz, M. P. Tornai, R. L. McKinley, and J. E. Bowsher, "3D data acquisition sampling strategies for dedicated emission mammotomography for various breast sizes," *2005 IEEE Nucl Sci Symp & Med Imag Conf*, vol. 4, pp. 2596-2600, 16-22 Oct. 2004 2004.

[15] S. J. Cutler, C. N. Brzymialkiewicz, and M. P. Tornai, "Investigating the effects of energy resolution in dedicated emission mammotomography," *2005 IEEE Nucl Sci Symp & Med Imag Conf*, vol. 5, pp. 2537-2541, 23-29 Oct. 2005 2005.

[16] M. P. Tornai, C. N. Brzymialkiewicz, and R. L. McKinley, "Comparison of scintimammography and dedicated emission mammotomography," in *2004 IEEE Nucl. Sci. Symposium & Med. Imaging Conference*, Rome, Italy, 2004, pp. 2818-2822.

[17] M. P. Tornai, C. N. Brzymialkiewicz, R. L. McKinley, J. E. Bowsher, and E. Samei, "Development of Dedicated 3D Molecular Mammotomography with SPECT and Quasi-Monochromatic X-ray Computed Mammotomography," in *Workshop on Alternatives to Mammography*, Winnepeg, Manitoba, 2004.

[18] R. L. McKinley, "Development and characterization of a dedicated computed mammotomography system," *Ph. D.Thesis*, 2006.

[19] M. P. Tornai, R. L. McKinley, C. N. Brzymialkiewicz, P. Madhav, S. J. Cutler, D. J. Crotty, J. E. Bowsher, E. Samei, and C. E. Floyd, "Design and development of a fully-3D dedicated x-ray computed mammotomography system," *2005 Proc SPIE: Phys Med Imag*, vol. 5745, pp. 189-197, 12-18 Feb. 2005 2005.

Appendix E

2008 IEEE Nuclear Science Symposium & Medical Imaging Conference Record

Dynamic Laser-Guided Contouring for Dedicated Emission Mammotomography

Spencer J. Cutler, *Member, IEEE*, Dominic J. Crotty, Martin P. Tornai, *Senior Member, IEEE*

***Abstract*–The dedicated breast CZT-based SPECT imaging system in our lab implements novel 3D camera trajectories that can minimize breast-detector separation, thus improving resolution and image quality. Current trajectories are manually customized for each patient by measuring breast-detector separations at several positions and interpolating. This study seeks to transition from this manual method to an automated contouring solution for routine patient SPECT imaging, given the vast array of uncompressed breast shapes in women.**

In the initial effort to model "typical" SPECT camera trajectories for patients, a sub-study was conducted of 103 MRI breast data sets to categorize the shape and size of uncompressed, pendant breasts. Obtained parameters include measured nipple-to-chest wall (mean=8.4cm), superior-inferior (mean=10.8cm), medial-lateral distances (mean=14.3cm), and estimated breast volume (mean=720mL). These images will be used as digital "phantoms" when utilizing computer models for orbit optimization and system development purposes.

Automated breast surface contouring is implemented using a dual-layer, low divergence, ribbon laser feedback sensor system mounted along the edge of the SPECT camera. The upper and lower sensor layers consist of two laser-detector pairs that identify the region on the camera face that has been penetrated, defining a virtual plane. In both layers, receivers sense reduced signal intensity when the beam path is interrupted by the breast surface. The ROR can then be automatically adjusted such that the breast is within ~1cm of the camera face, but no closer than 0.5cm, thus safely keeping the camera face as close to breast as possible. Robustness of the contouring system is assessed using flexible anthropomorphic breast phantoms to model various pendant breast shapes and sizes. Initial results indicate that dynamic contouring both improves image quality and potentially adds comfort to the patient by shortening scan setup time.

I. Introduction

Our lab has developed a novel single photon emission computed tomography (SPECT) system that is now coupled with a CT system, allowing for uncompressed 3D dedicated SPECT-CT molecular breast imaging or "mammotomography" [1, 2]. The current prototype system includes a cadmium zinc telluride (CZT) based compact gamma camera (*LumaGEM™ 3200S, Gamma Medica*, Northridge, CA) with 2.5 mm discrete pixels, a measured mean energy resolution of 6.8 % FWHM at 140 keV, and sensitivity of 37.9 cps/MBq [3]. The gantry consists of a goniometric cradle, providing polar tilt; a motorized laboratory jack for radius-of-rotation (ROR) control; and a rotational stage for azimuthal positioning. Image acquisition and gantry movement are synchronized and precisely computer controlled. This versatile positioning gantry allows for fully 3D imaging anywhere within a hemispherical volume about the pendant breast and overcomes physical proximity restrictions of standard clinical gamma cameras or compact systems without 3D motion [4].

Novel acquisition orbits are currently defined by creating a file listing the ROR, polar tilt angle, and rotation degree for each desired projection. Polar tilt and rotation angles have limits mostly defined by the patient bed and can be quickly defined using existing software algorithms developed in the lab for a number of complex orbits. The ROR measurements essential for close contouring, however, are more complex to define for a non-uniform object. To closely contour a non-uniform uncompressed breast currently requires first manually moving the camera to several positions around the breast, taking measurements, and interpolating the points around the breast. Even for a stationary phantom this process can become time consuming, and any movement of the system or phantom requires adjustments to the orbit file. This study seeks to transition from this manual method to an automated contouring solution for routine patient SPECT imaging, given the vast array of uncompressed breast shapes in women.

This work is divided into two parts. First, in an effort to model "ideal" SPECT camera trajectories for patients, a study was conducted of retrospective MRI breast data to analyze the shape and size of uncompressed, pendant breasts. Second, a prototype automated breast surface contouring is implemented using a dual-layer, low divergence, ribbon laser feedback sensor system mounted along the edge of the SPECT camera.

II. MRI Study

Similar to the SPECT-CT imaging procedure in our lab, clinical MRI images are acquired with patients lying prone, and provide views of a complete 3D uncompressed breast volume. An IRB approved study of 103 unique, existing clinical MRI breast data was conducted to obtain several parameters of uncompressed breasts to categorize shape and size, and in an effort to model an ideal range of contoured

Manuscript received November 14, 2008. This work was funded by the National Cancer Institute of the National Institutes of Health (R01-CA096821), and the Department of Defense Breast Cancer Research Program (W81XWH-06-1-0765), and in part by Duke BME.

The authors are with the Multi-Modality Imaging Lab in the Department of Radiology at Duke University Medical Center, the Department of Biomdical Engineering, and the Medical Physics Graduate Program at Duke University, Durham, NC 27710, USA (email:spencer.cutler@duke.edu).

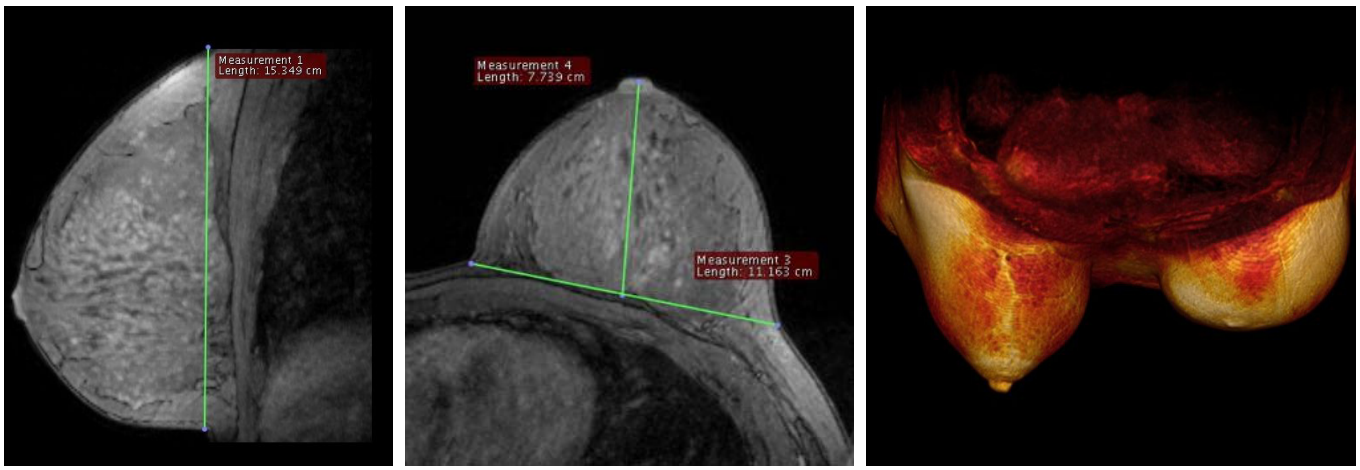

Fig. 1. Sample breast MRI sagittal (LEFT) and transverse (MIDDLE) slices with illustrated superior-inferior, nipple-chest, and medial-lateral measurements. A volumetric rendering (RIGHT) was also created for each subject.

orbits that may be used with patients when they would come for a SPECT-CT scan. MRI scans were acquired previously during patients' regular visits to Duke Radiology, and represent a random sampling of high risk breast cancer patients at the Duke University Medical Center. The volumetric data were completely de-identified except for age.

Using open-source *OsiriX* imaging software [5], breast parameters were obtained for a database consisting of measured pendant breast sizes: nipple-to-chest wall distance, superior-inferior distance, and medial-lateral distance (Fig. 1). From the 103 subjects, a total 202 uncompressed breasts were measured (several women had complete unilateral mastectomies and therefore only the remaining intact breast could be measured). Estimated volumes of the breasts were also calculated by first segmenting the images and then using voxel integration of the MRI images. Results are tabulated in Table I and the frequency distributions are displayed in Fig. 2. A weighted mean was calculated from the distributions. Moderate compression did occur for some larger breasts due to the fixed size of the MRI breast coil holes, and thus, true dimensions may have been slightly larger than measured.

A 3D surface rendering of the external breast shape was also generated in order to visualize challenges of contouring the breasts (Fig. 1, RIGHT) and to generally classify the data according to volumetric shape (Fig. 3). These MRI breast image sets can thus be used as the digital "phantoms" when utilizing computer models for system development and orbit optimization purposes (Fig. 4).

TABLE I: RESULTS FOR BREAST SIZES OBTAINED FROM MRI STUDIES

	Age (Yr)	Nipple-to-Chest (cm)	Medial-Lateral (cm)	Superior-Inferior (cm)	Vol. (mL)
Mean	45.8	8.4	10.8	14.3	720
Std Dev	7.6	2.7	2.4	1.6	415
Min	23	2.9	5.5	8	130
Max	66	19.1	16.9	17.3	2970

This study was helpful in visualizing the challenging variety of breast shapes and volumes to be contoured during the SPECT-CmT scanning procedure. Encouragingly, the polar tilts possible with our current complex orbits (Fig. 4) will sufficiently sample the majority of the shapes and volumes observed, but the ROR cannot rely on linearly interpolated points to accurately contour the breast, as is currently the protocol.

While the relatively low number of subjects measured

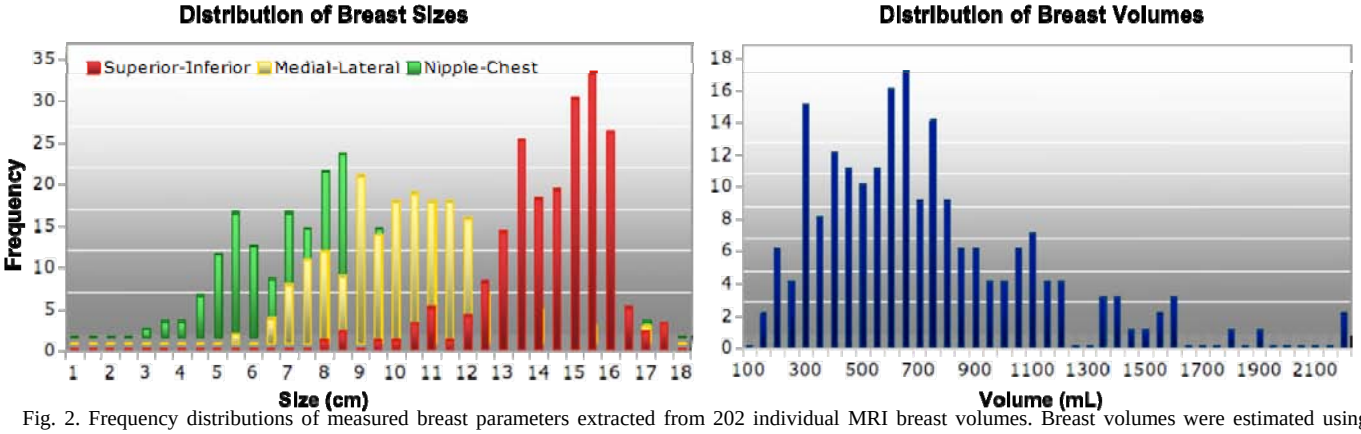

Fig. 2. Frequency distributions of measured breast parameters extracted from 202 individual MRI breast volumes. Breast volumes were estimated using segmentation and mesh volume calculations.

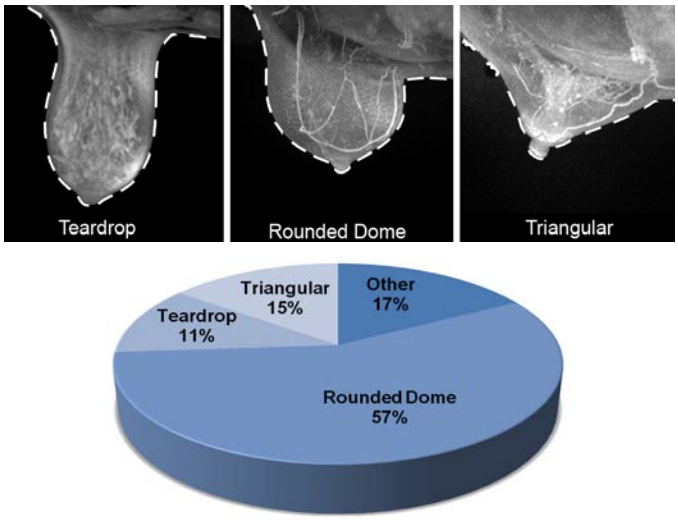

Fig. 3. (TOP) Representative examples of shape labels used to classify each subject. (BOTTOM) Distribution of general breast shapes over the 103 subjects. The "Other" category includes mastectomy and miscellaneous shaped breasts that didn't fit into the other three general classifications.

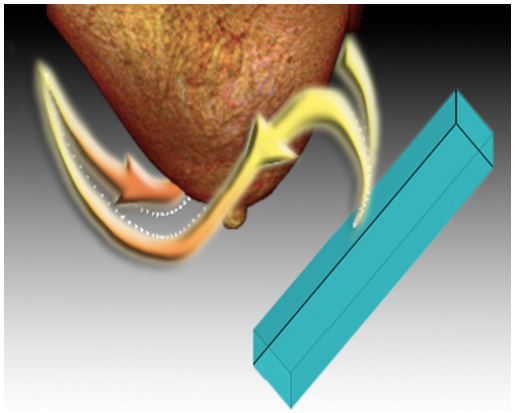

Fig. 4. A complex projected sine wave (PROJSINE) imaging acquisition orbit shown about a volume rendered digital breast "phantom"

prevents us from making any broad statistical classifications for the general population of women, the minimum, maximum, and mean measurements provide a starting estimate of ROR ranges for the gamma camera in our lab.

Prior to this study, one compressible and six incompressible breast phantoms were fabricated to our general specifications at *Radiology Support Devices, Inc.* (*RSD, Inc.*, Newport Beach, CA) [6]. These phantoms vary in shape and overall fillable volume, and were molded to resemble prone or pendant breasts. The measured MRI breast sizes from this study retrospectively validate the range of shapes and sizes of these custom shaped pendant breast phantoms. The compressible phantom dimensions are close to the mean value measurements of the MRI subjects, and the incompressible phantoms allow us to physically test from minimum to maximum extremities.

III. Dynamic Laser-Guided Contouring Implementation

The unique pendant breast shapes observed in the MRI study reinforce the need to automate the ROR component of an orbit. We have developed and implemented a prototype dual-layer optical barrier for real-time laser feedback, automated ROR control for arbitrary breast contouring. A single optical barrier only reports that the barrier is compromised, without any knowledge of how close an object (e.g. breast surface) could be. Having a second layer at a known small distance from the camera face provides information that the object has penetrated the first layer, and is therefore within some distance to the camera, but that it has/has-not penetrated the second layer (Fig. 5). Commercially available, low divergence, ribbon laser feedback sensors (*Keyence*, 4cm wide lasers (model LV-51M) and detectors (LV-H300)) were purchased to implement this design. The upper layer consists of independent ribbon lasers that help identify the region on the camera face that has been penetrated, while the lower layer consists of a single, multiply reflected beam defining a virtual plane. In both layers, a receiver senses the signal intensity drop when the path of the beam is interrupted. Therefore, we can know that a breast is within ~1cm of the camera face, but not closer than 0.5 cm, and also at what relative location along the camera face. Changes in ROR to keep the camera close can thus easily be made. We successfully bench tested this principle with the ribbon lasers and measured a change in beam intensity even using our clear breast phantoms [6].

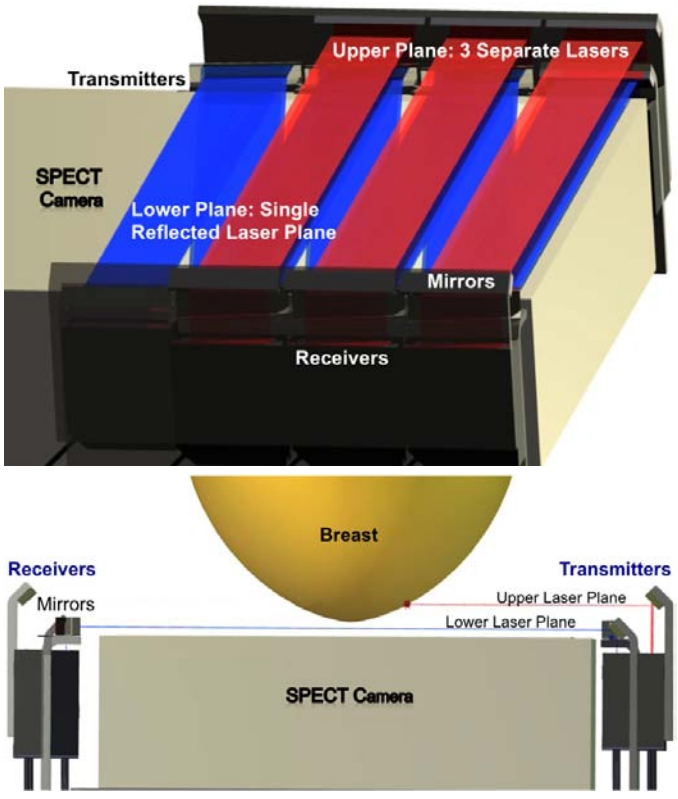

Fig. 5. (TOP) Automated breast surface contouring implementation using a dual-layer, low divergence, ribbon laser feedback sensor system mounted along the edges of the SPECT camera. The upper sensor layer (shown above in red) consists of three laser-detector pairs that identify the region on the camera face that has been penetrated, while the lower layer (shown above in blue) consists of a single, multiply reflected beam defining a virtual plane. (BOTTOM) Side view of the SPECT camera with breast penetrating the upper optical sensor plane.

Next, a working prototype was completed, allowing for dynamic laser-guided contouring for the SPECT system. A circuit was designed and built to power the sensor amplifiers and to channel the output receiver voltages (feedback) into the analog-to-digital converter of the Newport ESP7000 motion controller (Fig. 6). The data acquisition and motion control software were then modified to read in the digitized signals via an RS-232 serial interface, and new algorithms were created to position the camera based on the feedback from the lasers.

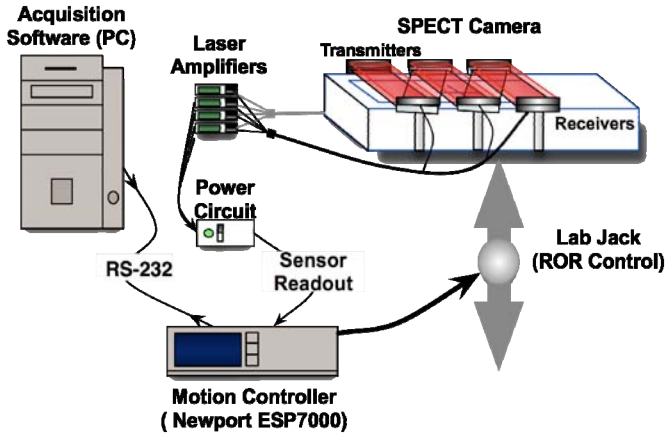

Fig. 6. Illustration of the laser contouring electronics and data flow. Sensors provide feedback to the acquisition software via the motion controller ADC, followed by the computer adjusting the ROR accordingly.

For the initial prototype, a 2x2 array of transmitter-receiver laser pairs were mounted on a thin piece of acrylic plastic, effectively creating two virtual planes with independent upper and lower positional data in each plane (Fig. 7, LEFT). After bench-top tests, this plastic sheet was adhered to the face of the SPECT camera, allowing functional scans with small additional attenuation due to the 6 mm thick plastic sheet.

Compared to a manually defined contour with the lasers, the automated approach kept the camera significantly closer during the scan (Fig. 8).

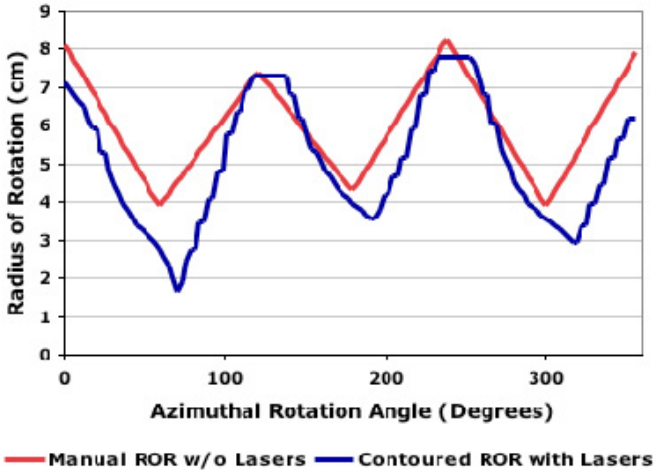

Fig. 8. 360° SPECT radius-of-rotation (ROR) trajectories about a 700 mL breast phantom. Laser guided contouring (blue) keeps the camera significantly closer to the breast (smaller ROR is better) during the scan compared to the manually created orbit (red)

Mini-cold rod image data, acquired prior to the sensor implementation, illustrate the proof-of-principle distance-dependant fall-off in spatial resolution with varying the radii-of-rotation. The 2.6 cm long rods were arranged in six sectors of equal diameters of 4.7, 3.9, 3.1, 2.3, 1.5, and 1.1 mm, on a pitch of twice their diameters. 15 mCi of 99mTc in water filled the interstitial spaces. The phantom was suspended vertically with the mini-rods in the center of the camera's field of view and parallel to the camera surface. The cold rods were first imaged as close as possible to the camera (4.4 cm constant ROR), and then with the camera backed away to a 7

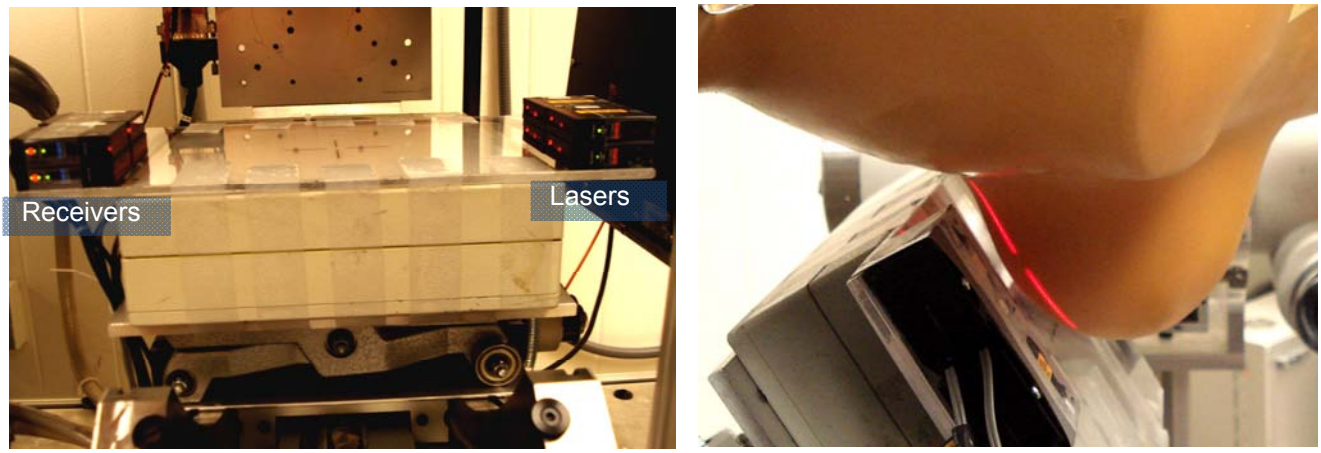

Fig. 7. (LEFT) Dual-layer prototype ribbon laser *(Keyence* Model HV300*)* contouring system attached to face of the SPECT camera. Sensor outputs are channeled through an ADC into the gantry motion controller (*Newport* ESP7000) that monitors and adjusts the ROR accordingly. (RIGHT) Separate 35 mm wide top-layer ribbon laser beams are seen on the breast phantom skin, as the camera dynamically contours at a minimal radius of rotation to improve resolution and image quality.

Using the functional prototype, we were able to automatically contour a 700 mL breast phantom with no initial setup time (Fig. 7, RIGHT). Trajectory repeatability for a fixed breast phantom was found to be very high, with only a few slight differences of less than 1 mm over multiple measurements.

cm ROR. Spatial resolution and contrast degradation are evident with increasing ROR (Fig. 9). The 4.7 and 3.9mm rods are visible in both cases, but the 3.1 mm rods are distinguishable only with the closest contouring (4.4 cm) ROR. Thus we anticipate that automated close contouring will

improve spatial resolution, especially with concomitant incorporation of resolution modeling using the feedback ROR data.

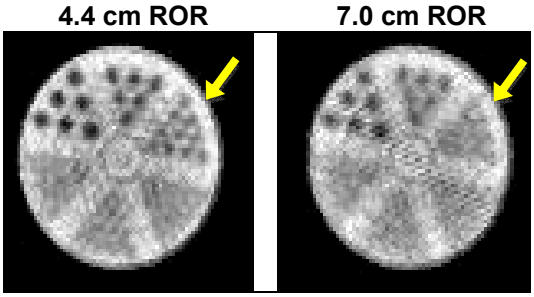

Fig. 9. Proof-of-principle reconstructed mini-cold rod image data illustrating the distance-dependant fall-off in spatial resolution with ROR that differ by only 2.6 cm. The largest 4.7 and 3.9 mm rods are visible in both cases, but the 3.1 mm rods (yellow arrow) are distinguishable only with the closest contouring (4.4 cm) ROR.

Automated orbits have been shown to both simplify and significantly expedite the overall SPECT imaging process (Table II). Contoured acquisition times take slightly longer due to longer gantry motion times from the increased range of ROR motion. This should be improved combining the gantry's physical capability of moving faster, and smarter software algorithms to "anticipate" the next ROR position based on positional information from the upper sensor plane and the current polar tilt of the system. The elimination of manual orbit setup time, however, more than makes up for the minimally increased scan time.

TABLE II: EFFECT OF AUTOMATED CONTOURING ON TOTAL IMAGING TIME

	Setup Time	Acquisition Time	Total
Without Lasers	6-8 min	11 min	*17-19 min*
With Lasers	0 min	11-13 min	*11-13 min*

A permanent fixed hardware design is in progress with the sensors mounted vertically on the sides of the camera (Fig. 5) and then reflected across the face in order to minimize obstructing area of the protruding sensors. This is important to avoid contact with the patient or obscuring the CT-cone beam mounted orthogonal to the SPECT system. Future modifications will also focus on adjusting the polar tilt of the camera based on the positional information from the upper plane of sensors, as well as potentially adding ranging sensors to the tip of the SPECT camera to allow polar-tilts to dynamically contour a patient's protruding shoulder and chest area.

IV. CONCLUSIONS

In an effort to characterize a range of breast shapes and sizes anticipated in the dedicated, uncompressed breast imaging paradigm, a retrospective study of breast shapes, sizes, and volumes provided useful guidelines for system and orbit optimization. The range of pendant breast shapes observed in the MRI study reinforce the need to automate the radius of rotation component of the dedicated breast SPECT orbit to contour to the wide variety of individual breast shapes. A simple, but effective method for automated dynamic laser-guided contouring system has been shown to both simplify and expedite the overall SPECT imaging process. A dual-layered system was implemented to allow modest determination of breast distance in addition to utilizing the optical barrier for safety (i.e. collision avoidance) concerns. Automated orbits created using this prototype system are highly robust, repeatable, and potentially improve overall image quality. More in-depth image quality comparisons will be undertaken once the final mounting hardware is fixed and software acquisition software is fully optimized. The implementation of dynamic laser-guided contouring will facilitate a smoother scanning process for ongoing clinical patient studies in the Duke Multi-modality Imaging Laboratory.

ACKNOWLEDGMENT

The authors thank V. L. Seewaldt and A. O. Bilska-Wolak for providing access to IRB approved de-identified MRI data used in this study. MPT is the inventor of the SPECT imaging technology, and is named as an inventor on the patent for this technology applied for by Duke. If this technology becomes commercially successful, MPT and Duke could benefit financially.

REFERENCES

[1] P. Madhav, D. J. Crotty, R. L. McKinley, and M. P. Tornai, "Initial development of a dual-modality SPECT-CT system for dedicated mammotomography," *2006 IEEE Nucl Sci Symp & Med Imag Conf*, vol. 4, pp. 2382 - 2386, 2006.

[2] M. P. Tornai, J. E. Bowsher, C. N. Archer, J. Peter, R. J. Jaszczak, L. R. MacDonald, B. E. Patt, and J.S. Iwanczyk, "A 3D gantry single photon emission tomograph with hemispherical coverage for dedicated breast imaging," *Nucl. Instr. Meth. Phys. Res. A*, vol. 497, pp. 157-167, 2003.

[3] C. N. Brzymialkiewicz, M. P. Tornai, R. L. McKinley, and J. E. Bowsher, "Evaluation of fully 3D emission mammotomography with a compact cadmium zinc telluride detector," *IEEE Trans. Med. Imag.*, vol. 24, pp. 868-877, 2005.

[4] C. N. Archer, M. P. Tornai, J. E. Bowsher, S. D. Metzler, B. C. Pieper, and R. J. Jaszczak, "Implementation and initial characterization of acquisition orbits with a dedicated emission mammotomograph," *IEEE Trans. Nucl. Sci.*, vol. 50, pp. 413-420, 2003.

[5] A. Rosset, L. Spadola, and O. Ratib, "OsiriX: An Open-Source Software for Navigating in Multidimensional DICOM Images," *Journal of Digital Imaging*, vol. 17, pp. 205-216, 2004.

[6] M. P. Tornai, R. L. McKinley, S. J. Cutler, D. J. Crotty, and C. N. Brzymialkiewicz, "Anthropomorphic breast phantoms for preclinical imaging evaluation with emission or transmission imaging," *2005 Proc SPIE: Phys Med Imag*, vol. 5746, pp. 825-834, 2005.

Appendix F

2008 SPIE Medical Imaging Conference Record

Initial Investigation of Novel Trajectories to Improve Chest Wall Imaging in a Dedicated Breast Computed Tomography System

Dominic J. Crotty[a,b], Randolph L. McKinley[c], Priti Madhav [a,b], Spencer J. Cutler[a,b], Martin P. Tornai[a,b]

[a]Department of Radiology, Duke University Medical Center, Durham, NC 27710
[b]Department of Biomedical Engineering, Duke University, Durham, NC 27708
[c] Zumatek Incorporated, Chapel Hill, NC 27514

ABSTRACT

In current dedicated breast computed tomography (mammotomography) systems, comfortable patient positioning on a stationary bed restricts the practicable range of source-detector trajectories, thus compromising the system's ability to adequately image the patient's anterior chest wall. This study examines the effect on detecting small, low-contrast lesion-like-spheres using limited angle x-ray source-detector trajectories and trajectories that intentionally raise the tomographic imaging system mid-acquisition. These modified acquisition paths may increase chest wall visualization, simplify the design of the imaging system and increase patient comfort by allowing the design of an improved patient bed. Thin walled balloons of various volumes filled with iodine act as surrogate high contrast lesions to initially investigate the effect of these novel trajectories. Then, stacks of 5mm acrylic spheres regularly spaced in concentric circles are placed in water to simulate a low contrast environment in a uniform scatter medium. 360° azimuthal scans are acquired at various bed heights with contiguous projections subsequently removed to create limited angle acquisitions from 240-360°. Projections from the different bed heights are interwoven to form trajectories that mimic discontinuously raising the imaging system mid-acquisition. The resulting iteratively reconstructed volumes are evaluated with an observer study. Initial images suggest that using limited angles and raising the system is possible while increasing the observer's ability to visualize objects near the chest wall. Based on the results of this study, an improved patient bed to facilitate chest wall imaging will be designed, and the feasibility of vertical system motion to increase imaged breast volume explored.

Keywords: CT, CTCB, MG, PER, breast CT, mammotomography, complex trajectory, cone beam CT

1. INTRODUCTION

Several researchers are currently developing devices dedicated to 3D breast imaging using computed tomography (CT or mammotomography) [1]. Our lab has developed a prototype dedicated dual-modality breast imaging system that integrates independent cone beam x-ray CT and single photon emission computed tomography (SPECT) sub-systems onto a common mechanical gantry and having a common field of view (FOV) (Fig. 1). The imaging technique used in dedicated breast CT calls for the patient to lie prone with one uncompressed breast hanging pendant through a flexible opening incorporated into the torso section of the bed. The imaging system then acquires projection data while rotating beneath the patient, with the CT system currently restricted to a fixed height and source-detector tilt relative to the rotation plane.

Experience gained from initial patient scans have shown that a combination of challenges in effective patient positioning and device dead zones inherent in the components of the CT sub-system [2, 3] ensure that the top plane of the CT cone beam is invariably separated from the chest wall (Fig. 1, Right and Right, inset) [4, 5]. This study investigates novel trajectories to overcome these limitations and enable the CT system to maximize the imaged volume of the patient's breast and anterior chest area. A number of potential solutions to enable direct viewing through the chest wall are investigated: (1) partial or limited angle tomography, i.e. using incomplete (< 360°) trajectories to acquire projections, and (2) vertically raising the imaging system mid-acquisition for a portion of the azimuthal rotation. An observer study is used to evaluate the effect of these trajectories, and the results are reported.

2. METHODOLOGY

In the prototype compact dual-modality system (Fig. 1), both the SPECT and CT sub-systems are secured to a common rotation stage (model RV350CCHL, *Newport Corp*., Irvine, CA) capable of 360° azimuthal rotation around the vertical chest-nipple axis of the breast. The SPECT sub-system is positioned orthogonal to the x-ray source-detector axis. In this study, only the CT sub-system is investigated as the full 3D positioning flexibility of the SPECT ensures that the breast and anterior chest wall is adequately sampled using the dedicated emission tomography system [6].

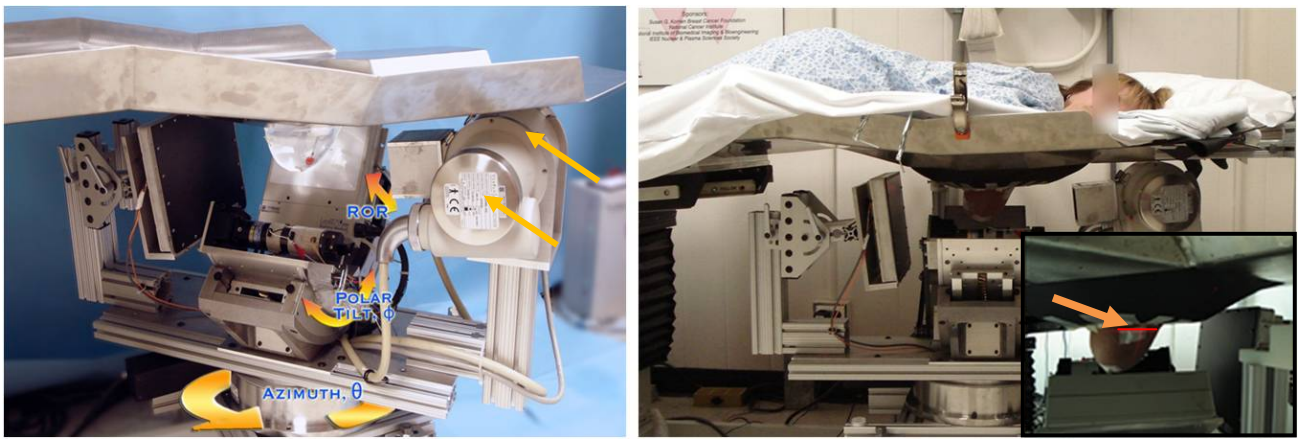

Fig. 1. (Left) The integrated hybrid SPECT-CT system is shown rotating below the custom made patient bed. A clear breast phantom hangs suspended from the torso section of the bed in the common field of view (FOV). The inner and outer circular edges of the x-ray tube housing are indicated (orange arrows). (Right) Photograph of a prone subject being imaged, with the x-ray tube passing under the subject's head. (Right, inset) The approximate position of the uppermost plane of the x-ray cone beam is delineated by the highlighted red positioning laser line.

2.1 Dedicated Breast CT System

The CT sub-system consists of a rotating tungsten target cone-beam x-ray source (model Rad-94, 0.4mm focal size, 14° anode angle, *Varian Medical Systems*, Salt Lake City, UT) and CsI(T1)-based amorphous silicon digital x-ray detector (model *Paxscan* 2520, *Varian Medical Systems*, Salt Lake City, UT) with a grid size of 1920x1536 and 127μm pixel pitch. The source and detector are secured to a ½" thick aluminum plate underneath the SPECT goniometer which is then attached to a common azimuthal rotation stage. A Ce 100th attenuating value layer (0.0508cm, calculated at 60kVp) filter (Z=58, ρ=6.77g/cm^3, K-edge=40.4keV, *Santoku America, Inc.*, Tolleson, AZ) was used to yield a mean x-ray beam energy of ~36keV and FWHM of 15%. Such a quasi-monochromatic x-ray source can (1) lower the x-ray dose for an image; (2) minimize beam hardening and may (3) improve the visualization of tissues with very small differences in attenuation coefficients. For these studies, a 60cm source-to-image distance (SID) was used with a magnification of 1.57 for an object located at the system's center of rotation. Unlike the SPECT sub-system, the current CT sub-system is restricted to simple circular motion at a 6.25° fixed tilt. A statistically iterative ordered subset transmission reconstruction algorithm can accommodate system shifting through modification of a user-defined orbit file that is read into the reconstruction algorithm.

2.2 Patient Bed System

A customized bed was designed to provide patient comfort while enabling the maximum volume of breast to be imaged (Fig. 1). Composed of ⅛" thick stainless steel, the bed is lined with thin layers of lead, polyurethane foam and neoprene to protect the patient from errant radiation, enhance comfort during the scan and provide support for the prone patient. The resultant tiered design (including an octagonal torso section and angled waist and head sections) both supports the patient and allows enough flexibility in the neoprene support to suspend her chest into the common system FOV [2, 3]. The octagonal torso section, positioned over the imaging FOV, allows the system to rotate underneath, and a removable insert can be replaced by radiolucent materials to enable imaging up to and, ideally, through the chest wall.

The bed is attached to a positioning system (model 830-058, *Biodex Medical Systems*, Shirley, NY) which has five degrees of movement to aid in extending maximal subject breast volume into the FOV and to negate bowing in the cantilevered bed due to the weight of the subject [7]. The most pertinent movement involved in this study is the ability of the bed to be raised or lowered vertically, thus modifying the distance between the under surface of the bed and the top plane of the CT cone beam.

2.3 Computer Aided Design (CAD) Simulation of the Benefits of Vertically Raising the System

With the CT sub-system restricted to azimuthal trajectories at a fixed height above the ground and at a fixed radius around the vertical axis of rotation, it is the section of the bed that is at the lowest height above the ground (i.e. the head section) that is therefore the critical limiting factor for allowing full azimuthal trajectories (see Figs. 1, 2). The flexibility of the bed positioning system allows implementation of a number of novel imaging trajectories. Several such trajectories were investigated by using a combination of raising or lowering the bed in this simulation and rotating the modeled x-ray tube around the vertical axis of rotation until the tube housing (Sapphire housing, *Varian Medical Systems*, Salt Lake City, UT) made contact with the bed.

Using design software, accurate 3D models of all components in the current CT sub-system configuration were produced (Fig. 2). Initial design simulations were performed to assess the changes in breast volume imaged using the various trajectories described in the paragraph below. The breast was modeled as an approximate 1000mL hemi-ellipsoid with a 12cm chest to nipple distance. The chest wall of the simulated breast was not explicitly modeled but was assumed to begin directly above the uppermost edge of the simulated breast.

Three potential trajectory setups were tested. The first (A) simulates raising the bed just enough to allow for full 360° rotation of the imaging system, including underneath the head section, trading increased tomographic sampling for a reduction in imaged breast volume (since the bed is raised to allow for full rotation it therefore increases the separation of the chest wall from the top plane of the cone beam). The second and third scenarios (B and C) simulate lowering the bed until the system is able to rotate up to the inner and outer circular edges of the sapphire housing, respectively (see Figs. 1,2).

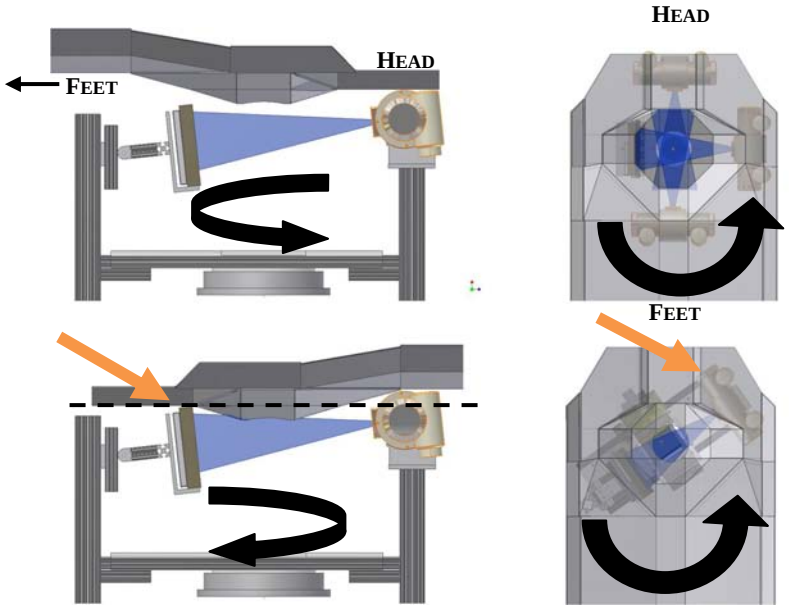

Fig. 2. (Top Row, Left) CAD image of the raised patient bed allowing the x-ray tube to rotate underneath the head section. Note the separation of the top plane of the modeled x-ray cone beam (blue) from the under surface of the bed. (Top Row, Right) Top down view of the modeled x-ray tube completing a full 360° trajectory with the raised bed. (Bottom row, Left) The patient bed is lowered, with the top plane of the cone beam now penetrating through the octagonal section of the bed i.e. penetrating the assumed position of the chest wall of the patient. Note the top of the x-ray tube is above the level of the head section (black broken line) (Bottom Row, Right) In this configuration, with a circular trajectory at a single height, the increase in imaged breast volume comes at the expense of the azimuthal range of the CT system affected by the reduced angular range of x-ray tube before it impacts the head section of the bed – conversely, the detector remains capable of traversing under the head section (orange arrows).

2.4 Qualitative study of the effect of using novel trajectories on lesion visibility

Fig. 3 shows the phantom used in a set of experiments that examined the visibility of high-contrast simulated lesions of various sizes imaged using novel trajectories described in more detail below. Each phantom consists of 4 thin walled balloon lesions (*Harvard Appartus Inc.*, Holliston, MA), of volume 2600, 500, 140 and 70µL arranged on the same radius circle at 90° intervals. The lesions were filled with CT contrast (1:60 Iodine:water concentration). Attached to an acrylic ring, two such planes of simulated lesions were stacked approximately 3cm apart (Fig. 3, Center), placed in a water-filled cylinder (to mimic dense breast tissue) and suspended in the FOV of the CT imaging system.

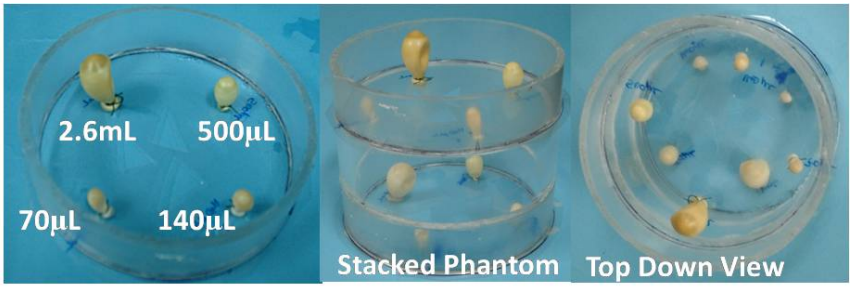

Fig. 3. Photographs of the thin-walled balloon phantom (Left) with the different-sized lesions noted and (Center and Right) the stacked phantom.

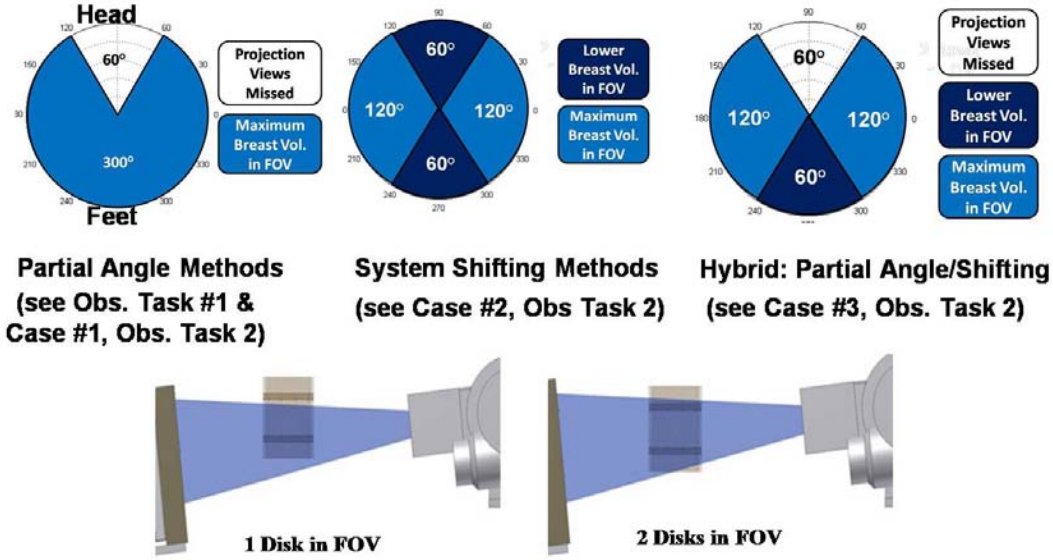

Fig. 4. A sample of post-processed (Top Row, Left) partial angle, (Top Row, Center) system shifted and (Top Row, Right) combined partial angle/shifting trajectories are also shown. Please see Fig. 1 for orientation of the head and feet directions of the bed. (Bottom Row) CAD drawings of the phantom being imaged in the FOV at both heights are also shown. Polar plots detail the positions of projection angles that are removed or how system shifted data sets are created.

Two separate and complete tomographic data sets were acquired. The first scan acquired 360 projections at 1° intervals with only one (the lower) plane in the system FOV (60kVp, 100mA, 2.5mAs per projection - see Fig. 4, Bottom Row). The disk phantom was then lowered and a follow up 360° data set acquired with both disks in the FOV using the same imaging parameters. The tomographic data sets were post-processed to mimic both partial angle and vertically shifted data sets (Fig. 4, Top Row). Partial angle data sets were created by simply removing projections in contiguous sectors from desired positions around the phantom. Vertically shifted data sets were created by concatenating projections in specific sectors from the first data set containing one visible disk with projections from the second data set where both disks were visible (Fig.4, Bottom Row). In that way, a variety of data sets were created to model the limits of the current equipment in the lab.

2.5 Observer Study of Low-Contrast Objects Imaged using Novel Trajectories

An observer study was additionally used to quantify the ability of observers to detect low-contrast spherical acrylic 'lesions' in water using both partial angle and system shifting techniques. Partial angle techniques were initially investigated using a data set acquired using a phantom consisting of a single plane of acrylic spheres of varying size (1 to 14.3mm) positioned equidistant from a common center point (Fig. 5, Left) [8].

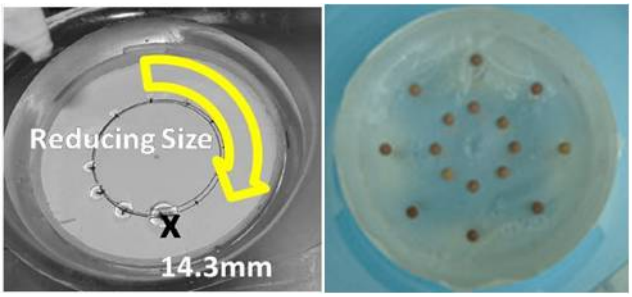

Fig. 5. (Left) The phantom consisting of acrylic spheres of continually decreasing size (14.3 – 1mm) arranged on a single circle of fixed radius, and (Right) circular disk phantom with 5mm acrylic spheres separated at regular 45° intervals.

In this case, a full 360° of data was acquired using 240 equally-spaced projections at 60kVp, 100mA and 25ms per projection. Projections were removed in different sectors around the clock to create partial angle tomography data.

5 observers each assessed 58 images. The first observer Task 1 initially used this phantom with contiguous 60° sectors removed from the full data set of raw projections. These partial angle data sets were reconstructed, and the resulting images shown to observers who were tasked with recording the number of visible spheres, in addition to the perceived quality of the images (on a 1 to 10 interval scale, 10 being best). The task was repeated using images reconstructed from the same data set with 120° of angles removed from various sectors.

The second observer task considered the effect on the detectability of very low contrast 5mm acrylic spheres in the circular disk phantom of vertically shifting the system mid-scan. The circular disk phantom (Fig. 5, Right) consisted of concentric circles of 5mm acrylic spheres in two concentric circles spaced at 45° intervals around a disk. Two such disks were stacked approximately 3cm apart in a water-filled cylinder to yield a low contrast imaging task (~1% intrinsic contrast at 36keV). Three potential solutions were investigated to enable increased access to the chest wall (see Fig. 4, Top Row for illustrations): Case #1 - raising the bed so that the system can azimuthally traverse 60° or 120° under the head section of the bed only; Case #2 - raising the system at both head and feet for 60° or 120° each; Case #3 – raising the bed either at the head or feet along with an additional partial angle of 60° and 120° of projection data removed completely from the other end (see Fig. 4, Top Row). Observers were asked to note the number of visible spheres from each of the two planes of the reconstructed phantom data, and the objective quality (on a 1 to 10 interval scale, 10 being best) of the images of the spheres.

3. RESULTS

3.1 CAD Simulation

Representative images of the setup for the simulated cases are shown in Fig. 2 with the breast and anterior chest wall (not shown in Fig. 2) modeled as hanging pendant from the center of the octagonal opening in the bed. Table 1 lists quantifiable tradeoffs involved in vertically shifting the system in order to allow more of the breast and chest wall to be included in the FOV. A negative number in the far right column indicates that the top plane of the cone beam lies anterior to the simulated chest wall, i.e. the chest wall is not sampled. A positive number indicates that the top plane of the cone beam images into and through the chest wall. While mindful of not truncating the nipple region from the distal side of the cone beam, the optimal result would be to image as much chest wall as possible, making this positive number as large as possible.

Table 1. Effect of partial angle acquisitions on ability to increase the volume of breast imaged near the anterior chest wall

Partial Angle Setup	Setup	Total azimuthal projection range	Distance between anterior chest wall and cone beam (mm) *
A	Tube passes below head section of the bed	360°	-10
B	Tube housing inner circular edge impacts bed	300°	-2.9
C	Tube housing outer circular edge impacts bed	240°	+9.3

* Negative values indicate the top plane of the cone beam is anterior to the chest wall, positive values mean the beam penetrates the chest wall.

A 120° azimuthal segment arises from the difference between a full 360° rotation at a lower system height where the x-ray tube is allowed to pass below the head section of the bed (Setup A) and a 240° trajectory with the system raised up to view more of the breast, but where the outer edge of the tube housing impacts the head section (Setup C) (see Fig. 2); the azimuthal angle is measured with respect to the projection angle of the central ray. If this 120° reduction in azimuthal sampling is acceptable, simulation results then indicate that there is an approximate 19mm increase in visualization towards the chest wall. This result demonstrates the potential advantages for using novel system trajectories to view more of the breast tissue.

It can be additionally seen that a trajectory involving vertical shifting of the system can also be used to concurrently satisfy a full 360° azimuthal sampling of a lower portion of the breast while accepting partial azimuthal sampling of the full breast volume. Such a trajectory could be implemented by imaging at one height for a portion of the trajectory (e.g. setup B or C in Table 1) and at a lower height for the remainder of the trajectory (i.e. setup A) to complete the 360° rotation by passing beneath the head section of the bed.

3.2 Breast CT imaging using novel trajectories

Fig. 6 shows sample projections of the imaged iodine-contrast phantom with a (Left) single and (Second from Left) both planes of balloon lesions in the FOV – see Fig. 4 for CAD representations of this setup. Fig. 7 shows reconstructed maximum intensity projection (MIP) images of the balloons acquired with both system shifting and partial angle methods. The range of projections included for partial angle tomography that includes vertical shifting is noted on each image. For example, 'Partial 280°' means that 280° of projection data was included in the reconstruction with the other 80° missing entirely and 'Shifted 280°' means that both planes of balloons were in the FOV for 280° of projections, with the other 80° containing only the lower plane of balloons. The projection data set acquired with both planes of balloons in the FOV for 360° is also reconstructed (16 subsets, 8 iterations) and is taken as the standard against which the quality of images reconstructed using partial angle and system shifting methods are compared.

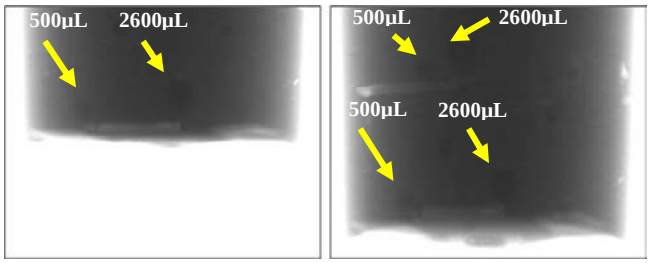

Fig. 6. Sample projection images of the phantom with (Left) only the lower plane and (Right) both planes in the FOV. These projection images are adjusted to illuminate the iodine-filled balloons (at arrows). Only the two larger balloons on both planes are visible in these projections.

As expected, increasing distortion is evident in images where the number of removed projections is increased. This is especially evident for the shifted data sets, where the upper plane of lesions is sampled in the FOV for only a subset of the total projection range. However, even for shifted data sets the lower plane is always in the FOV and yields reconstructions with image quality similar to that of the full 360° data set. The ability to maintain lesion visibility despite

a reduction in sampling further enforces the results of another study undertaken by us [9]. Smaller lesions become harder to visualize as more projections are removed from the full 360°; again this is particularly true for system shifted data. Shown in Fig. 8 are profiles obtained from both shifted and limited angle reconstructions across each separate lesion in only the upper plane of lesions. The profiles emphasize the trend in increased lesion distortion and a reduction in peak reconstructed attenuation coefficient value (both contrast and absolute value degradation).

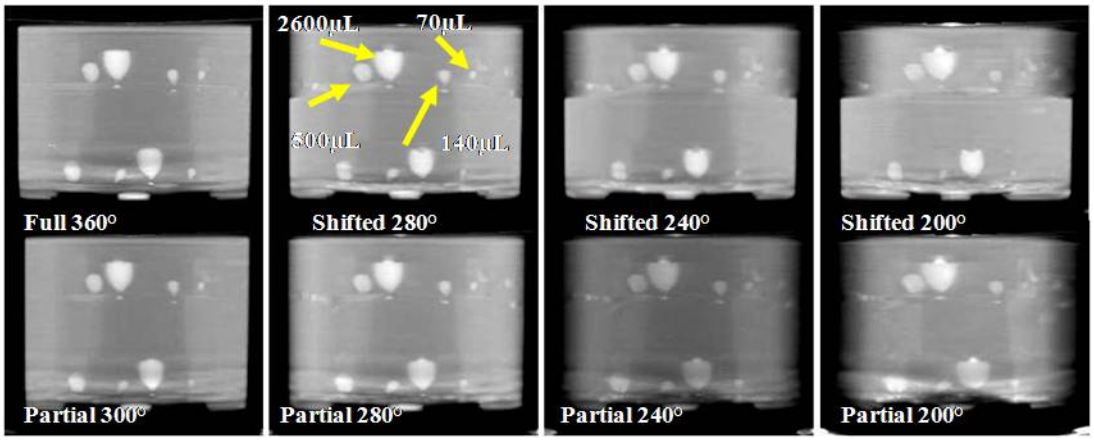

Fig. 7. Reconstructed MIP images showing all the balloons in both the upper and lower planes with the full 360° acquisition (upper and lower planes in the FOV for 360° of projections) (Top Row, Left) contrasted with images from (Top Row) shifted and (Bottom Row) partial angle data sets (see Methods section). Note the increased distortion in lesion shape, most apparent in the 2600µL lesion on the upper plane, as projections are increasingly removed.

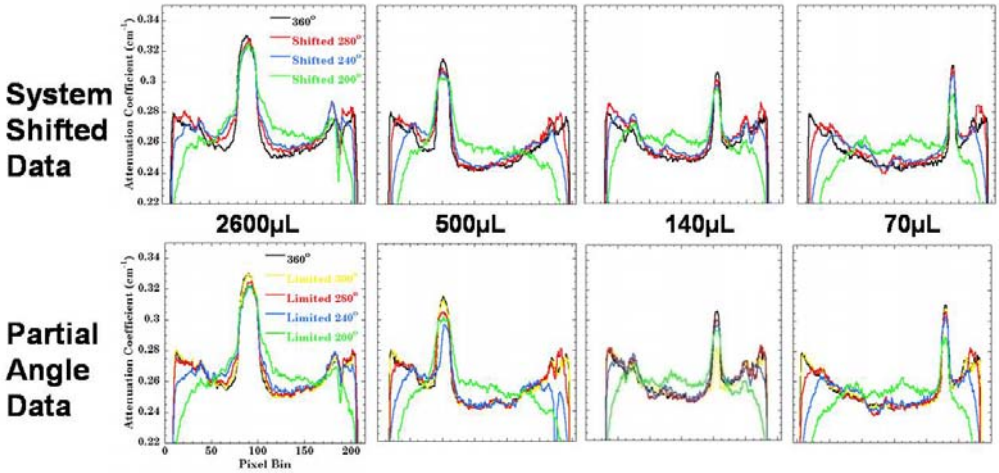

Fig. 8. Separate profiles taken from reconstructed single slices through the four balloon "lesions" on the upper plane (2600µL to 70µL from left to right) for (Top Row) shifted data sets and (Bottom Row) under partial angle (Limited) conditions. Note the increased distortion in the profiles towards the lesion edges as projections are increasingly removed while the peak 'lesion' values generally reduce.

3.3 Observer Study of Low-Contrast Objects Imaged using Novel Trajectories

Partial Angle Imaging

Fig 9 illustrates three sample images of the phantom made with acrylic spheres of decreasing size (see Fig 5, Left). Presented with images from datasets reconstructed missing 60° and 120° of projections as well as the full 360° of data, observers were asked how many spheres they could visualize. The mean sphere size was determined from observers' responses, and the statistical significance evaluated. Given that different sized spheres were present in the phantom, it was necessary to remove equivalent sectors of angles from several possible positions in the phantom. Therefore, 60°

were removed from 6 different contiguous sectors around the scan (0 to 60°, 60 to 120°, etc); for the 240° scans, 3 contiguous sectors of 120° were removed in 3 different acquisitions (0 to 120°, 120 to 240°, 240° to 360°).

Using the different sized spheres, with 60° removed, there was no significant difference between any of the sectors and the full 360° scan in terms of the smallest sized detectable sphere (3.5mm). However, with the 240° scan, a significant difference exists between the data set missing projections from 0-120° and the full 360° scan, with the smallest detectable sphere size increasing from 3.5mm to 3.75mm.

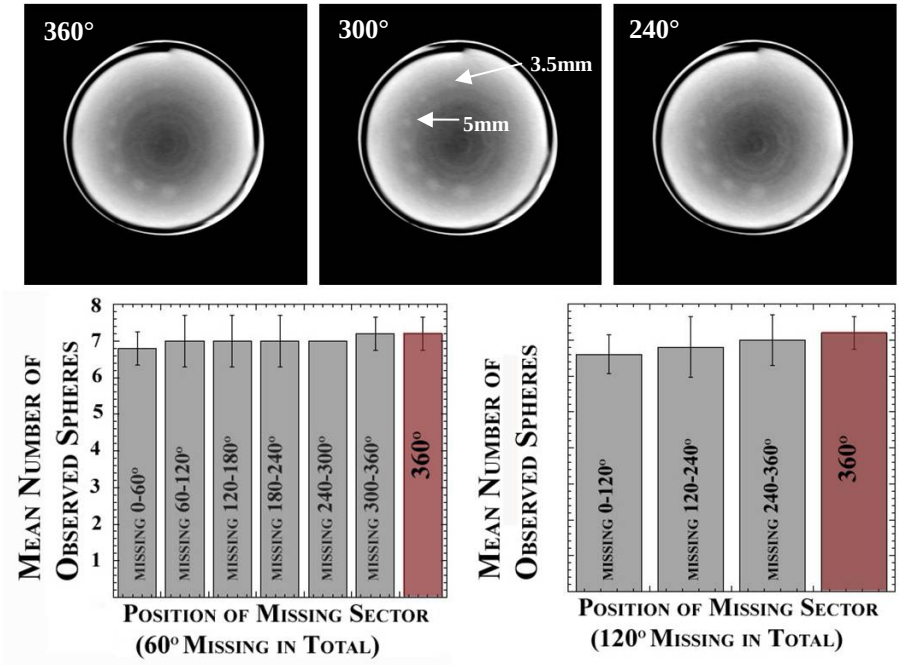

Fig. 9. (Top Row) Reconstructed images of the changing sized acrylic spheres having different segments of projection angles removed (ranges indicated). Also shown (Bottom Row) are the observers' responses when asked to indicate the number of spheres visible with 60° of projections (Bottom Row, Left) removed from different sectors around the 360° of projections – no significant difference in response was observed. The same question was asked of the observers (Bottom Row, Right) using 120° of missing data in different sectors with a significant difference being recorded for spheres reconstructed missing data from 0-120°.

Vertical System Shifting in Mid Scan

Shown in Fig. 10 are images of the circular disk phantom (see also Fig. 5, Right) reconstructed using trajectories that incorporate shifting the imaging system in mid-scan. Note the readily apparent distortion in the outer edges of the cylinder due to missing views for trajectories where the bed is raised to allow the x-ray tube to pass underneath both the head and feet sections (Case #2, see also Fig. 4, Top Row, Center); spheres located in the inner portion of the cylinder are still visible. Observers were asked how many of the spheres were noticeably distorted or of lower visibility than the others. For Case #2 with 60° removed at both head and feet, 3.4±2.3 spheres on the upper plane were considered distorted, while for spheres on the lower plane, 1.2±1.6 were considered distorted. Observers indicated the number of low-contrast 5mm spheres visible from images reconstructed from data sets missing 60° and 120° of projections. Given the wide variability in observer response, no significant difference was measured, however, it is clear that on average, the upper plane of spheres (with lower number of sampled angles) had additional distortion not found in the lower plane of spheres. It is unknown whether more realistic, irregularly shaped 'lesions' with fuzzy borders would show any significant observer difference. Importantly, the visibility of 'lesions' reconstructed from images acquired with two different system heights is well maintained with 60° spans of shifted data.

In terms of image quality assessment on a scale of 1 to 10, the results in Fig. 10 indicate that there was no statistically significant difference in the overall quality of the reconstructed spheres assessed by observers, despite obvious artifacts towards the edge of the image and a general decline in image quality as projection views of the upper plane are missed.

The presence of artifacts is particularly apparent for the upper layers which are only partially sampled in cases where shifting occurs. For Cases #2 and 3 for the 120° missing projection data span (not shown, although the images are degraded even compared to the image in Case #2, 60° shown in Fig. 10), the reconstructed imaged volume was so visually poor that the spheres could not be adequately assessed; some observers stated that only 2 or 3 spheres were visible. In fact, the reconstructed spheres were so distorted that it is difficult to envision corrections that would enable adequate image quality and content. Therefore, Cases #2, 3 for 120° were not considered.

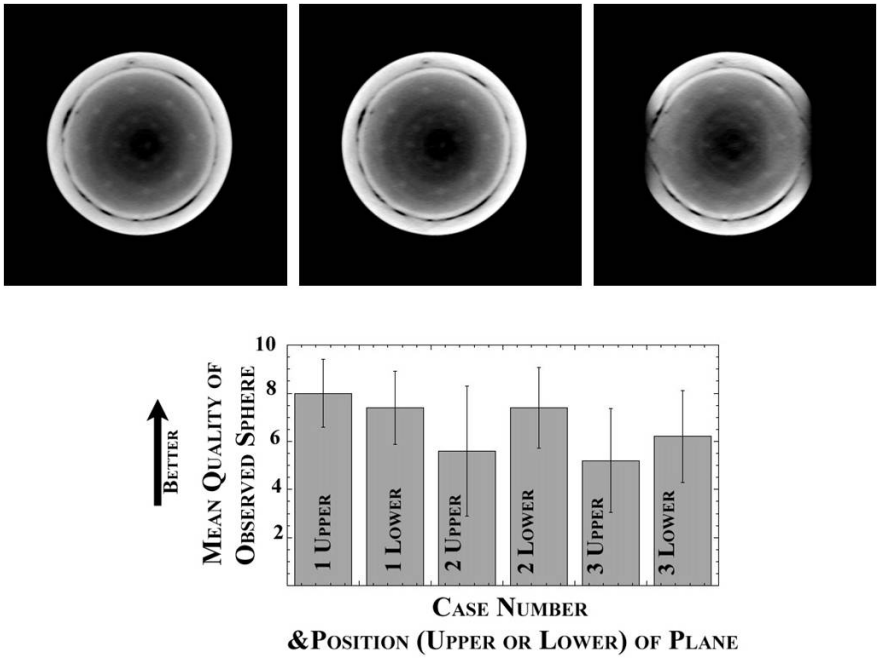

Fig. 10. (Top Row) Images of the upper plane of 5mm acrylic spheres in water, reconstructed using different schemes involving system shifting indicated on the images (see also Fig. 4 for sample setups for each Case). (Bottom Row) The observer response when asked to evaluate the mean quality of images on the upper and lower planes using various shifting cases as described above. Despite a general decline in image quality, no significant difference was seen between fully sampled and the shifted data.

4. DISCUSSION AND CONCLUSIONS

An important challenge associated with breast computed tomographic imaging is the ability of the system to reliably image the patient's chest wall. In this study, the use of novel source-detector trajectories to increase the visualization of breast tissue close to or into the anterior chest wall of a prone subject is investigated. CAD simulations are initially made, followed by qualitative assessment of high contrast images using combined partial angle and system shifting techniques. Finally the quantative results of an observer study are reported concerning the efficacy of using these trajectories to visualize low-contrast objects similar to a small lesion embedded in glandular tissue.

The cumulative finding from this study indicates that an approximate 300° acquisition trajectory or potentially using a combination of partial angle tomography of the breast in addition to accurately shifting the system with respect to the patient, produces minimal volumetric image degradation compared to a simple-circular, full 360° data set. This therefore may be a solution to viewing more of the chest wall and circumventing the physical restrictions caused by the bed design. Visibility of small low-contrast objects (similar to the scenario encountered when trying to observe a small lesion embedded in normal glandular breast tissue) becomes significantly affected when approximately 120° of data is removed from the full projection data set.

For prone patient imaging, the design of the patient bed is a vital component of the overall system and a key determinant in its ultimate clinical utility. The design must satisfy the competing demands of ensuring patient comfort to help minimize motion artifacts in raw projections while also maximizing access for the imaging system to the breast and chest wall. The current bed design, constrained by these competing demands, helps to practically separate the top of the

CT cone beam from the patient's chest wall, thus limiting the system's ability to image this important area. Novel source-detector trajectories using iterative reconstruction techniques may help to satisfy both the ergonomic and technical requirements of patient imaging, increase visualization of the chest wall, and may increase patient comfort by allowing a more comfortable bed design. Future studies incorporating the fully-suspended CT system in this hybrid configuration will emphasize the practical challenges of realizing this in a patient-imaging context, and ideally present similar high quality volumetric imaging data as for the CT-only system has in the past. When using cone beam imaging for such a dedicated application, better volumetric sampling clearly has a benefit on the final image quality.

5. ACKNOWLEDGEMENTS

This work was supported by DOD grants W81XWH-08-1-0352, W81XWH-06-1-0791,W81XWH-06-1-0765 and NIH grants R43-CA125924 and R01-CA096821. MPT is a shareholder and consultant of Zumatek. MPT is the inventor of this imaging technology, and is named as an inventor on the patent for this technology applied for by Duke. If this technology becomes commercially successful, MPT and Duke could benefit financially.

REFERENCES

[1] S. J. Glick, "Breast CT," *Annual Review of Biomedical Engineering*, vol. 9, pp. 501-526, 2007.

[2] D. J. Crotty, P. Madhav, R. L. McKinley, and M. P. Tornai, "Patient bed design for an integrated SPECT-CT dedicated mammotomography system," in *2006 Workshop on the Nuclear Radiology of Breast Cancer*, San Diego, CA, 2006.

[3] D. J. Crotty, P. Madhav, R. L. McKinley, and M. P. Tornai, "Investigating novel patient bed designs for use in a hybrid dual modality dedicated 3D breast imaging system," *2007 SPIE Med Imag Conf*, vol. 6150, 2007.

[4] P. Madhav, S. J. Cutler, D. C. Crotty, K. L. Perez, R. L. McKinley, L. Wilke, T. Wong, and M. P. Tornai, "Pilot Patient Studies Using a Dedicated Dual-Modality SPECT-CT System for Breast Imaging " in *2008 AAPM* Houston TX, 2008.

[5] P. Madhav, S. J. Cutler, K. L. Perez, D. J. Crotty, R. L. McKinley, T. Z. Wong, and M. P. Tornai, "Initial patient study with dedicated dual-modality SPECT-CT mammotomography," in *2007 IEEE Nucl Sci Symp & Med Imag Conf*, Honolulu, HI, USA, 2007, pp. 3781-7.

[6] C. N. Brzymialkiewicz, M. P. Tornai, R. L. McKinley, and J. E. Bowsher, "3D data acquisition sampling strategies for dedicated emission mammotomography for various breast sizes," *2005 IEEE Nucl Sci Symp & Med Imag Conf*, vol. 4, pp. 2596-2600, 16-22 Oct. 2004 2004.

[7] K. L. Perez, P. Madhav, D. J. Crotty, and M. P. Tornai, "Analysis of patient bed positioning in SPECT-CT imaging for dedicated mammotomography," in *Medical Imaging 2007: Physics of Medical Imaging*, San Diego, CA, USA, 2007, pp. 651037-8.

[8] R. L. McKinley and M. P. Tornai, "Preliminary investigation of dose for a dedicated mammotomography system," *2006 Proc SPIE: Phys Med Imag*, vol. 6142, pp. 60-70, 11-17 Feb. 2006 2006.

[9] S. J. Cutler, P. Madhav, K. L. Perez, D. J. Crotty, and M. P. Tornai, "Comparison of reduced angle and fully 3D acquisition sequencing and trajectories for dual-modality mammotomography," in *2007 IEEE Nucl Sci Symp & Med Imag Conf*, Honolulu, HI, USA, 2007, pp. 4044-50.

Appendix G

Co-authored Peer Reviewed Manuscript accepted for publication in Physics in Medicine and Biology

IOP PUBLISHING PHYSICS IN MEDICINE AND BIOLOGY

Phys. Med. Biol. **54** (2009) 3659–3676 doi:10.1088/0031-9155/54/12/004

Evaluation of tilted cone-beam CT orbits in the development of a dedicated hybrid mammotomograph

P Madhav[1,2], D J Crotty[1,2], R L McKinley[3] and M P Tornai[1,2]

[1] Department of Radiology, Duke University Medical Center, Durham, NC 27710, USA
[2] Department of Biomedical Engineering, Duke University, Durham, NC 27708, USA
[3] Zumatek Incorporated, Chapel Hill, NC 27519, USA

E-mail: priti.madhav@duke.edu

Received 13 February 2009, in final form 13 April 2009
Published 28 May 2009
Online at stacks.iop.org/PMB/54/3659

Abstract

A compact dedicated 3D breast SPECT-CT (mammotomography) system is currently under development. In its initial prototype, the cone-beam CT sub-system is restricted to a fixed-tilt circular rotation around the patient's pendant breast. This study evaluated stationary-tilt angles for the CT sub-system that will enable maximal volumetric sampling and viewing of the breast and chest wall. Images of geometric/anthropomorphic phantoms were acquired using various fixed-tilt circular and 3D sinusoidal trajectories. The iteratively reconstructed images showed more distortion and attenuation coefficient inaccuracy from tilted cone-beam orbits than from the complex trajectory. Additionally, line profiles illustrated cupping artifacts in planes distal to the central plane of the tilted cone-beam, otherwise not apparent for images acquired with complex trajectories. This indicates that undersampled cone-beam data may be an additional cause of cupping artifacts. High-frequency objects could be distinguished for all trajectories, but their shapes and locations were corrupted by out-of-plane frequency information. Although more acrylic balls were visualized with a fixed-tilt and nearly flat cone-beam at the posterior of the breast, 3D complex trajectories have less distortion and more complete sampling throughout the reconstruction volume. While complex trajectories would ideally be preferred, negatively fixed-tilt source–detector configuration demonstrates minimally distorted patient images.

(Some figures in this article are in colour only in the electronic version)

1. Introduction

Over the past decade, dual-modality tomographic imaging systems have grown in both clinical and preclinical popularity and offer great promise in the detection and staging of numerous

cancerous diseases, monitoring and prediction of treatment therapies and improving precision of surgical biopsies. The main benefit of acquiring 3D transmission and emission data is in the ability to fuse the anatomical framework of an object obtained from a transmission image with an emission image that provides the *in vivo* localization of the molecular tracer, e.g. in a tumor. Additionally, the transmission data can be used as an attenuation map to compensate the emission data for photon attenuation and absorption by overlapping structures, making the molecular images more quantitatively and spatially accurate. It is anecdotally observed that integrating complementary anatomical and molecular functional information can lead to further improvements in visual quality and quantitative accuracy over independent systems alone (Shreve 2000, Israel *et al* 2001, Hany *et al* 2002, Hasegawa *et al* 2002, Schillaci and Simonetti 2004).

Our lab has been working on developing such a dual-modality single photon emission computed tomography (SPECT) and computed tomography (CT) imaging system specifically dedicated to fully 3D breast imaging (Crotty *et al* 2005, 2006, Madhav *et al* 2006). With the compact, high performance gamma camera of the SPECT system (Brzymialkiewicz *et al* 2006) and the novel quasi-monochromatic x-ray cone-beam of the CT system (McKinley *et al* 2005b), both systems have independently yielded visualization of small lesions in the breast, especially ones closer to the chest wall. Each system was first developed on its own 3D positioning gantry which permitted simultaneous azimuthal and polar tilting motion capabilities (Brzymialkiewicz *et al* 2005, McKinley *et al* 2005a). This allowed the source–detector combinations to be positioned anywhere in a hemisphere about a pendant, uncompressed breast during a tomographic acquisition.

In its initial hybrid integration described here, the SPECT system retains its fully 3D positioning capability. However, the CT system is placed at a fixed-tilt angle and restricted to only a 360° circular rotation around the vertical axis of a pendant breast. Various groups that have developed cone-beam dedicated breast CT tomographic scanners have also been limited to using a circular scan during image acquisition (Chen and Ning 2002, Vedula and Glick 2003, Chen *et al* 2005, Boone *et al* 2006). This limits the CT system in its ability to image deep into the breast and chest wall, and introduces insufficient sampling which has previously been shown to be eliminated by using 3D complex acquisition trajectories (Kudo and Saito 1990, Zeng *et al* 1994, Junhai *et al* 2003, McKinley *et al* 2005a, Tornai *et al* 2005). In this study, we describe the configuration of the dual-modality SPECT-CT system and evaluate the effects on object distortion with the CT system at different stationary tilts. It is necessary to determine if a stationary tilt will (1) permit maximal access to the patient's breast; and (2) provide sufficiently sampled information.

2. Materials and methods

2.1. Overview of the SPECT-CT system

The first prototype compact dual-modality SPECT-CT system was built (figure 1) for imaging pendant uncompressed breasts (Madhav *et al* 2006). Both systems, using separate detectors to view an object in the common field-of-view (FOV), rest on a common rotation stage (model RV350CCHL, Newport Corp., Irvine, CA) to allow an azimuthal rotation of 360° around the vertical axis of the breast. The SPECT system is positioned 90° relative to the x-ray source–detector axis. With both systems on the same gantry, the subject is not required to move in between the SPECT and CT acquisitions. A customized patient bed, placed above the hybrid system, is built to allow for patient comfort, shield from scatter x-rays and avoid collision with the equipment below (Crotty *et al* 2007a).

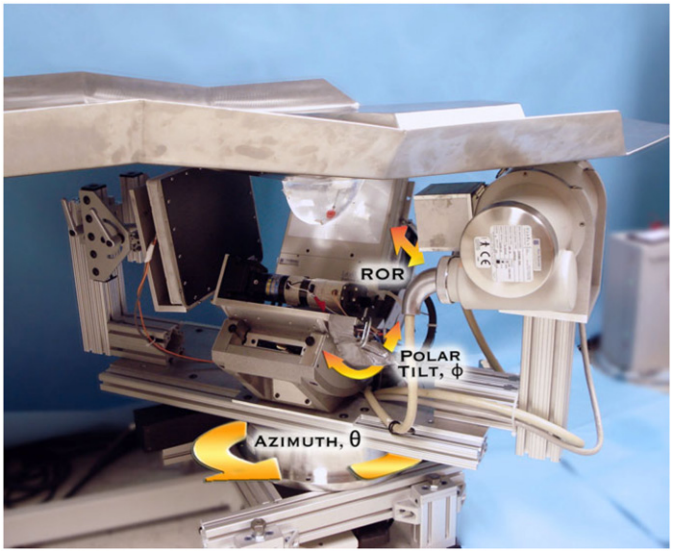

Figure 1. Photograph of the prototype dual-modality dedicated breast imaging tomographic system. The SPECT sub-system (center, back) is placed orthogonally to the x-ray tube (right, front) and digital flat-panel detector (left, toward back). The arrows illustrate system motions (azimuthal, polar and radius of rotation (ROR)). A customized patient bed is located above the hybrid system, shown with a breast phantom pendant through the center opening in the table. Note that the lesion-containing breast phantom is in the common FOV of both systems.

Our current parallel-beam emission tomography system uses a compact 16 × 20 cm^2 field-of-view Cadmium Zinc Telluride (CZT) gamma camera (model LumaGEM 3200S^{TM}, Gamma Medica, Inc., Northridge, CA) with discretized crystals, each 2.3 × 2.3 × 5 mm^3 on a 2.5 mm pitch. The measured energy resolution of the gamma camera at 140 keV is 6.7% FWHM and the collimator sensitivity is 37.9 cps MBq^{-1} (Brzymialkiewicz *et al* 2005). Higher energy resolution is the primary reason for using the CZT camera over a scintillator-based camera for the SPECT system. This system has a parallel-hole collimator with hexagonal holes (1.2 mm hole size flat-to-flat, 0.2 mm septa and 25.4 mm height). The camera is attached to a laboratory jack (model M-EL120, Newport Corp., Irvine, CA) and a goniometric cradle (model BGM200PE, Newport Corp., Irvine, CA) permitting various radius of rotations (RORs) and polar tilts (ϕ), respectively.

Our existing cone-beam transmission tomography system uses a rotating tungsten target x-ray source (model Rad-94, Varian Medical Systems, Salt Lake City, UT) with a 0.4/0.8 mm nominal focal spot size and 14° anode angle and a 20 × 25 cm^2 FOV CsI(T1)-based amorphous silicon digital x-ray detector (model Paxscan 2520, Varian Medical Systems, Salt Lake City, UT) with a grid size of 1920 × 1536 pixels and 127 μm pitch. Source and detector are secured to the same aluminum plate as the SPECT system. A custom-built collimator is attached to the x-ray source to hold ultra-thick K-edge beam shaping filters to produce a quasi-monochromatic beam (McKinley *et al* 2005b). The advantages of using a quasi-monochromatic source are (1) improving the visualization of tissues with very small differences in attenuation coefficients; (2) using a low x-ray dose and (3) minimizing beam hardening effect. For these studies, a 60 kVp x-ray beam and a 0.051 cm cerium filter ($Z = 58$, $\rho = 6.77$ g cm^{-3}, K-edge = 40.4 keV, Santoku America, Inc., Tolleson, AZ) were used. This filter was approximately a 100th attenuating value layer which reduced the exposure of the incident x-ray beam by a factor of 100 and yielded a spectrum that had a mean energy of approximately 36 keV and the

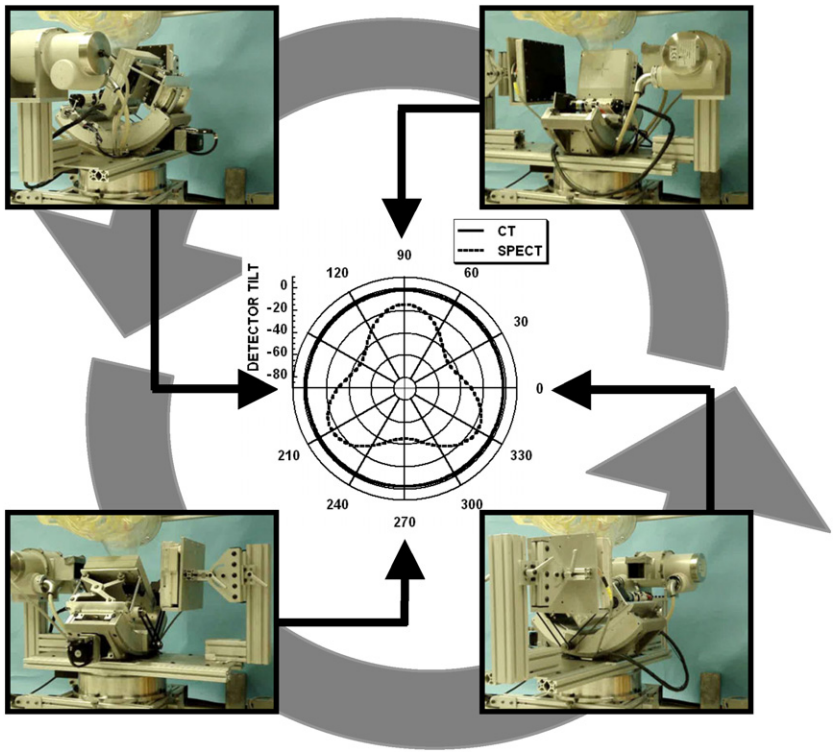

Figure 2. Photographs at different positions of the dual-modality system rotating around a pendant, uncompressed breast and torso phantoms. Polar plot (center) is shown for the SPECT (3D noncircular trajectory) and CT sub-systems (simple fixed-tilt circular orbit).

FWHM of 15% (McKinley *et al* 2004). In the current hybrid setup, the source-to-image distance (SID) is 60 cm and source-to-object distance (SOD) is 38 cm resulting in a magnification of 1.57 for an object located at the center of rotation of the system.

Figure 2 illustrates the current dual-modality SPECT-CT system rotating around a pendant uncompressed breast phantom. As shown in the corresponding polar plot, the SPECT sub-system has fully 3D positioning capabilities while the CT sub-system remains at a fixed polar tilt as the system rotates 360° around the breast. Along with the parallel-beam imaging geometry of the SPECT sub-system, the entire volume of the breast is in the FOV of both systems even at different cone-beam CT tilts (figure 3).

2.2. Data acquisition

Object visualization, distortion and frequency dependence at different planes of the image volume were measured using a Defrise-type disk phantom (model ECT/MI-DEF/P, 5 mm disk thickness, 5 mm disk spacing, Data Spectrum Corp., Hillsborough, NC) with and without 3.5 mm acrylic balls placed in the interstitial spaces between the disks (figure 4, left). Another measurement utilized a breast phantom consisting of numerous acrylic balls suspended throughout the entire volume. These 'suspended spheres' were created by arranging 5 mm diameter acrylic balls on 10 mm center-to-center pitch in a cross pattern on a thin plastic sheet. Each plastic sheet was stretched and glued to the bottom of a circular acrylic frame (20 mm height). These circular bands of varying diameters were stacked together to roughly

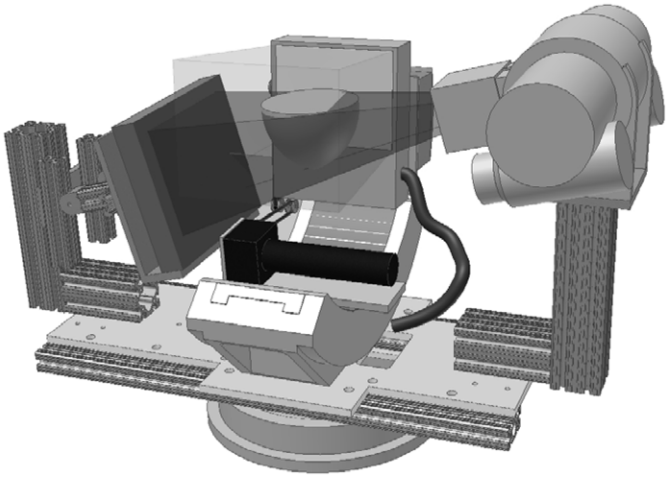

Figure 3. 3D CAD model of the SPECT-CT system with a breast placed at the center of rotation. The breast is in the common FOV of both systems regardless of the tilt of the CT sub-system. Translucent volumes illustrate the intersection of both the parallel-beam of the SPECT sub-system and the cone-beam of the CT sub-system.

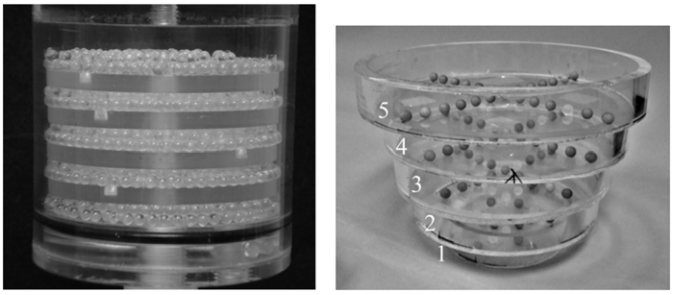

Figure 4. (left) Photograph of the disk phantom with 3.5 mm acrylic beads in the gaps between the disks. (right) Photograph of 5 mm diameter acrylic spheres suspended on thin plastic sheets inside each circular band. Each frame or level is labeled 1 through 5, with 1 being the smallest diameter frame.

contour the shape of the breast (figure 4, right). The frames could also be immersed in liquids while retaining the distribution of spheres on a single, nominally attenuating plane. For this set of experiments, five circular concentric frames were placed in a 1050 mL breast phantom shell (nipple-to-chest distance of 11 cm, medial-to-lateral distance of 17 cm and superior–inferior distance of 18 cm). Throughout this paper, each frame of this phantom will be referred to by a number with one representing the circular band with the smallest diameter (nearest the pendant nipple).

Several measurements were taken in air and with the breast uniformly filled with mineral oil to provide different contrasts between the acrylic spheres and breast background. Due to the physical distortion of the breast phantom after filling it with oil (i.e. due to the added weight), only the four smallest annular disks fit in the breast shell. Mineral oil has an intrinsic density of 0.87 g cm^{-3} and acrylic has a density of 1.19 g cm^{-3}.

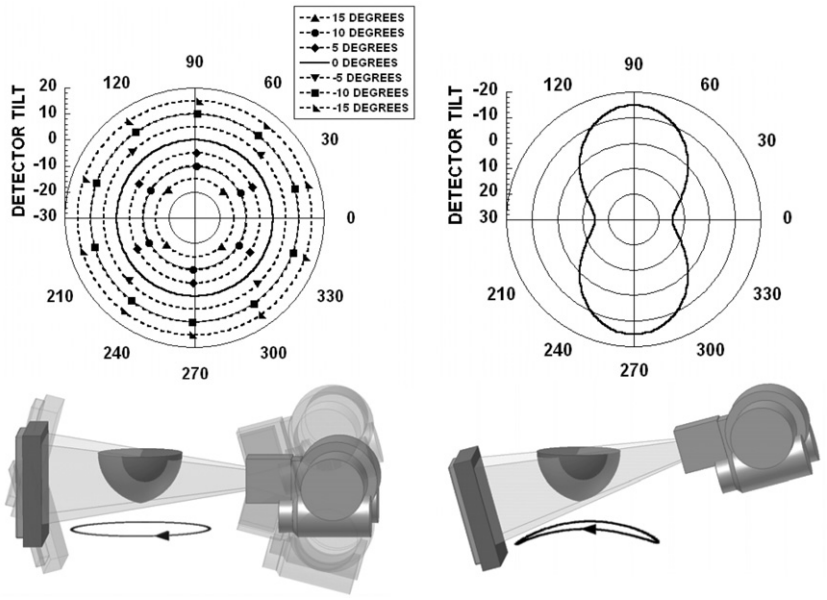

Figure 5. (top) Polar plots for (left) simple tilted circular orbits and (right) 3D saddle trajectory. Polar tilt is defined by the radius of the circle, and the azimuthal angle (location) is defined around the circumference of the circle. (bottom) The 3D CAD drawings of the CT system setup and dark circles underneath are shown to illustrate the location(s) of the source–detector pair during an acquisition. Negative polar tilt is defined as the x-ray detector moving down (or the x-ray source moving closer to the patient bed).

Initial measurements were obtained using a simple circular trajectory at 0°, ±5°, ±10° and ±15° fixed polar tilts (figure 5, left), and a saddle trajectory having +15° to −15° ranging polar tilts (figure 5, right). The CT system pivots at the intersection point between the central ray of the cone-beam and center-of-rotation axis. A prior study showed that using a noncircular acquisition orbit (i.e. saddle trajectory) will improve sampling (satisfying Tuy's data sufficiency condition) and reduce distortion (McKinley *et al* 2005a). Note that a negative polar tilt is defined as the x-ray source moving up (closer to the patient bed) and the detector moving down (closer to the ground). For ease of acquiring images using the various tilted circular orbits and complex 3D trajectory motion, all acquisitions were taken on the independent CT system which had a 55 cm SID, 35 cm SOD and 1.57 magnification. In this setup, the x-ray source and detector were affixed on their own base plate which rested on top of the goniometer and rotation stage. Similar to the SPECT sub-system on the hybrid device, the goniometer allowed the CT system to be tilted in the polar direction to provide the flexibility to acquire tomographic projection data at various fixed tilted circular orbits and complex trajectories. Tube potential was set at 60 kVp with a 1.25 mAs exposure per projection (McKinley and Tornai 2006). Projection images were collected every 1.5° through a 360° azimuthal acquisition for a total of 240 projections. The total scan time for each acquisition was 6 min. Although the breast is somewhat truncated (seen in figure 5), the suspended sphere phantom was placed in the breast volume such that it was in the center of the field-of-view and not truncated.

2.3. Patient study

A volunteer with biopsy confirmed breast cancer (adenocarcinoma) in her left breast was imaged with the dedicated breast CT sub-system having a tilted circular orbit, under a protocol

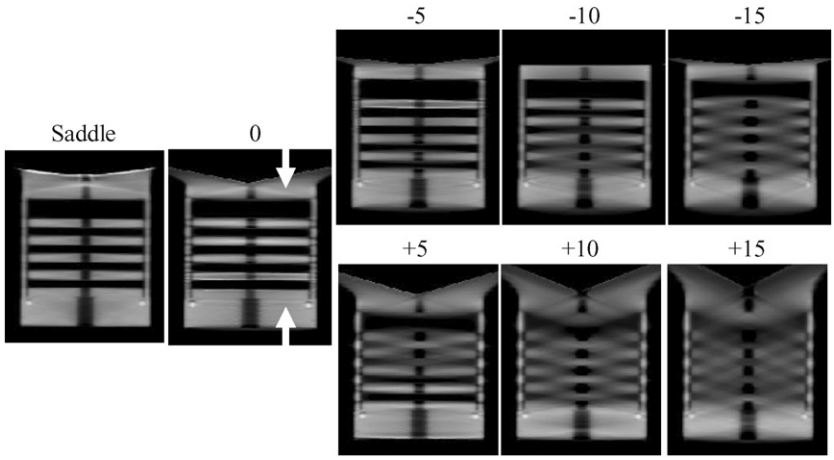

Figure 6. Sagittal reconstructed slices of the disk phantom for 0, ±5, ±10 and ±15, and saddle acquisition trajectories.

approved by the Duke University Medical Center institutional review board (IRB). Informed written consent was obtained.

The subject was scanned with the hybrid system and a customized patient bed. The CT sub-system was at a -6.2° tilt for the entire 360° acquisition. Tube potential was set at 60 kVp with a 1.25 mAs exposure using our standard Ce filtration.

2.4. Image reconstruction and data analysis

Image reconstruction was performed on the CT projection images by increasing the log likelihood via the iterative ordered-subset transmission reconstruction algorithm (OSTR) (Erdogan and Fessler 1999), using a ray-driven image reconstruction code, CT-Map (Bowsher *et al* 2002), which also accounted for the 3D motion of the CT system (McKinley *et al* 2005b). Projection images were corrected for gain and offset and binned to 4×4 pixels. Reconstruction parameters were set to 5 iterations, 16 subsets, a $350 \times 350 \times 384$ reconstruction grid and a 508 μm^3 voxel size. The total reconstruction time in this iterative framework was 4 h.

Object distortion was observed using the sagittal and coronal reconstructed slices of the disk and suspended sphere phantoms collected for all acquisition orbits. Horizontal and vertical line profiles were also drawn through the disks and acrylic balls to compare the differences in image distortion and artifacts for all acquisition trajectories.

3. Results and discussion

3.1. Disk phantom without acrylic balls

The sagittal reconstructed slices of the disk phantom (figure 6) show that the tilted cone-beam acquisition orbits result in disk distortion especially for images acquired at higher positive tilts, where it becomes more difficult to visibly separate out each of the five disks. At some locations in the reconstructed volumes, the apparent positions of the disk and air layer appear to be reversed, a common problem with aliased or highly undersampled tomographic data. Tuy's data sufficiency condition states that for cone-beam imaging, each plane crossing the object must intersect the orbit of the focal point at least once (Tuy 1983, Smith 1985). Due to

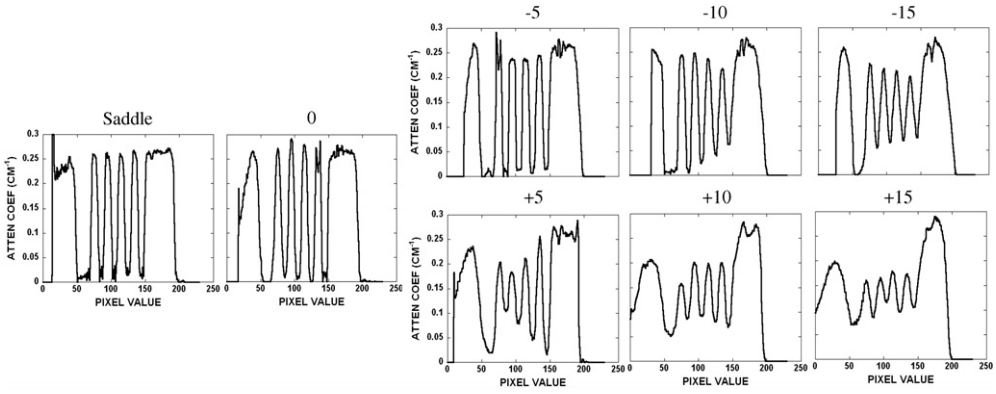

Figure 7. Line profiles obtained vertically through the disks in the disk phantom for all acquisition trajectories. Values indicate degrees of tilt or complex trajectory. Figure 6 indicates the position of the line profile shown between the white arrows.

the failure to meet this condition with a wide cone-beam, reconstruction of slices for locations further away from the flat plane of the beam (which is parallel to the ground and intersects the focal point) contains significant distortion and errors. This incompleteness in circular trajectories with cone-beam acquisitions has been seen to degrade the reconstructed images, especially with the use of large cone angles (Webb *et al* 1987, Kudo and Saito 1990, Davis 2005, McKinley *et al* 2005a).

Figure 5 (bottom left) illustrates the cause of the insufficient sampling in our experimental setup. When the CT system is at a -10° tilt with the detector positioned down (closer to the ground), the cone-beam is relatively flat near the top of the phantom. This location would be nearer to a patient's chest wall. Better sampling and minimal disk distortion are seen in the top area of the reconstructed images since these planes intersect the orbit of the vertex of the cone-beam (figure 6, top row). A loss in resolution and inaccuracy in reconstruction are observed when the x-rays travel at a large enough angle that intersects at least two disks. Not surprisingly, the reverse is true for the $+10^\circ$ tilt case, where the insufficient sampling now occurs for slices that are reconstructed from divergent x-rays away from the flat plane at the bottom of the cone-beam (figure 6, bottom row). Due to the large included cone-beam angle of 28°, geometric distortion increases with circular orbits. However, this limitation can be overcome by using a 3D complex acquisition trajectory such as a saddle orbit, which is easily implemented on our independent, 3D CT imaging system. As shown in the reconstructed image slices (figure 6, left), the saddle trajectory can reproduce the object with minimal geometrical distortion due to the improved sampling throughout the object volume.

A vertical line profile was obtained for all trajectories semi-quantitatively confirming the disk distortion (figure 7) seen in the earlier reconstructed images (figure 6). The shape of the line profile for the saddle acquisition has a relatively distortion-free and constant attenuation coefficient value through each of the five disks and cylindrical support structure, in contrast to the varying results from the tilted acquisition trajectories. Those other profiles illustrate definite distortion and artifacts especially for planes farther away from the flat, more completely sampled plane of the cone-beam acquisition. These distortions cause the profiles to have a greater variation in the attenuation coefficient value among each of the disks. For instance, in the -10° tilt situation, the profile taken through the disks near the top of the disk phantom is less distorted than the profile taken through the disks further away. Therefore, it is clearly illustrated how complex 3D acquisition trajectories can overcome these cone-beam

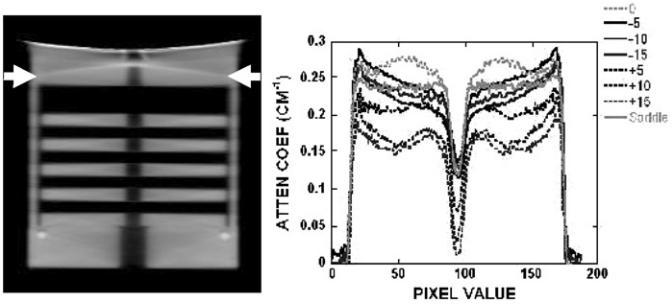

Figure 8. (left) Reconstructed sagittal slice of the disk phantom acquired with the saddle trajectory. (right) Horizontal line profile for all acquisition trajectories. Arrows indicate the position of the profile.

sampling artifacts, especially for the outer planes of the beam where distortions become more significant.

A horizontal line profile was also drawn across regions of the reconstructed images of the disk phantom (figure 8, right). For the profiles obtained with simple circular orbits, cupping artifacts were observed and became worse at locations further away from the flat horizontal plane of the cone-beam. Cupping artifacts are generally considered to be consisted of scatter and beam hardening in the projection images. Since the disks are virtually suspended in air, scatter is minimal in this experimental setup. Also, the independent dedicated breast CT system uses a quasi-monochromatic beam which virtually eliminates beam hardening (McKinley *et al* 2005b, Crotty *et al* 2007b). Therefore, the apparent cupping artifacts are most likely caused by data insufficiency. The profile in figure 8 shows the saddle trajectory having more constant profile values than the other tilted circular acquisition orbits. Using a table of x-ray mass attenuation coefficients, the measured attenuation coefficient of acrylic at 36 keV is 0.30 cm^{-1} (Hubbell and Seltzer 1996). The line profile shows a reduced attenuation coefficient value primarily due to the presence of scatter. Negative circular acquisition orbits display a slight cupping artifact due to the location of the flat plane of the cone-beam relative to the position of the line profile. A distinct and consistent decrease in attenuation coefficient values at higher positive angle acquisition orbits is observed since this region is in the outer planes (i.e. x-rays at larger angles) of the cone-beam, relative to where the profile was measured.

3.2. Disk phantom containing additional acrylic balls

Disk distortion due to undersampling was next examined with the disk phantom uniformly packed with 3.5 mm acrylic beads in the interstitial spaces between each disk. The intent with this modified disk phantom was to evaluate whether there was an object frequency dependence on the reconstructed image results by imaging both the disks and considerably smaller acrylic balls simultaneously. Figure 9 shows a not surprisingly similar disk distortion as seen for the disk-only phantom without the balls. Furthermore, despite the inaccurate reproduction of the disks located further away from the fully sampled plane of the cone-beam, some small acrylic beads can be singled out, and appear to be less distorted in these same areas. The saddle trajectory-acquired data, which clearly illustrate the visualization of all balls in that given slice, can be used as the standard with which to compare all the other acquired and reconstructed data. A line profile through the bottom row of acrylic balls in the phantom confirms that each can be distinctly separated (figure 10). These findings suggest that identifying an amorphous object in reconstructed space partly depends on the distribution of its frequency components (Bartolac

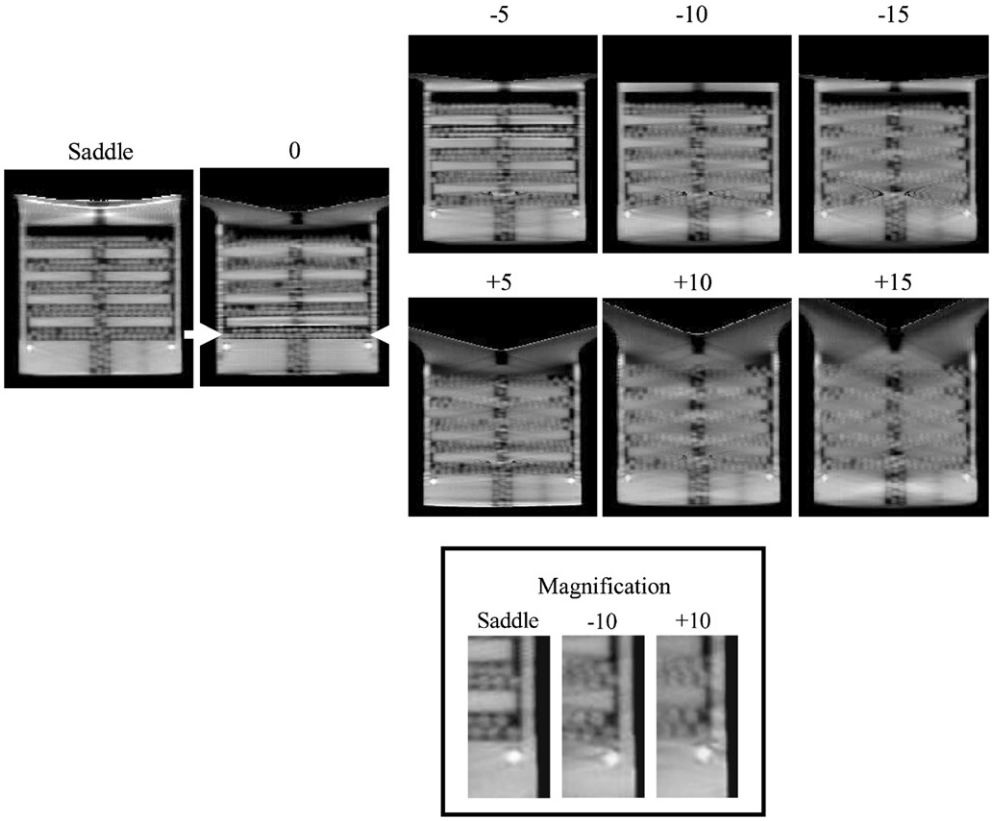

Figure 9. Sagittal reconstructed central slices of the disk phantom containing additional acrylic balls for 0, ±5, ±10 and ±15, and saddle acquisition trajectories. (Bottom) Magnification of a small area of the disk phantom for ±10 and saddle acquisition trajectories to illustrate the visualization of the acrylic balls.

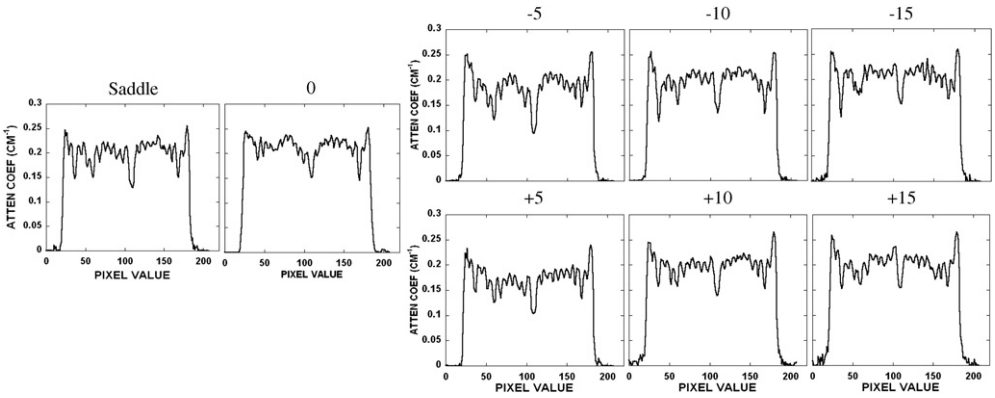

Figure 10. Horizontal line profile taken through the bottom row of acrylic balls in the disk phantom for all acquisition trajectories. Figure 9 indicates the position of the line profile shown between the white arrows.

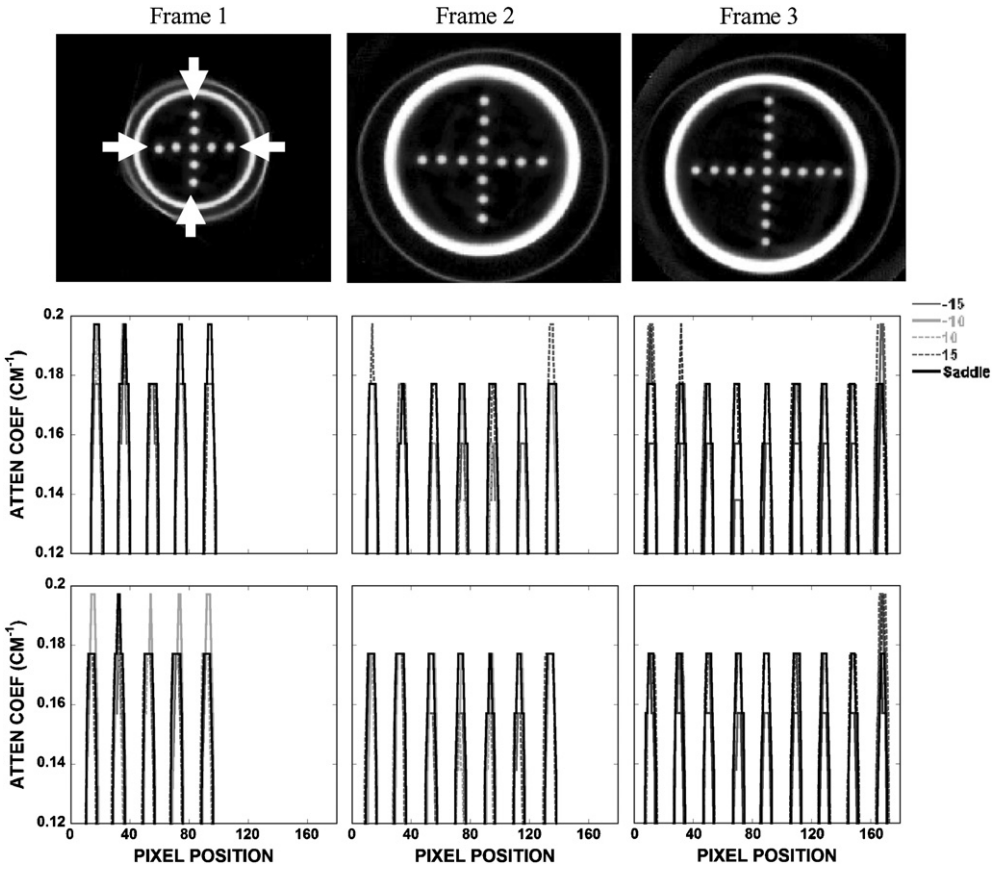

Figure 11. (top) Reconstructed coronal slices of the spheres arranged in a cross pattern acquired with saddle. Outer thin perimeter is the actual breast cup; inner thicker annulus is the acrylic frame supporting the sheet suspending the balls. (middle) Vertical and (bottom) horizontal profiles drawn through the acrylic balls along the directions indicated between the white arrows.

et al 2006). In this case, the high frequency and discrete objects (i.e. acrylic balls) remain more preserved than the low-frequency information (i.e. disks). One study has previously shown that data collected with larger cone angles sustained high-frequency details despite the distortion and artifacts associated with cone-beam imaging, while smaller cone angles maintained low-frequency details at the expense of the lower signal-to-noise ratio (Davis 2005). Our results with the dedicated mammotomographic imaging system are consistent with these previous findings. For all tilted orbits, figure 9 shows that the low-frequency information in the disks is preserved around the area of the flat plane of the cone-beam (i.e. small cone angles) while at locations further away (i.e. large cone angles) the high-frequency information of the acrylic spheres is kept regardless of the disk distortion. Not surprisingly, use of the more completely sampling saddle trajectory nearly completely eliminates these sampling-related distortions.

3.3. Suspended spheres in air in the breast phantom

Object distortion was additionally examined in different coronal slices of a breast-shaped phantom with the suspended sphere phantom inside its tiered frame. Horizontal and

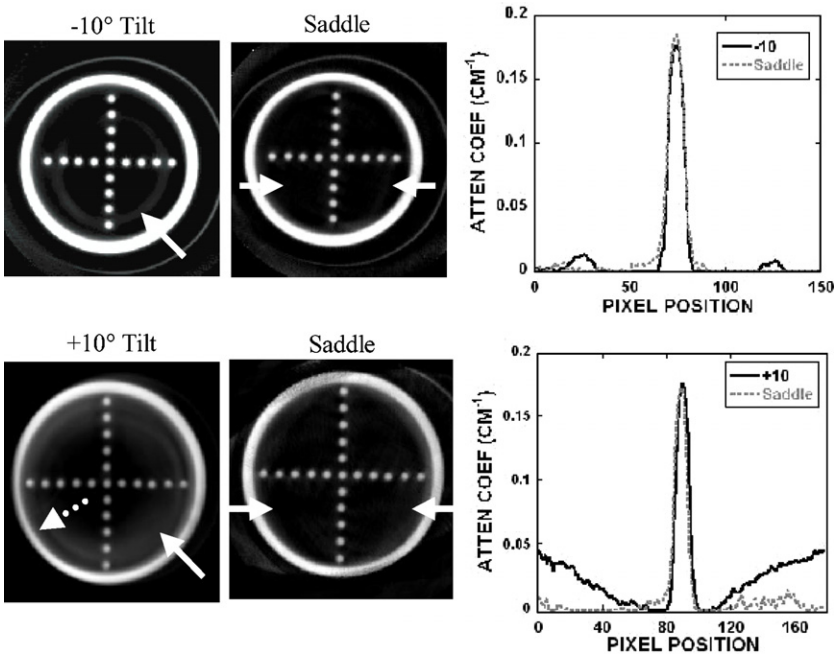

Figure 12. (top left) Reconstructed slice of frame 3 obtained with the −10° tilted orbit. (bottom left) Reconstructed slice of frame 4 obtained with the +10° tilted orbit. Solid arrow illustrates an overlapped region in which the frame below can also be seen in this single slice (shown at the arrow tip). Dotted arrow illustrates the geometric distortion of the acrylic frame. (middle column) Reconstructed slice of the same phantom acquired with the saddle trajectory. (right column) Line profile (obtained from between arrows on the saddle slice) shows some artifacts due to the overlapped regions in the slice acquired with the (top) −10° and (bottom) +10° tilts.

vertical lines drawn across images of the acrylic balls in the three smallest circular disks (frames 1–3) placed closest to the nipple showed negligible differences among different acquisition trajectories (i.e. fixed tilt or saddle) (figure 11). However, close inspection of the reconstructed coronal slices through each of the annular disks obtained using stationary polar tilt orbits revealed overlapping structures (figure 12). For the −10° tilt cone-beam acquisition, there is nearly complete sampling close to the top slice (near the chest wall) where all objects are more completely sampled and no overlapping (i.e. out-of-plane) structures can be seen there. However, with a negative system tilt, overlapping structures (i.e. from the frame below) become more noticeable in reconstructed slices closer to the nipple (figure 12, top left). Due to the insufficient polar sampling that does not 'fill in' additional views of the object in the FOV, out-of-plane information is inaccurately superimposed on any single plane of interest (shown by the white solid arrow in figure 12, top left). The reverse trend is true in the +10° tilt case (figure 12, bottom). However, using the saddle trajectory, there is more complete polar sampling yielding far fewer noticeable artifacts in the reconstructed slices (figure 12, middle column). The line profiles (figure 12, right column) illustrate how out-of-plane object information acquired with an incomplete sampling trajectory can contribute contaminated information into a given plane of interest. With 3D acquisition trajectories, such as saddle, there is more complete sampling of the object volume in the polar and azimuthal directions, resulting in the reduction of overlapping structures originating out-of-plane. Although more of the acrylic balls can be clearly seen when the top of the cone-beam is level (i.e. −10° tilt)

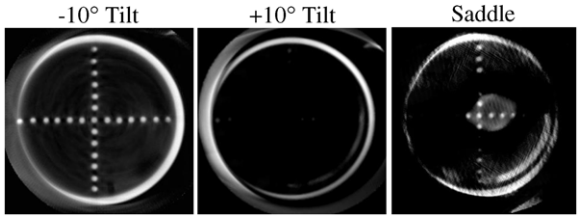

Figure 13. Reconstructed slice of frame 5 acquired at (left) -10°, (middle) $+10^\circ$ tilt and (right) saddle trajectory. The top plane at the -10° tilt is more uniformly sampled, whereas this frame is out of the FOV for many of the angles with the other two trajectories. Even though more acrylic balls are seen at the -10° tilt, 3D complex trajectories have less distortion and more complete sampling throughout the reconstruction volume.

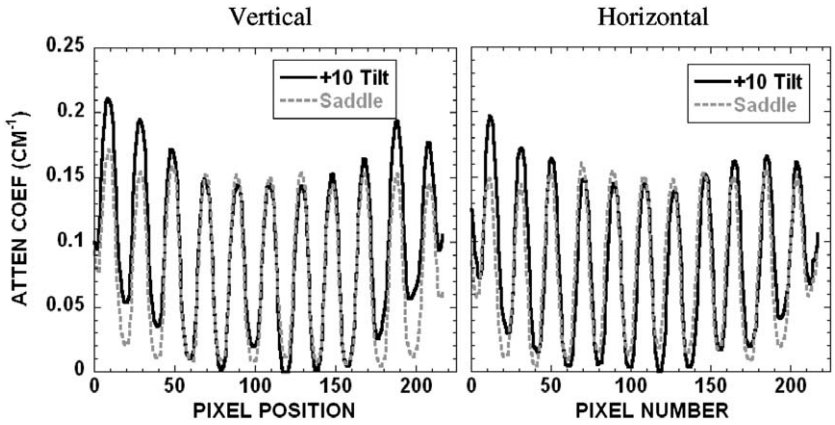

Figure 14. (left) Vertical and (right) horizontal profiles over lesions of frame 4 obtained with the $+10^\circ$ tilt and saddle shown in figure 12, bottom.

near the back of the pendant breast (i.e. near chest wall), complex 3D trajectories overall allow for less distortion and more complete sampling (figure 13).

Profiles drawn over the acrylic balls of frame 4 shown in figure 12, bottom, are illustrated in figure 14. Consistent with the earlier disk measurements (figure 8), the horizontal and vertical profiles also show that there is a cupping artifact with the fixed-tilt orbit by observing the intensities from the edge toward the center, which could be mistaken for scatter or beam hardening. This is missing from the saddle-acquired data due to its more sufficient sampling throughout the imaged volume.

Effects of insufficient sampling were also seen in the reoriented sagittal slices of the breast phantom (figure 15). When the system is at a -10° tilt, there is better sampling at the top of the reconstructed volume compared with the bottom. This is illustrated by the uniformity of the peak heights of the profiles across the FOV. This phenomenon is reversed for the $+10^\circ$ tilt, which again shows a similar cupping artifact as illustrated earlier, in which the plane was located at an extreme edge of the cone-beam. However, while the particular image shows artifacts at the top with a saddle trajectory, line profiles confirm that there is uniformity of signal amplitude through the entire reconstructed volume, for the indicated spheres.

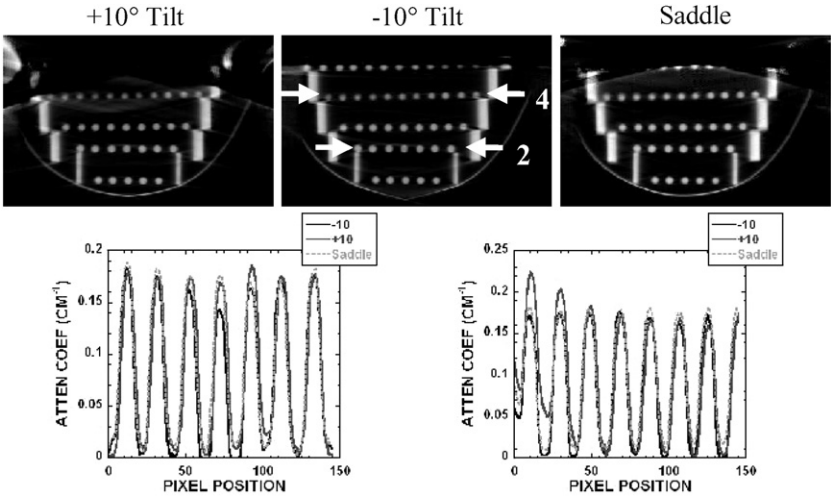

Figure 15. (top) Sagittal reconstructed slices of the ball phantoms acquired at indicated trajectories. (bottom) Profiles drawn through the ball phantom (bottom left) at frame 2 (indicated in the top-middle image) and (bottom right) at frame 4. Tilt at -10° shows greater peak uniformity at frame 4, while the $+10^\circ$ tilt shows more uniformity at frame 2. Saddle trajectory shows stable peak height uniformity throughout the reconstructed volume.

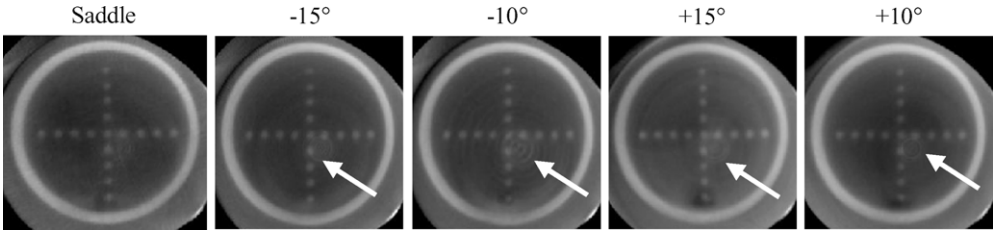

Figure 16. Reconstructed slices of frame 3 of the suspended sphere phantom in oil acquired at various acquisition trajectories as indicated. Although the breast phantom is truncated, the circular frames are completely in the FOV. Images acquired with a fixed polar tilt and circular orbit had a circular ring due to nonuniformity errors (indicated by an arrow) in some of the reconstructed slices. However, in the same slice for the saddle trajectory, there is no circular ring apparent.

3.4. Suspended spheres in oil in the breast phantom

In order to assess whether these phenomena are visible in lower contrast environment, the breast shell containing the suspended sphere phantom was uniformly filled with mineral oil. Figure 16 shows the reconstructed slices of frame 3 measured with the different indicated trajectories. When examining the images for all trajectories, a series of circular rings appear in the reconstructed slices, except for the saddle trajectory. Typically, these rings in reconstructed images occur due to the nonuniform response between detector elements, errors in detector gain calibration, etc. The advantage of using a 3D complex trajectory such as saddle is that since the same detector element does not always view the object from the same vantage point, the detector nonuniformity effect is not compounded hence amplified. For this reason, reconstructed images acquired with the 3D saddle trajectory tend to not have these artifacts.

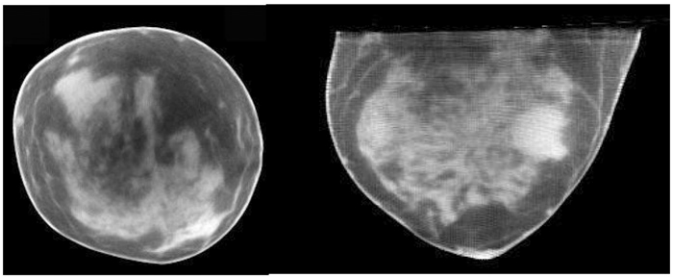

Figure 17. Reconstructed CT (left) coronal and (right) transverse image slices of human subject volunteer.

As with the experiments in air, horizontal line profiles (not shown here) drawn over the acrylic balls near the chest wall (or back of the breast phantom) also showed improved sampling for the negative tilted orbits, since this layer of the phantom was located closer to the flat part of the cone-beam.

3.5. Patient data

Figure 17 shows the result of our first CT patient study acquired with a -6.2° tilted orbit. The real human subject data are meant to illustrate here the high-frequency content as well as the nonuniform nature of the object ultimately intended to be imaged. Although the geometric phantoms have shown the known and consistent artifacts due to undersampling with circular cone-beam acquisitions, these patient images show that the perception of distortion and reconstruction inaccuracy are minimal and details are preserved (Madhav *et al* 2008). As described in the previous sections, this is due to small negative tilts having more complete sampling near the chest wall and the components of the breast consisting of more high-frequency detail.

4. Conclusion

Imaging with a dedicated dual-modality breast imaging tomographic system may help to improve identification and localization of lesions during patient screening, diagnostic work-ups and therapeutic monitoring of response. The two main advantages of having a dedicated versus a whole-body imaging system are that the x-ray radiation dose is limited to only the breast and axillary regions. Thus, imaging can be optimized for the breast, and potentially 'peer' into the chest wall and axillary region to improve the detection of small breast tumors without unduly contorting the subjects. Furthermore, this system can acquire images sequentially with the SPECT and CT sub-systems without transferring the subject from one location to another or moving the patient bed in between acquisitions. This should minimize acquisition time and allow SPECT and CT images to be consistent and correlate with each other for easier co-registration. Our current prototype dedicated SPECT-CT system can provide volumetric fully 3D registered and fused breast images. This system can image an entire breast close to the chest wall to facilitate the detection and biopsy of small tumors without breast compression. This system has common emission (SPECT) and transmission (cone-beam CT) FOVs that intersect each other, as opposed to being either on separate systems or linearly juxtaposed on separate gantries.

Here, the CT component of the hybrid assembly was characterized for various system orientations and acquisition trajectories. Imaging results of the disk phantom with and without

acrylic balls, and tiered cross-shaped ball phantoms suspended throughout the 3D breast volume acquired using stationary polar tilted simple circular orbits, demonstrated geometric distortions and reconstruction inaccuracies (i.e. overlapping structures, circular ring) that manifest themselves as cupping artifacts. These cupping artifacts are distinctly different from those commonly known to arise from scatter and beam hardening. Given that insufficient cone-beam sampling yields an additional component of reconstruction 'cupping', any general scatter correction algorithm applied to these regions may indeed 'flatten' the response across the image, but would incorrectly account for the measured scatter response. That resulting data could not explicitly be considered quantitative in terms of resulting attenuation coefficients. Blur around the disks in the disk phantom was progressively observed away from the horizontal plane of the cone-beam, which had the more complete sampling using simple circular orbits. From the results of this study, we suggest that these incomplete sampling-based cupping artifacts are an addition to but distinct from any scatter or beam hardening induced cupping artifacts, indicating that simple scatter correction algorithms present in some systems may thus overestimate the scatter correction. Additionally, the results also showed that high-frequency information (smaller object size) was more preserved in incompletely sampled data, implying that resolution recovery is also dependent on the frequency components of an object. One caveat to note about the object frequency dependence, however, is that there may still be incorrect information transferred from out-of-plane regions into any plane of interest due to incomplete sampling. Thus, interpreting absolute attenuation coefficients should be made cautiously unless the system has more complete polar sampling as well.

Currently in our prototype dual-modality dedicated mammotomography system, the CT component has a stationary tilt. Results indicate that having the cone-beam flat closer to the chest wall (i.e. negative CT system tilt) allows for more complete sampling near the chest wall, and more lesion-like small spherical objects can be clearly seen than for a completely sampled complex 3D trajectory. The drawback is that there are overlapping structures throughout the volume, geometric distortion and incomplete sampling in the rest of the reconstruction volume. Clinically, this can translate to decreased contrast and size estimation of a lesion in the breast, as well as inaccurate absolute attenuation coefficient determination. Regardless of these known inaccuracies due to insufficient sampling with circular cone-beam acquisitions, CT patient images have shown that distortion appears to be nominal with high resolution recovery. However, for more distortion-free images, use of complex 3D trajectories in imaging procedures having more complete and uniform sampling is suggested. Our ongoing goal is to develop a CT sub-system with a complex 3D trajectory capability as part of the hybrid system that would allow for more complete and uniform sampling of the entire image volume, and subsequently lead to more quantitative CT image content potentially useful in tissue characterization. A large number of complex 3D acquisition trajectories are possible with the completely flexible positioning CT system; many would facilitate better sampling and are under investigation and development (Crotty *et al* 2006). The volume limitation issue of complex sampling may be ameliorated by lowering the object farther into the FOV, provided it is possible to do so (Cutler *et al* 2007, Crotty *et al* 2008).

Acknowledgments

This work was supported by NIH R01-CA096821, and in part by DOD W81XWH-06-1-0791, W81XWH-08-1-0352 and DOD W81XWH-05-1-0280. MPT is the inventor of this breast CT and hybrid imaging technology, and is named as an inventor on the patent for this technology applied for by Duke. If this technology becomes commercially successful, MPT and Duke could benefit financially. MPT is a founder and consultant of Zumatek.

References

Bartolac S, Noo F, Clackdoyle R, Moseley D, Siewerdsen J and Jaffray D 2006 A local Fourier description of artifacts in circular cone beam computed tomography *Med. Phys.* **33** 2287

Boone J M, Kwan A L, Yang K, Burkett G W, Lindfors K K and Nelson T R 2006 Computed tomography for imaging the breast *J. Mammary Gland Biol. Neoplasia* **11** 103–11

Bowsher J E, Tornai M P, Peter J, Gonzalez Trotter D E, Krol A, Gilland D R and Jaszczak R J 2002 Modeling the axial extension of a transmission line source within iterative reconstruction via multiple transmission sources *IEEE Trans. Med. Imaging* **21** 200–15

Brzymialkiewicz C N, Tornai M P, McKinley R L and Bowsher J E 2005 Evaluation of fully 3D emission mammotomography with a compact cadmium zinc telluride detector *IEEE Trans. Med. Imaging* **24** 868–77

Brzymialkiewicz C N, Tornai M P, McKinley R L, Cutler S J and Bowsher J E 2006 Performance for dedicated emission mammotomography for various breast shapes and sizes *Phys. Med. Biol.* **51** 5051–64

Chen B and Ning R 2002 Cone-beam volume CT mammographic imaging: feasibility study *Med. Phys.* **29** 755–70

Chen L, Shaw C C, Tu S, Altunbas M C, Wang T, Lai C, Liu X and Kappadath S C 2005 Cone-beam CT breast imaging with a flat panel detector: a simulation study *Proc. SPIE: Phys. Med. Imaging* **5745** 943–51

Crotty D J, Brzymialkiewicz C N, McKinley R L and Tornai M P 2005 Optimizing orientation of SPECT and CT detectors through quantification of cross contamination in a dual modality mammotomography system *Proc. IEEE Med. Imaging Conf.* **3** 1672–6

Crotty D J, Brzymialkiewicz C N, McKinley R L and Tornai M P 2006 Investigation of emission contamination in the transmission image of a dual modality computed mammotomography system *Proc. SPIE: Phys. Med. Imaging* **6142** 664–74

Crotty D J, Cutler S J, McKinley R L, Madhav P, Perez K L and Tornai M P 2008 Improved chest wall imaging through combined circular trajectories in dedicated dual modality SPECT-CT breast molecular imaging *Proc. IEEE MRBC Conf.* pp 5650–65

Crotty D J, Madhav P, McKinley R L and Tornai M P 2007a Investigating novel patient bed designs for use in a hybrid dual modality dedicated 3D breast imaging system *Proc. SPIE: Phys. Med. Imaging* **6150** 65101H

Crotty D J, McKinley R L and Tornai M P 2007b Experimental spectral measurements of heavy K-edge filtered beams for x-ray computed mammotomography *Phys. Med. Biol.* **52** 603–16

Cutler S J, Madhav P, Perez K L, Crotty D J and Tornai M P 2007 Comparison of reduced angle and fully 3D acquisition sequencing and trajectories for dual-modality mammotomography *Proc. IEEE Med. Imaging Conf.* **6** 4044–50

Davis G 2005 Explicit control of image noise and error properties in cone-beam microtomography using dual concentric circular source loci *Nucl. Instrum. Methods Phys. Res.* A **547** 679–85

Erdogan H and Fessler J A 1999 Ordered subsets algorithms for transmission tomography *Phys. Med. Biol.* **44** 2835–51

Hany T F, Steinert H C, Goenes G W, Buck A and von Schulthess G K 2002 Improvement of diagnostic accuracy of PET imaging using an in-line PET-CT system—initial results *Radiology* **225** 575–81

Hasegawa B H, Wong K H, Iwata K, Barber W C, Hwang A B, Sakdinawat A E, Ramaswamy M, Price D C and Hawkins R A 2002 Dual-modality imaging of cancer with SPECT/CT *Technol. Cancer. Res. Treat.* **1** 449–58

Hubbell J H and Seltzer S M 1996 Tables of x-ray mass attenuation coefficients and mass energy-absorption coefficients 1 keV to 20 MeV for elements $Z = 1$ to 92 and 48 additional substances of dosimetric interest (Gaithersburg: National Institutes of Standards and Technology)

Israel O, Keidar Z, Iosilevsky G, Bettman L, Sachs J and Frenkel A 2001 The fusion of anatomic and physiologic imaging in the management of patients with cancer *Semin. Nucl. Med.* **31** 191–205

Junhai W, Hongbing L, Wei Z, Zigang W and Zhengrong L 2003 A study on truncated cone-beam sampling strategies for 3D mammography *Proc. IEEE Med. Imaging Conf.* **5** 3200–4

Kudo H and Saito T 1990 Feasible cone beam scanning methods for exact reconstruction in three-dimensional tomography *J. Opt. Soc. Am.* A **7** 2169–83

Madhav P, Crotty D J, McKinley R L and Tornai M P 2006 Initial development of a dual-modality SPECT-CT system for dedicated mammotomography *Proc. IEEE Med. Imaging Conf.* **4** 2382–6

Madhav P, Cutler S, Crotty D, Perez K, McKinley R, Marcom P, Wong T and Tornai M 2008 Pilot patient studies using a dedicated dual-modality SPECT-CT system for breast imaging *Med. Phys.* **35** 2894

McKinley R L, Brzymialkiewicz C N, Madhav P and Tornai M P 2005a Investigation of cone-beam acquisitions implemented using a novel dedicated mammotomography system with unique arbitrary orbit capability *Proc. SPIE: Phys. Med. Imaging* **5745** 609–17

McKinley R L and Tornai M P 2006 Preliminary investigation of dose for a dedicated mammotomography system *Proc. SPIE: Phys. Med. Imaging* **6142** 60–70

McKinley R L, Tornai M P, Samei E and Bradshaw M L 2004 Simulation study of a quasi-monochromatic beam for x-ray computed mammotomography *Med. Phys.* **31** 800–13

McKinley R L, Tornai M P, Samei E and Bradshaw M L 2005b Initial study of quasi-monochromatic beam performance for x-ray computed mammotomography *IEEE Trans. Nucl. Sci.* **52** 1243–50

Schillaci O and Simonetti G 2004 Fusion imaging in nuclear medicine: applications of dual-modality systems in oncology *Cancer Biother. Radiopharm.* **19** 1–10

Shreve P D 2000 Adding structure to function *J. Nucl. Med.* **41** 1380–2

Smith B D 1985 Image reconstruction for cone beam projections: necessary and sufficient conditions and reconstruction methods *IEEE Trans. Med. Imaging* **4** 14–25

Tornai M P, McKinley R L, Brzymialkiewicz C N, Madhav P, Cutler S J, Crotty D J, Bowsher J E, Samei E and Floyd C E 2005 Design and development of a fully-3D dedicated x-ray computed mammotomography system *Proc. SPIE: Phys. Med. Imaging* **5745** 189–97

Tuy H K 1983 An inversion formula for cone-beam reconstruction *SIAM J. Appl. Math.* **43** 546–52

Vedula A A and Glick S J 2003 Computer simulations of CT mammography using a flat panel imager *Proc. SPIE: Phys. Med. Imaging* **5030** 349–60

Webb S, Sutcliffe J, Burkinshaw L and Horsman A 1987 Tomographic reconstruction from experimentally obtained conebeam projections *IEEE Trans. Med. Imaging* **6** 67–73

Zeng G L, Clack R and Gullberg G T 1994 Implementation of Tuy's cone-beam inversion formula *Phys. Med. Biol.* **39** 493–507